Development of Soft Actuators and Flexible Sensors using Shape Memory Polymer

A doctoral dissertation presented to
Integrated Graduate School of Medicine, Engineering, and Agricultural Sciences
University of Yamanashi

September 2020

Yingjun An

Contents

Chapter 1 General Introduction

1.1 Research background

Now almost all the developed or developing countries are stepping to 'Aged Population Society'[1]. The aging population has become a serious problem for all the countries in the world. With the increasing of aged population, the development of health care devices which can provide force assistant to aged human or monitor human motion are important and necessary. Traditional health care devices, such as crutch, wheelchairs and so on, are hard, heavy, inconvenient and low efficiency. So the development of light, soft and wearable actuators[2-5] and sensors[6-10] are important.

Hard machines, such as gasoline engine, electromagnetic motor, hydraulic pump and so on, are the traditional actuators which can transfer chemical, electricity energy to mechanical energy, furthermore force can be generated. It is well knew that those hard machines play very important roles in our life at both this moment and in future. Most of them are heavy, expensive, noisy, the most significant drawback is that all of the devices are hard, they are very difficult to work as wearable devices to provide force assistant for human beings. In order to achieve the goal of force assistant, development of cheap, flexible, light weight and wearable actuators is necessary. On the other hand, the commercial sensors, consist of piezoelectric acceleration sensors, gas sensors, temperature sensors and as well as typical displacement sensors, are hard and expensive. Similar to those hard actuators, they are difficult to work as wearable health care devices to monitor human motions. Fig. 1-1 shows the typical hard actuators and sensors, which were useful in our word.

In order to achieve the goal of wearable devices which can provide force assistant and monitor human motions, many soft actuators and flexible sensors have been developed using functional polymers. The development of soft actuators and flexible sensors will be introduced in next sections.

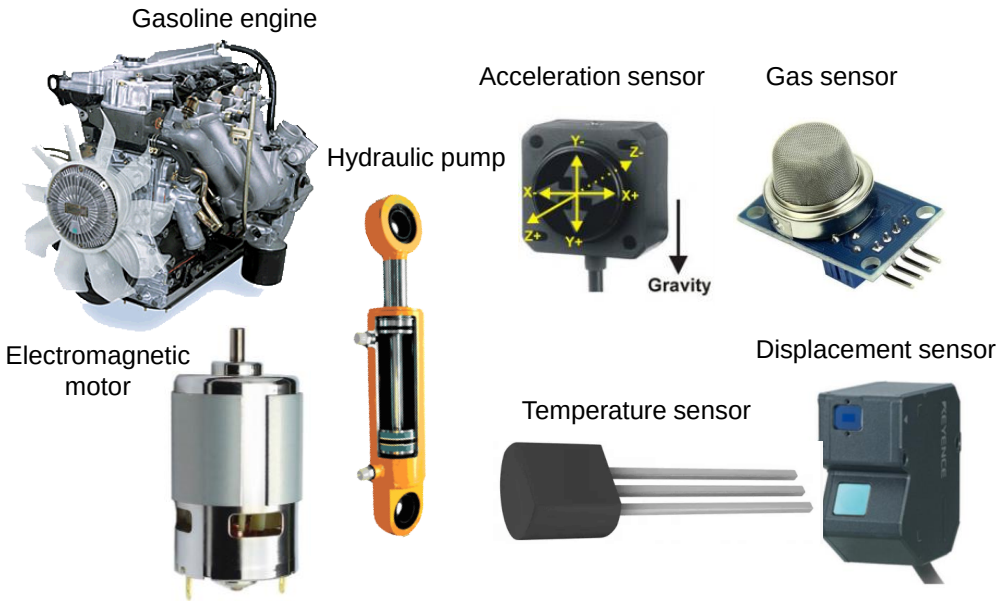

Figure 1-1 Traditional hard machines (gasoline engine, hydraulic pump and electromagnetic motor) and various hard sensors (acceleration, displacement, gas and temperature sensors).

1.2 Soft actuators

Many different types of electro-active soft actuators have been developed, such as ionic polymer metal composites (IPMC)[11-15], dielectric elastomer actuators (DEA)[16,17], polyvinyl chloride (PVC) gel[18-21] actuators, conductive polymer actuators[22-30] and so on, as shown in Fig. 1-2. Differing from conventional mechanical transducers such as electric motors, combustion engines, and hydraulic pumps in which the motion is generated via changes of relative positions between their components, the soft actuators exhibit flexible motion through shape or volume changes due to accumulation and integration of microscopic conformational changes at the molecular level into a macroscopic large deformation of the actuator materials. Ionic polymer metal composites (IPMC) is one of the most typical soft actuators[31-33]. Under an applied voltage, ion migration and redistribution due to the imposed voltage across a strip of IPMCs result in a bending deformation. The response time is fast, but the generated force is too weak. Furthermore, the actuation performance is strongly dependent on the relative humidity. The dielectric elastomer actuator (DEA)[34] will undergo larger deformation while the polyvinyl chloride (PVC) actuator[35] can generate larger force, under external high voltage, in the order of hundreds or kilos volt. Conductive polymers, such as polypyrrole[36], polythiophene[37], polyaniline[38], and their derivatives, are another typical electro-active actuators which show dimensional changes resulting from

electrochemical doping, characterized by transportation of solvated ions between the interior of the polymer matrix and the surrounding electrolyte solution, electrostatic repulsion, and/or structural distortion through oxidation of π-conjugated polymers. One the other hand, polypyrrole (PPy) and poly (3,4-ethylenedioxythiophene)/poly(4-styrenesulfonate) (PEDOT/PSS) undergo contraction in air under application of an electric field, due to the desorption of water vapor caused by Joule heating. The development of those materials had driven further progress in soft actuators not only from the fundamental view point of basic science and materials chemistry and physics but also from the engineering view point for the practical applications to light-weight, low-cost, less-noise, less pollution and high efficiency micro- and macro-artificial muscles and soft robotic systems.

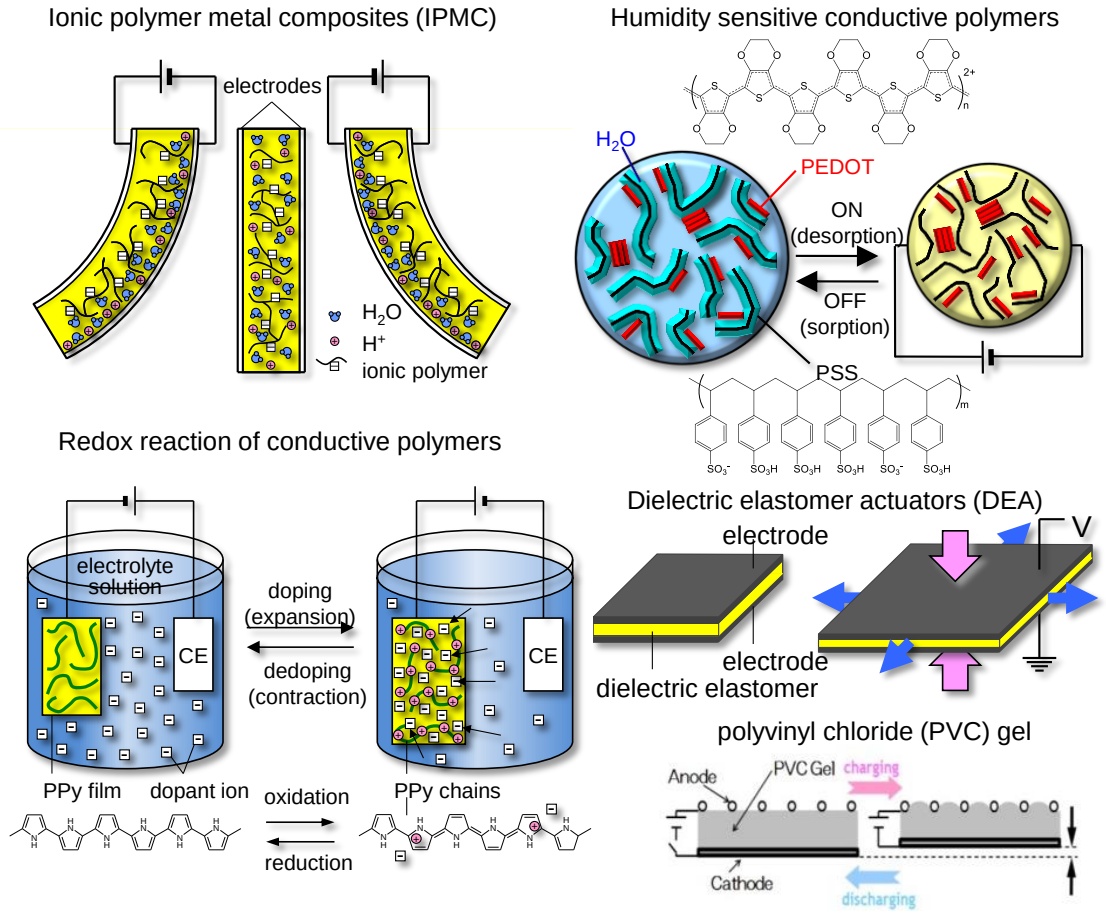

Figure 1-2 Various typical electro-active polymer (EAP) actuators, ionic polymer metal composites (IPMC), humidity sensitive conductive polymers, actuators based on redox reaction of conductive polymers, dielectric elastomer actuator (DEAs), and polyvinyl chloride (PVC) gels.

1.3 Flexible sensors

Internet of Things (IoT) is a system that connects between people and things, and between things through the Internet such as health monitoring using heart rate sensors[39], remote control of appliances using wearable devices[40], and gait measurement using sole sensors[41]. Here, soft and flexible sensors are key devices for the wearable electronics in the world of IoT. Recently, as the rapid development of IoT has substantially increased sensors demands, especially flexible multi-functional or non-powered sensors. In general, the flexible sensors can be categorized into two types, one is resistive sensor, and the other is capacitive one[42]. The resistive sensor detects changes in resistance of conductors, such as metal wires[43], carbon nanotubes[44] and graphene[45], under mechanical deformation. However, electric power consumption of the resistive sensors is relatively high, due to electric current always flows through the conductor. On the other hand, the capacitive sensor detects changes in capacitance of a dielectric such as silicones[46], polyurethanes[47], and acrylpolymers. But difficult to distinguish the direction of deformation, which is not suitable for a motion sensor. Recently, various non-power sensors were developed, such as piezoelectric[48], triboelectric[49] and piezoionic[50] sensors. After the sensors were bended, an electric signal can be generated, like voltage and current or electric charges. The output signals of piezoelectric and triboelectric sensors are spike-like peak of voltage while the piezoionic sensors can generate stable output voltage. In order to monitor and determine the motions, acceleration, displacement and bending direction are the most important parameters in the characterization of an object's movement. Usually, the acceleration and displacement sensors are based on force sensing mechanisms, including piezoresistive, piezoelectric or differential capacitance, has been widely applied in navigation[51], industrial engineering[52] and robots[53]. In the view of energy consumption and precise determine the displacement and acceleration motions, piezoresistive strain sensors, piezoelectric, triboelectric and capacitive sensors are not suitable to use as motion sensors.

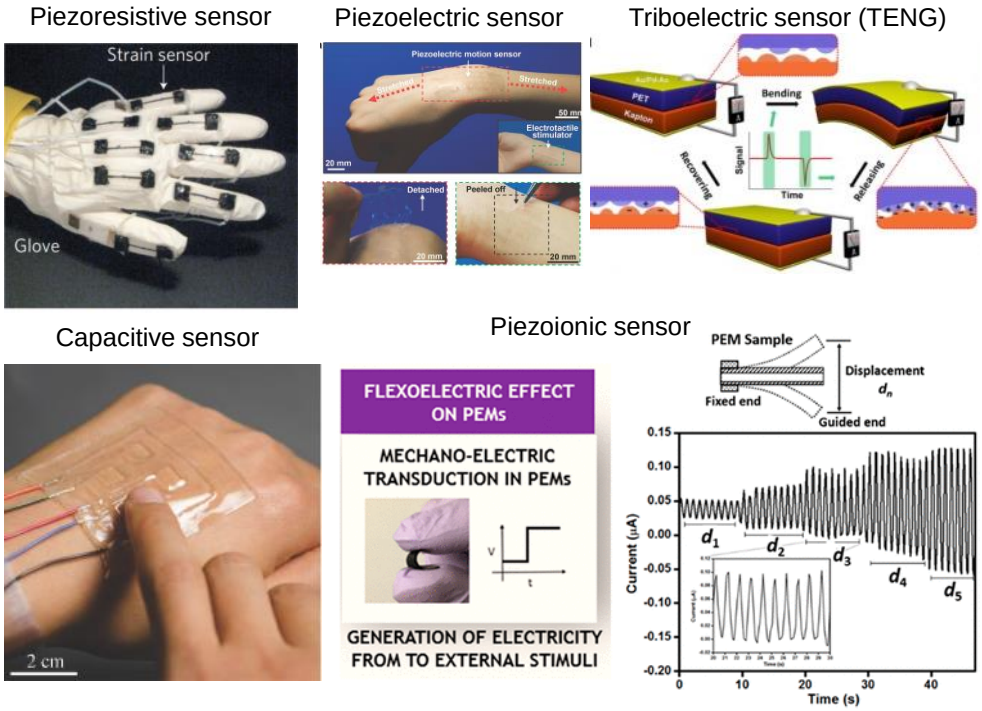

Figure 1-3 Various wearable strain sensors, piezoelectric sensors, capacitive sensors, piezoelectric sensors, triboelectric sensors and piezoionic sensors.

1.4 Objective and scope of thesis

Shape memory polymers (SMPs) are one type of very important smart materials. SMPs can be fixed in a temporary shape, and recover to the original shape upon exposing to external stimulus like heat, solvent, electric field, or magnetic field. That is because there are two segments in the polymer chains. One is stable polymer network, another is revisable switch. The hard segments form physical cross-links arising from polar interactions, hydrogen bonding, and crystallization in the hard domain, while the soft segments form the reversible phase because of molecular motion in a rubbery state[54-57]. So SMP is a good candidate for the application of soft actuators. For the thermo-responsive SMPs, they can recover to their original shape by being heated above their transition temperature. After the thermo-responsive SMP was put into hot water, it would recover from temporary shape to the original shape. In this research, novel electric SMP and ionic SMP were developed. The electric SMP works as soft actuators while the ionic SMP can be applied to flexible sensors.

In chapter 2, a novel electric SMP was fabricated. It is well known that the thermo-sensitive

SMPs can be fixed to a temporary shape and recover to its initial shape once it was heated above the glass transition temperature (T_g). So SMP is a good candidate for the application of soft actuator. But direct heating is very inconvenient and low efficiency. So composited SMPs with conductive materials is a common way to solve those problems. There are many conductive materials, like graphene[58], carbon nanotubes (CNTs)[59], carbon black (CB)[60] and poly(3,4-ethylenedioxythiophene):poly(styrene sulfonate) (PEDOT:PSS). Even though those materials show high electrical conductivity, but they are difficult to dissolve or disperse homogeneously in organic solvents. As the result, they are difficult to composite homogeneously with SMPs in solution. Some researchers had tried to composite those conductive fillers with SMPs using melt mixing method. But the conductivity of those conductive filler/SMP composites was very low, it was because the conductive particles couldn't disperse very well in the polymer matrix. Of course, the conductivity of those electric SMP can be improved by increasing conductive filler content, but on the other hand, the shape memory properties will drop drastically at the same time. Recently, we have successfully synthesized a novel conductive polymer, fully soluble self-doped poly(3,4-ethylenedioxythiophene) (S-PEDOT)[61,62], with an electrical conductivity greater than 1000 S cm^{-1}. Since the S-PEDOT can dissolve not only in water but in some organic solvents such as dimethyl sulfoxide (DMSO), formic acid (FA) and ethylene glycol (EG), composites with various polymers are available by a solution mixing method. A novel electro-active SMP was fabricated with fully soluble self-doped poly(3,4-ethylenedioxythiophene) (S-PEDOT) and SMP using a solution mixing method at various S-PEDOT weight ratios ($W_{S\text{-}PEDOT}$). The percolation analysis showed an extreme low percolation threshold of 0.38 vol% and critical exponent of 1.15, which was associated with the S-PEDOT conductive networks formed by phase separation in the S-PEDOT:SMP composite. The shape memory characteristics were observed at WS-PEDOT $\leqslant$ 30 wt%, while the glass transition temperature (T_g) was almost constant ca. 50 °C. The S-PEDOT:SMP composite film at $W_{S\text{-}PEDOT}$ = 10 wt% showed electrical conductivity (σ), shape fixing ratio (R_f), and shape recovery ratio (R_r) of 29 S cm^{-1}, 95.4%, and 90.1%, respectively. Furthermore, an electro-active SMP soft actuator, fabricated using the S-PEDOT:SMP composite film at $W_{S\text{-}PEDOT}$ = 10 wt%, quickly recovered from a temporary bent shape to its original open shape within 5 s upon application of 6 V.

In chapter 3, a multifunctional ionic liquid-shape memory polymer (IL-SMP) gel was fabricated using 1-ethyl-3-methylimidazolium bis(trifluoromethylsulfonyl)imide (EMI^+TFSI^-) and SMP at

various EMI^+TFSI^- weight ratios (W_{IL}). The EPMA elements mapping images showed the good miscibility between IL and SMP. The ionic conductivity increased in proportion to IL content, achieved 1.85×10^{-5} S cm^{-1} at W_{IL} = 30 wt%. The mechanical bending induced electric charge of the ionic polymer sensors was measured firstly. Furthermore, the electric current was evaluated by differential electric charges with time. Interestingly, it was found that both electric charges and current increased in proportion to the acceleration, indicates the ionic SMP composite has the potential to work as acceleration sensor to detect the acceleration of movement, such as human motions and so on. The acceleration sensitivity was characterized in chapter 3. Notably, the ionic SMP composites exhibit higher acceleration sensitivity, as high as 8.6 nA m^{-1} s^2 at W_{IL} = 30 wt%. On the other hand, voltage was induced under mechanical stimulate. It was found that the mechanical bending induced voltage increases in proportion to the bending displacement, less dependent on the acceleration, indicates that it is suitable to work as non-power displacement sensor. Notably, we claim that the generated voltage is strongly dependent on the total transferred charges (ΔQ)[63,64] under the mechanical stimulate and the capacitance (C) of the ionic SMP gel composites. Notably, the highest voltage was achieved at W_{IL} = 25 wt%, as high as 9.8 mV, which can be explained by the largest ΔQ (total transferred electric charges) and relative lower C (capacitance). On the other hand, the mechanical bending induced voltage was strongly dependent on the bending displacement, while regardless with velocity as well as acceleration. The ionic SMP /PEDOT:PSS with 25 wt% of EMI^+ $TFSI^-$ exhibits displacement sensitivity of 1.25 V m^{-1}. The ionic SMP/PEDOT:PSS composite can work as multi-functional motion sensor to detect acceleration and displacement. Interestingly, the generated voltage of the ionic SMP/PEDOT:PSS composite (W_{IL} = 10 wt%) also exhibits transition behavior while the ambient temperature is around T_g. The thermomechanical analysis measurement revealed that the ionic SMP gels exhibit acceptable shape memory property while $W_{IL} \leq 10$ wt%, as R_f = 86.9 %, R_r = 89.8 % at W_{IL} = 10 wt%.

In chapter 4, 3D printable electroactive soft actuators and multi-functional ionic SMP gel were fabricated using fused deposition modeling (FDM) 3D printing technology. 3D printing technology, also was named as additive manufacturing, has many advantages compared with traditional manufacturing technology, as fast manufacture, low cost and so on. Many different types of commercial 3D technology has been developed, like stereolithography (SLA), selective laser sintering (SLS), 3D plotting/direct-write (3DP) and fused deposition modeling (FDM). Due to the

novel electric SMP (chapter 2) and ionic SMP (chapter 3) exhibit T_g at ca. 50 and lower 50 ºC, these novel SMPs have the potential to apply to FDM 3D printing technology. In chapter 4, the novel electric SMP and ionic SMP were applied to FDM 3D printing technology, 3D printable electroactive soft actuators and ionic SMP gel with shape memory properties were fabricated.

Furthermore, in chapter 5, a stretchable conductive gel was fabricated. It is well known that, the flexible and stretchable electrodes play very important role in wearable devices[65-67]. The stretchable and highly conductive polymer (S-CP) hydrogels were fabricated by casting a water solution of poly(3,4-ethylenedioxythiophene) doped with poly(4-styenesulfonate) (PEDOT:PSS) and polyacrylamide (PAAm) and subsequent swelling in water. The mechanical properties, electrical conductivity, and structure of the S-CP gels with different weight ratios of the PAAm (W_{PAAm}) were investigated by means of the tensile test, four-probe method, scanning electron microscopy (SEM), and electron probe micro analysis (EPMA). It was found that the S-CP gels were composed of soft and stretchable PAAm-rich porous network surrounded by the PEDOT:PSS-rich conductive network layers, exhibiting excellent electrical conductivity (17 S cm^{-1}) and fracture strain (110%) though it contained 92% of water at W_{PAAm} = 64 wt%. Furthermore, the electrical conductivity of the S-CP gel was improved by stretching up to 75% due to the orientation of the PEDOT:PSS-rich conductive network layers so as to keep the resistance constant, which had potential applications to smart electrodes for soft sensors and actuators in a new field of wet electronics using hydrogels, so called 'gelectronics'.

1.5 References

1) Nations U. World Population Ageing 2017-Highlights. Department of Economic and Social Affairs, 2017.
2) A. Katchalsky, M. Zwick. Mechanochemistry and ion exchange. J. Polym. Sci. **16**, 221, 1955.
3) E. Smela. Conjugated polymer actuators for biomedical applications. Adv. Mater. **15**, 481, 2003.
4) Y. Osada, J. Gong. Soft and wet materials: polymer gels. Adv. Mater. **10**, 827, 1998.
5) P. Brochu and Q. Pei. Advances in dielectric elastomers for actuators and artificial muscles. Macromol. Rapid. Commun. **31**, 10, 2010.
6) F. Zhao, L. Wang, Y. Zhao, L. Qu and L. Dai. Graphene oxide nanoribbon assembly toward

moisture-powered information storage. Adv. Mater. **29**, 1604972, 2017.

7) C. Liu and J. Choi. An embedded PDMS nanocomposite strain sensor toward biomedical application. 31st Ann. Int. Conf. IEEE EMBS, 6391, 2009.
8) T. Giorgino, P. Tormene, F. Lorussi, D. Rossi and S. Quaglini. Sensor evaluation for wearable strain gauges in neurological rehabilitation. IEEE Trans. Neural Syst. Rehabil. Eng. 409, 2009.
9) F. Lourussi, E. Scilingo, M. Tesconi, A. Tognetti and D. Rossi. Strain sensing fabric for hand posture and gesture monitoring. IEEE Trans. Inf. Technol. Biomed. 372, 2005.
10) C. Liu and J. Choi. Patterning conductive PDMS nanocomposite in an elastomer using microcontact printing. J. Micromech. Microeng. **19**, 085019, 2009.
11) A. Grodzinsky, Electromechanics of Deformable Polyelectrolyte Membranes, Sc. D. Dissertation, Dept. of Elec. Eng., MIT, Cambridge, June 1974.
12) M. Shahinpoor. Conceptual design, kinematics and dynamics of swimming robotic structures using ionic polymeric gel muscles. Smart Mater. Struct. Int. J., **1**, 91, 1991.
13) K. Asaka, K. Oguro, Y. Nishimura, M. Mizuhataand and H. Takenaka. Bending of polyelectrolyte membrane–platinum composites by electric stimuli I. Response characteristics to various waveforms. Polym. J. **27**, 436, 1995.
14) M. Shahinpoor. Continuum electromechanics of ionic polymeric gels as artificial muscles for robotic applications. Smart Mater. Struct. **3**, 367, 1994.
15) K. Kim and M. Shahinpoor. A novel method of manufacturing three-dimensional ionic polymer–metal composites (IPMCs) biomimetic sensors, actuators and artificial muscles. Polymer. **43**, 797, 2002.
16) R. Pelrine, R. Kornbluh, Q. Pei and J. Joseph. High-speed electrically actuated elastomers with strain greater than 100%. Science. **287**, 836, 2000.
17) R. Pelrine, R. Kornbluh, J. Joseph, R. Heydt, Q. Pei, S. Chiba. High-field deformation of elastomeric dielectrics for actuators. Mater. Sci. Eng. C. **11**, 89, 2000.
18) T. Hirai, T. Ogiwara, K. Fujii , T. Ueki, K. Kinoshita and M. Takasaki. Electrically active artificial pupli showing amoeba-like pseudopodial deformation. Adv. Mater. **21**, 2886, 2009.
19) M. Ali, T. Ueki, D. Tsurumi, and T. Hirai. Influence of plasticizer content on the transition of electromechanical behavior of PVC gel actuator. Langmuir. **27**, 7902, 2011.

20) K. Asaka and M. Hashimoto. Electrical properties and electromechanical modeling of plasticized PVC gel actuators. Sens. Actuators B Chem. **273**, 1246, 2018.

21) Y. Li and M. Hashimoto. PVC gel soft actuator-based wearable assist wear for hip joint support during walking. Smart Mater. Struct. **26**, 125003, 2017.

22) T. Mirfakhrai, J. Madden, R. Baughman. Polymer artificial muscles. Mater. Today. **10**, 30, 2007.

23) S. Hara, T. Zama, W. Takashima and K. Kaneto. Free-standing gel-like polypyrrole actuators doped with bis(perfluoroalkylsulfonyl)imide exhibiting extremely large strain. Smart Mater. Struct. **14**, 1501, 2005.

24) K. Kaneto, H. Hashimoto, K. Tominaga and W. Takashima. Shape retention in polyaniline artificial muscles. Jpn J. Appl. Phys. **50**, 021603, 2011.

25) H. Okuzaki and T. Kunugi. Adsorption-induced bending of polypyrrole films and its application to a chemomechanical rotor. J Polym Sci B Polym Phys. **34**, 1735, 1996.

26) H. Okuzaki and T. Kunugi. Electrically induced contraction of polypyrrole film in ambient air. J Polym Sci B Polym Phys. **36**, 1591, 1998.

27) H. Okuzaki, H. Suzuki and T. Ito. Electrically driven PEDOT/PSS actuators. Synth. Metal. **159**, 2233, 2009.

28) D. Hohnholz, H. Okuzaki and A. MacDiarmid. Plastic electronic devices through line patterning of conducting polymers. Adv. Funct. Mater. **15**, 51, 2005.

29) G. Spinks, V. Mottaghitalab, M. Bahrami, P. Whitten, G. Wallace. (2006) Carbonnanotube-reinforced polyaniline fibers for high-strength artificial muscles. Adv. Mater. **18**, 637, 2006.

30) H. Okuzaki, T. Kuwabara, K. Funasaka and Tomooki Saido. Humidity-sensitive polypyrrole films for electro-active polymer actuators. Adv. Funct. Mater. **23**, 4400, 2013.

31) K. Asaka and H. Okuzaki. Soft actuators: materials, modeling, applications, and future perspectives. Springer Nature, 2019.

32) H. Schneider and M. ShahinpoorIonic polymer metal composites (IPMCs): Smart multi-functional materials and artificial muscles. Royal Society of Chemistry, 2015.

33) I. Asiri. Ionic Polymer Metal Composites for Sensors and Actuators. Springer, 2019.

34) S. Koh, T. Li, J. Zhou, X. Zhao, W. Hong, J. Zhu and Z. Suo. Mechanisms of large actuation strain in dielectric elastomers. J Polym Sci B Polym Phys. **49**, 504, 2011.

35) Y. Li and M. Hashimoto. Design and prototyping of a novel lightweight walking assist

wear using PVC gel soft actuators. Sens. Actuator A Phys. **239**, 26, 2016.

36) H. Okuzaki, T. Kondo and T. Kunugi. Characteristics of water in polypyrrole films. Polymer. **40**, 995, 1999.

37) N. Vandesteeg, P. Madden, J. Madden, P. Anquetil and I. Hunter. Synthesis and characterization of EDOT-based conducting polymer actuators. Smart Struct Mater EAPAD. **5051**, 349, 2003.

38) K. Kaneto, Y. Min, A. MacDiarmid. Conductive polyaniline laminates. U.S. Patent 5,556,700, 1994.

39) C. Boutry, A. Nguyen, Q. Lawal, A. Chortos, S. Gagné and Z. Bao. A sensitive and biodegradable pressure sensor array for cardiovascular monitoring. Adv. Mater. **18**, 6954, 2015.

40) S. Mallineni, Y. Dong, H. Behlow, A. Rao andR. Podila. A wireless triboelectric nanogenerator. Adv. Energy Mater. **8**, 1702736, 2018.

41) S. Chen, T. Huang, H. Zuo, S. Qian, Y. Guo, L. Sun, D. Lei, Q. Wu, B. Zhu, C. He, X. Mo, E. Jeffries, H. Yu, Z. You. A single integrated 3D-printing process customizes elastic and sustainable triboelectric nanogenerators for wearable electronics. Adv. Funct. Mater. **14**, 1805108, 2018.

42) X. Liao, Q. Liao, X. Yan, Q. Liang, H. Si, M. Li, H. Wu, S. Cao and Y. Zhang. Flexible and Highly Sensitive Strain Sensors Fabricated by Pencil Drawn for Wearable Monitor. Adv. Funct. Mater. **25**, 2395, 2015.

43) S. Gong, W. Schwalb, Y. Wang, Y. Chen, Y. Tang, J. Si, B. Shirinzadeh, and W. Cheng. A wearable and highly sensitive pressure sensor with ultrathin gold nanowires. Nat. Commun. **5**, 1, 2014.

44) T. Yamada, Y. Hayamizu, Y. Yamamoto, Y. Yomogida, A. Najafabadi, D. Ftaba and K. Hata. A stretchable carbon nanotube strain sensor for human-motion detection. Nat. Nanotechnol. **6**, 296, 2011.

45) T. Yang, X. Jiang, Y. Zhong, X. Zhao, S. Lin, J. Li, X. Li, J. Xu, Z. Li and H. Zhu. A wearable and highly sensitive graphene strain sensor for precise home-based pulse wave monitoring. ACS Sens. **2**, 967, 2017.

46) X. Wang, T. Li, J. Adams and J. Yang. Transparent, stretchable, carbon-nanotube-inlaid conductors enabled by standard replication technology for capacitive pressure, strain and

touch sensors. J. Mater. Chem. A. **1**, 3580, 2013.

47) Y. Liu, Y. Hu, J. Zhao, G. Wu, X. Tao and W. Chen. Self-powered piezoionic strain sensor toward the monitoring of human activities. Small. **12**, 5074, 2016.

48) S. Lim, D. Son, J. Kim, Y. Lee, J. Song, S. Choi, D. Lee, J. Kim, M. Lee, T. Hyeon and D. Kim. Transparent and stretchable interactive human machine interface based on patterned graphene heterostructures. Adv. Funct. Mater. **25**, 375, 2015.

49) H. Zhang, Y. Yang, Y. Su, J. Chen, K, Adams, S. Lee, C. Hu and Z. Wang. Triboelectric nanogenerator for harvesting vibration energy in full space and as self-powered acceleration sensor. Adv. Funct. Mater. **24**, 1401, 2014.

50) N. Kamamichi, M. Yamakita, K. Asaka, Z. Luo and T. Mukai, Sensor Property of a Novel EAP Device with Ionic-liquid-based Bucky Gel, SENSORS, 2007 IEEE, Atlanta, GA, 221, 2007.

51) C. Xiang, C. Liu, C. Hao, Z. Wang, L. Che and X. Zhou. A self-powered acceleration sensor with flexible materials based on triboelectric effect. Nano Energy. **31**, 469, 2017.

52) D. Lee, H. Hong, M. Lee, C. Park, and N. Min. A prototype high sensitivity load cell using single walled carbon nanotube strain gauges. Sens. Actuators, A. **180**, 120, 2012.

53) T. Someya, T. Sekitani, S. Iba, Y. Kato, H. Kawaguchi, and T. Sakurai. A large-area, flexible pressure sensor matrix with organic field-effect transistors for artificial skin applications. Proc. Natl Acad. Sci. USA. **101**, 9966, 2004.

54) A. Lendlein, and S. Kelch, Shape-memory polymers. Angew. Chem. Int. Ed. **41**, 2034 , 2002.

55) J. Hu, Y. Zhu, H. Huang, and J. Lu, Recent advances in shape-memory polymers: Structure, mechanism, functionality, modeling and applications. Prog. Polym. Sci. **37**, 1720, 2012.

56) Q. Zhao, H. Qi, and T. Xie, Recent progress in shape memory polymer: New behavior, enabling materials, and mechanistic understanding. Prog. Polym. Sci. **49**, 79, 2015.

57) T. Xie, Recent advances in polymer shape memory. Polymer. **52**, 4985, 2011.

58) J. T. Kim, H. J. Jeong, H. C. Park, H. M. Jeong, S. Y. Bae, and B. K. Kim, Electroactive shape memory performance of polyurethane/graphene nanocomposites. React. Funct. Polym. **88**, 1, 2015.

59) J. Cho, J. Kim, Y. Jung, and N. Goo, Electroactive shape-memory polyurethane composites incorporating carbon nanotubes. Macromol. Rapid Commun. **26**, 412, 2005.

60) J. Leng, X. Lan, Y. Liu, and S. Du, Electroactive thermoset shape memory polymer nanocomposite filled with nanocarbon powders. Smart Mater. Struct. **18**, 074003, 2009.

61) H. Yano, K. Kudo, K. Marumo, and H. Okuzaki, Fully soluble self-doped poly (3,4-ethylenedioxythiophene) with an electrical conductivity greater than 1000 S cm^{-1}. Sci. Adv. **5**, eaav9492, 2019.

62) H. Yano, M. Nishiyama, S. Hayashi, K. Kudo, and H. Okuzaki, Synthesis and Characterization of a Novel Self-Doped Water-Soluble Conducting Polymer. Kobunshi Ronbunshu, **75**, 607, 2018.

63) S. Imaizumi, Y. Kato, H. Kokubo, and M. Watanabe. Driving mechanisms of ionic polymer actuators having electric double layer capacitor structures. J. Phys. Chem. B. **116**, 5080, 2012.

64) V. Woehling, G. Nguyen, C. Plesse, Y. Petel, Y. Dobashi, J. Madden, C. Michal and F. Vidal. Study of the piezoionic effect and influence of electrolyte in conducting polymer based soft strain sensors. Multifunct. Mater. **2**, 045002, 2019.

65) H. Klauk ed. Organic Electronics: Materials, Manufacturing and Applications Wiley-VCH, Weinheim, 2006. H. Klauk ed. Organic electronics II: More Materials and Applications Wiley-VCH, Weinheim, 2010.

66) A. Elschner, S. Kirchmeyer, W. Lövenich, U. Merker and K. Reuter eds. PEDOT Principles and Applications of an Intrinsically Conductive Polymer CRC Press, 2010.

67) H. Okuzaki ed. PEDOT: Material Properties and Device Applications, Science & Technology. 2012.

Chapter 2 Novel electro-active shape memory polymers for soft actuators

2.1 Introduction

Electro-active polymer (EAP) soft actuators, the size or shape of which change upon application of an electric field as a result of contraction or bending deformation, can be used as artificial muscle and organic robots.[1-3] So far, a variety of EAP soft actuators, such as ionic polymer metal composites (IPMC),[4,5] polyvinyl chloride (PVC) gels[3] and conductive polymers[2,6-8] have been investigated. Shape memory polymers (SMPs), exhibiting the ability to switch from temporary to their original shape upon heating above the glass transition temperature, are one of the candidates for soft actuators.[9-13] Although it is difficult to control the actuation of SMPs by direct heating, a straightforward approach for indirect heating is Joule heating by voltage application.[14] The electro-active SMPs have been generally fabricated by mixing the SMP with electrically conductive fillers, such as carbon black (CB),[15] carbon nanotubes (CNTs),[16] and graphene.[17] Cho et al.[16] synthesized electro-active SMP composites by solution mixing with multi-walled carbon nanotubes (MWCNTs), where the MWCNT:SMP composite with an electrical conductivity of 10^{-3} S cm^{-1} recovered to its original shape in 10 s under 40 V. On the other hand, Raja et al.[18] fabricated CNT:SMP composite actuators with an electrical conductivity of 10^{-2} S cm^{-1} by a melt mixing method, where the shape recovery time was 15 s under 40 V. The low performance of these electro-active SMPs is ascribed to the low electrical conductivity of the composites due to poor dispersibility of the conductive fillers in the SMP matrix.

Recently, we have successfully synthesized a novel conductive polymer, fully soluble self-doped poly(3,4-ethylenedioxythiophene) (S-PEDOT), with an electrical conductivity greater than 1000 S cm^{-1}.[19] Since the S-PEDOT can dissolve not only in water but in some organic solvents such as dimethyl sulfoxide (DMSO), formic acid (FA) and ethylene glycol (EG), composites with various polymers are available by a solution mixing method. This study deals with the fabrication of novel electro-active SMP using S-PEDOT and characterization of S-PEDOT:SMP composites by means of electron probe microanalyzer (EPMA), X-ray diffraction (XRD), atomic force microscope (AFM), dynamic mechanical analysis (DMA), and thermomechanical analysis (TMA). It was found that the electrical conductivity of the S-PEDOT:SMP composite with 10 wt% S-

PEDOT attained 29 S cm^{-1} and the electro-active SMP soft actuator was driven at lower driving voltage (6 V) with faster recovery response (5 s).

2.2 Experimental methodologies

2.2.1 Materials

A fully soluble self-doped poly(3,4-ethylenedioxythiophene) (S-PEDOT) water solution (1.3 wt%) was synthesized in our laboratory as previous reports.[19,20] A polyurethane-based shape memory polymer (SMP, MM-5520) with a nominal glass transition temperature (T_g) of 55ºC was purchased from the SMP Technologies Inc. The chemical formula of the SMP is shown in Fig. 2-1[21] inferred from the previous patents.[22,23] Dimethyl sulfoxide (DMSO) used as a solvent (Junsei Chemical) was used as received.

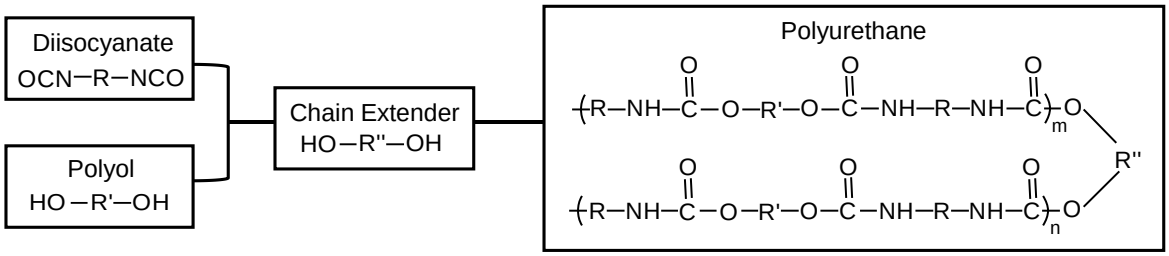

Figure 2-1 Synthetic rout of polyurethane-based SMP.

2.2.2 Fabrication of S-PEDOT:SMP composites

The S-PEDOT water solution was freeze dried using a freeze dryer (DC400, Yamato Scientific). The S-PEDOT powder and SMP pellets were dissolved in DMSO with concentrations of 1 and 10 wt%, respectively, and both solutions were mixed with different weight ratios of the S-PEDOT ($W_{S\text{-}PEDOT}$). After vigorous stirring, the mixed solution was drop cast and dried at 120°C on a glass slide or Teflon dish. Finally, the S-PEDOT:SMP composite films as electro-active SMPs were obtained by heating at 200°C for 1 h in vacuum to remove the residual solvent completely (Figure 2-2).

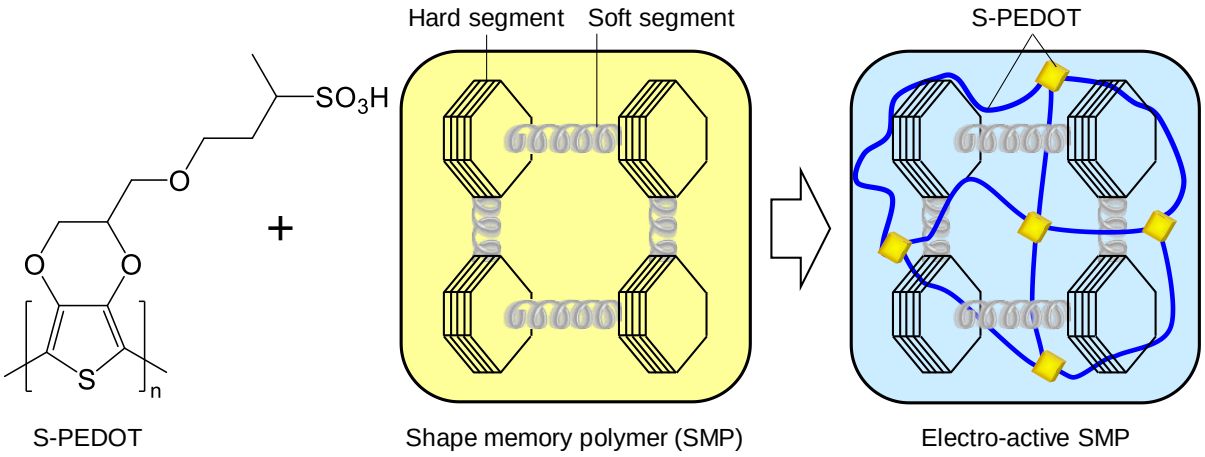

Figure 2-2 Schematic illustration of electro-active shape memory polymer (SMP) composing of S-PEDOT and SMP.

2.2.3 Characterization of S-PEDOT:SMP composites

The distribution of oxygen, nitrogen, and sulfur elements in the S-PEDOT:SMP composite films was characterized with an electron probe micro analyzer (EPMA) (JXA-8200, JEOL) at an accelerating voltage of 10 kV. The electrical conductivity was measured by van der Pauw method (HEM-2000, EGK), where at least five films were prepared and measured for each electrical conductivity. The volume fraction of the S-PEDOT in the composite film ($\phi_{S\text{-}PEDOT}$) was calculated using the densities of S-PEDOT ($d_{S\text{-}PEDOT}$ = 1.50 g cm^{-3}) and SMP (d_{SMP} = 1.23 g cm^{-3}) measured by Archimedes' principle at room temperature. Assuming that the values of $d_{S\text{-}PEDOT}$ and d_{SMP} are the same in the composite without cracks and voids, the $\phi_{S\text{-}PEDOT}$ (vol%) was calculated as follows.

$$\phi_{S\text{-}PEDOT} = W_{S\text{-}PEDOT} \times d_{S\text{-}PEDOT} / (W_{S\text{-}PEDOT} \times d_{S\text{-}PEDOT} + W_{SMP} \times d_{SMP}) \times 100 \quad (2\text{-}1)$$

The XRD patterns were measured by an X-ray diffractometer (MiniFlex600, Rigaku) at 40 kV and 15 mA, where crystallinity was evaluated by PDXL power diffraction software (Rigaku). The atomic force microscopic (AFM) images were obtained using a scanning probe microscope (SPM-9600, Shimadzu) in tapping mode. The dynamic mechanical analysis (DMA) of the S-PEDOT:SMP composite films (10 mm long, 2 mm wide, and ca. 150 μm thick) was carried out using TMA/SS6200 (Hitachi High-Tech) under a constant tension measured at a heating rate of 2°C min^{-1} and a frequency of 0.1 Hz. The differential scanning calorimetry (DSC) curves were measured with DSC 3100S (Netzsch) under a nitrogen flow from room temperature to 100°C at a heating rate of 5°C min^{-1}. The thermomechanical analysis (TMA) was performed with the

TMA/SS6200 (Hitachi High-Tech) using a tensile fixture at a force control mode. The EAP actuator properties of the S-PEDOT:SMP composite film were recorded with a video camera and infrared thermal imaging camera (TVS-500EX, Nippon Avionics) under application of a voltage. The recovery force generated in the actuator was measured with a small-capacity load cell (LTS-50GA, Kyowa).

2.3 Results and discussion

2.3.1 Miscibility and electrical properties

Figure 2-2 shows element mapping images of S-PEDOT:SMP composite film (cross section) measured by EPMA. It was found that sulfur, nitrogen, and oxygen originated from S-PEDOT, SMP, and both S-PEDOT and SMP, distributed homogeneously in the composite film. This clearly indicates the high miscibility between S-PEDOT and SMP achieved by the solution mixing method. The SEM and EMPA element mapping images of the film surface (Figure 2-3) also support homogeneous distribution of elements and smooth surface without aggregations at the microscopic level.

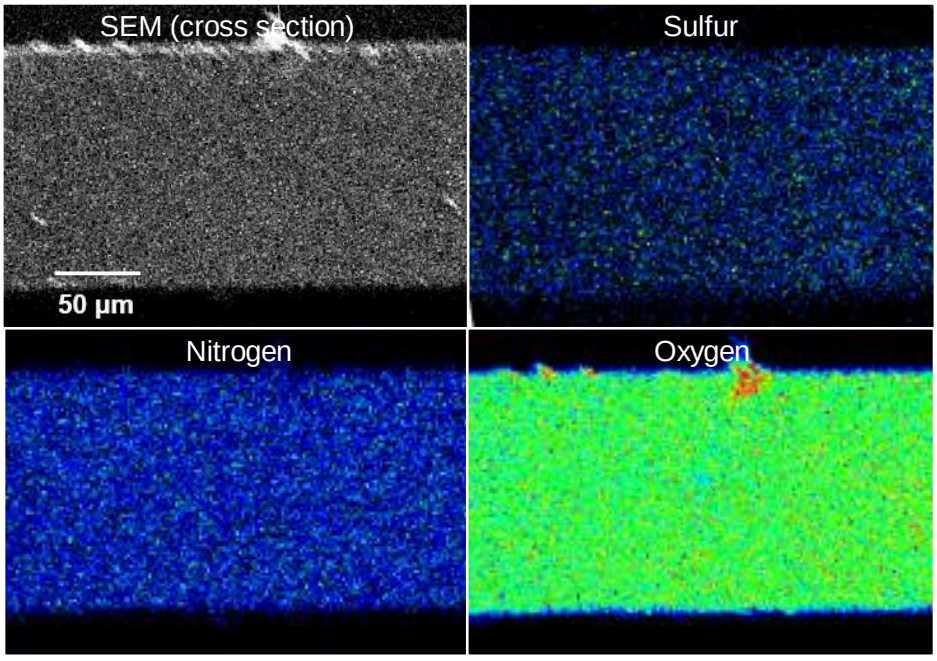

Figure 2-2 EPMA element mapping images of S-PEDOT:SMP composite film (cross section) at $W_{S\text{-}PEDOT}$ = 10 wt%.

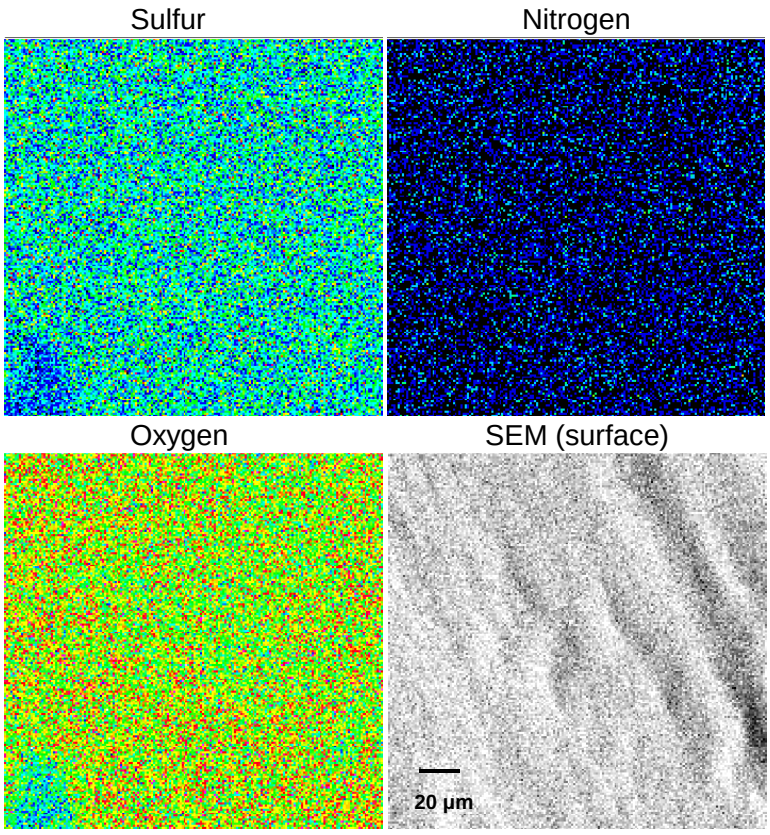

Figure 2-3 EMPA element mapping images of S-PEDOT:SMP composite film (surface) at $W_{S\text{-}PEDOT}$ = 10 wt%.

The electrical conductivity of the S-PEDOT:SMP composite films is shown in Figure 2-4. The electrical conductivity linearly increases with increasing the volume fraction of S-PEDOT ($\phi_{S\text{-}PEDOT}$) and attains 579 S cm^{-1} at $\phi_{S\text{-}PEDOT}$ = 100 vol%. The result shows a typical insulator-conductor transition usually described by the percolation theory[24] using the following equation,

$$\sigma = \sigma_0 (\phi - \phi_c)^t \quad (2\text{-}2)$$

where σ_0 is the proportionality constant related to the intrinsic conductivity of the conductive filler, ϕ is the volume fraction of the conductive filler, ϕ_c is the critical volume fraction of the filler at percolation threshold, and t is the critical exponent relating to the system dimensionality of electric composites. At $\phi < \phi_c$, no conducting pathways can be established because the average distance between conductive fillers is too large to transport charge carriers. Once the conductive pathway is formed at $\phi \geq \phi_c$, electric current can flow under electric field through the neighboring conductive fillers.[24] For the S-PEDOT:SMP composite films, the best fitting result highly agreed with the experimental data (the red line in Figure 2-4), where σ_0 = 576 S cm^{-1}, ϕ_c = 0.38 vol% and

t = 1.15, respectively. Compared to other conductive composites containing various conductive fillers such as CB, CNTs, and graphene listed in Table 1, the S-PEDOT:SMP composite films show extremely lower ϕ_c and higher σ values. This is associated with the higher electrical conductivity (σ_0 = 576 S cm^{-1}) and miscibility of the S-PEDOT. It is also noted that t = 1.15 is smaller than the theoretical values of three-dimensional (t = 2) and two-dimensional percolations (t = 1.33),[24] indicative of low-dimensional conductive pathways that will be discussed later.

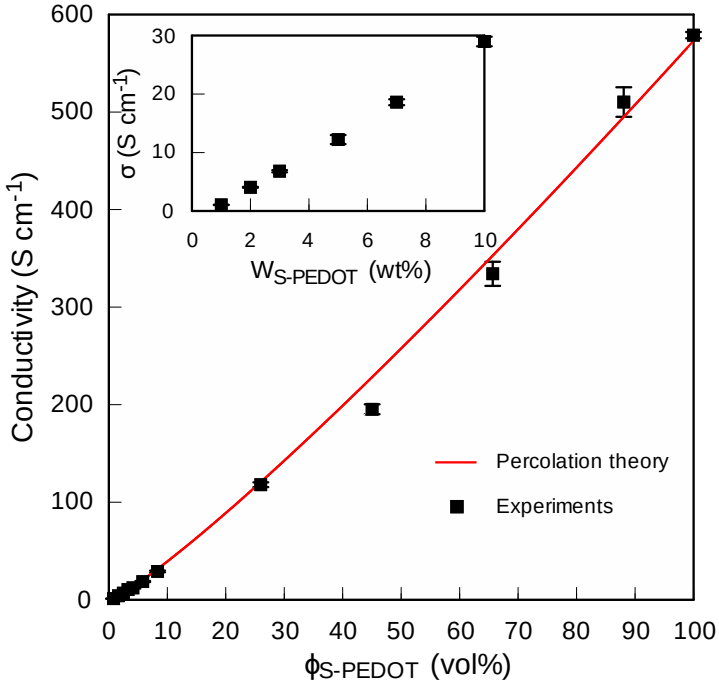

Figure 2-4 Relation between electrical conductivity (σ) and volume fraction of S-PEDOT ($\phi_{S\text{-}PEDOT}$) for S-PEDOT:SMP composite films. Inset: Relation between σ and $W_{S\text{-}PEDOT}$.

Table 1 Comparison of percolation parameters and electrical conductivity for various polymer composites with different conductive fillers.

Composites	Percolation threshold	σ_0 (S cm^{-1})	t	σ (S cm^{-1})	Conductive filler	Ref.
CB/SMP	3.8 vol%	0.1	2	~0.1	10 vol%	Leng et al.[25]
CB/HDPE	0.4 vol%	2.1×10^{-3}	1.4	$\sim10^{-3}$	~2 vol%	Yoon et al.[26]
CNTs/PS	1.5 wt%	-	-	10^{-2}	5.5 wt%	Loos et al.[27]
CNTs/PLA	0.5 wt%	-	-	~ 0.1	2 wt%	Villmow et al.[28]
Graphene/PS	1 wt%	-	-	0.15	2 wt%	Tkalya et al.[29]
PEDOT:PSS/PU	2.4 wt%	166	1.27	25	25 wt%	Wallace et al.[30]
PEDOT:PSS/PU	0.5 wt%	554	1.175	185	40 wt%	Li et al.[31]
PEDOT:PSS/PAAm	0.46 vol%	766	1.65	17	36 wt%	An et al.[32]
S-PEDOT:SMP	0.38 vol%	576	1.15	29	10 wt%	This work

2.3.2 Structure and morphology

In order to clarify the detailed structure of S-PEDOT:SMP composite films, an XRD measurement was carried out and the results are shown in Figure 2-5. The pure SMP ($W_{S\text{-}PEDOT}$ = 0 wt%) shows a broad diffraction around 2θ = 20°, indicating that the SMP is almost amorphous. On the other hand, the pure S-PEDOT ($W_{S\text{-}PEDOT}$ = 100 wt%) reveals peaks at 2θ = 5.0, 10.1 and 24.6°, corresponding to the diffractions from (100), (200), and (020) planes of the S-PEDOT crystallites, respectively.[19] Here, an increase of $W_{S\text{-}PEDOT}$ from 10 wt% to 70 wt% results in the decrease of the broad diffraction from amorphous SMP but an increase of the diffraction peaks from crystalline S-PEDOT at the same diffraction angles. This suggests that the S-PEDOT and SMP are phase separated with no significant interactions at the molecular level, in which the S-PEDOT forms crystalline structure in the amorphous SMP matrix. In fact, the crystallinity of the composite increases in proportion to the $W_{S\text{-}PEDOT}$ as shown in the inset of Figure 2-5.

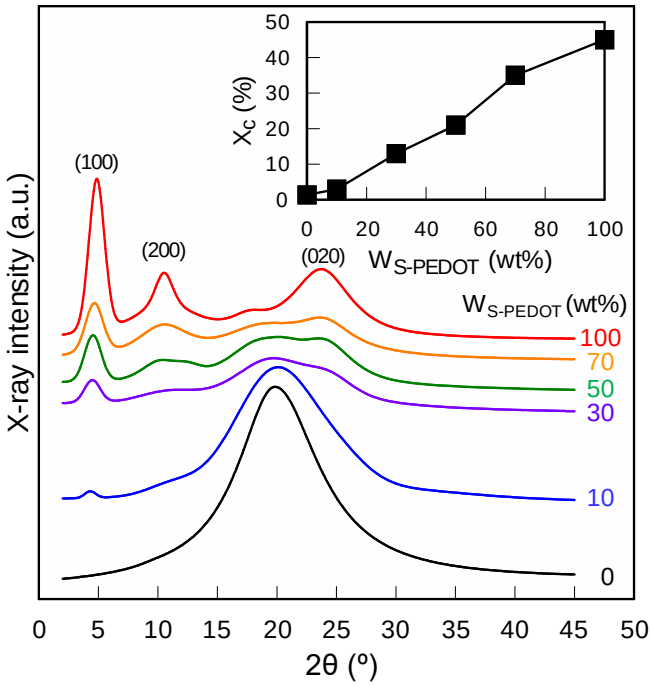

Figure 2-5 XRD patterns of S-PEDOT:SMP composite films with different $W_{S\text{-}PEDOT}$. Inset: Relation between crystallinity (X_c) of S-PEDOT:SMP composite films and $W_{S\text{-}PEDOT}$.

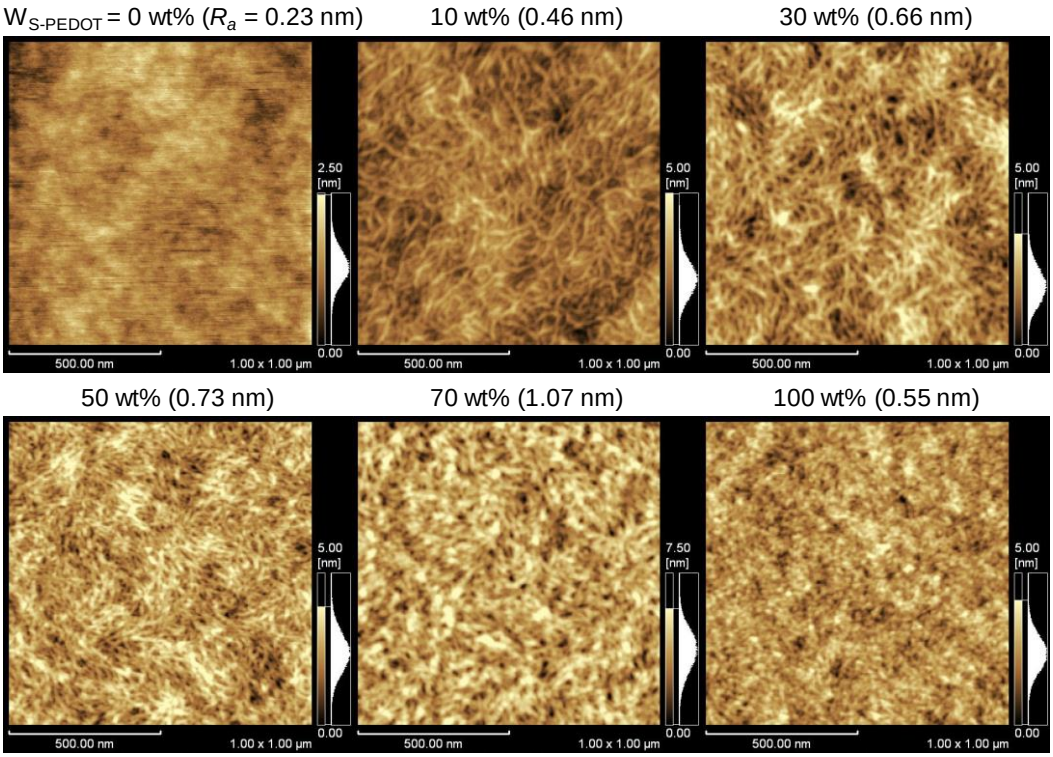

Figure 2-6 AFM surface morphology and surface roughness (R_a) of various S-PEDOT:SMP composite films with different $W_{S\text{-}PEDOT}$.

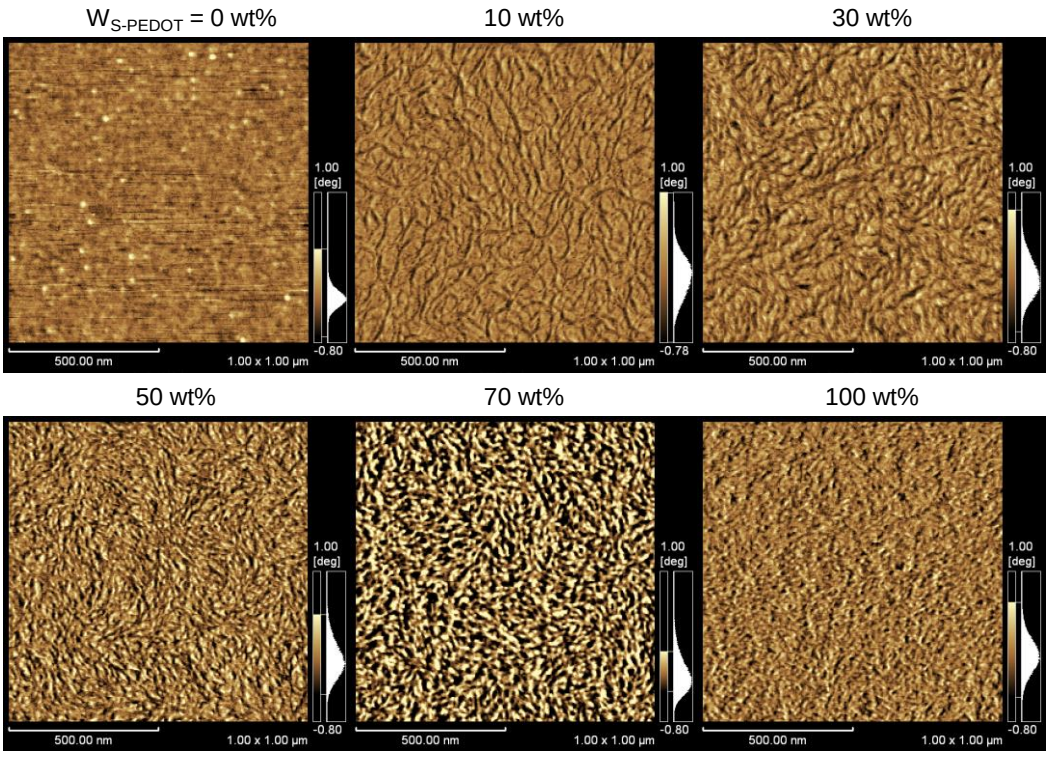

Figure 2-7 AFM phase images of various S-PEDOT:SMP composite films with different $W_{S\text{-}PEDOT}$.

For further analysis of phase separation, surface morphology of various S-PEDOT:SMP composite films was measured by AFM. It is seen from Figure 2-6 that the SMP shows a smooth surface with a small surface roughness (R_a) of 0.23 nm. Interestingly, the S-PEDOT:SMP composite films ($W_{S\text{-}PEDOT}$ = 10 ~ 70 wt%) show fibrils (average diameter is 17 nm) with higher R_a values (0.46~1.07 nm). Since the pure S-PEDOT shows low R_a (0.55 nm) and numerous small grains (average diameter is 16 nm) the fibrils in the S-PEDOT:SMP composites may correspond to the hard S-PEDOT molecular chains. The fact that the fibrils are harder than the matrices from phase images (Figure 2-7) suggests that the crystalline S-PEDOT forms conductive networks due to the phase separation in the SMP matrices, which will be responsible for the low-dimensional percolation mechanism as shown in Figure 2-4.

2.3.3 Shape memory characteristics

In general, thermally induced shape memory characteristics of the SMP consist of two processes as shown in Figure 2-8. One is the programing process where the SMP heated above T_g is deformed by an external force (strain changes from ε_0 to ε_1), and then cooled down below T_g to fix the temporary shape (strain relaxes from ε_1 to ε_2). The other is the recovery process where the heating

of the deformed SMP above the T_g will release the accumulated stress, which results in a recovery of the SMP from the temporary to its original shape (strain recovers from ε_2 to ε_3).[9,33] The fixing ratio and recovery ratio can be evaluated by ε_1, ε_2 and ε_3, respectively.

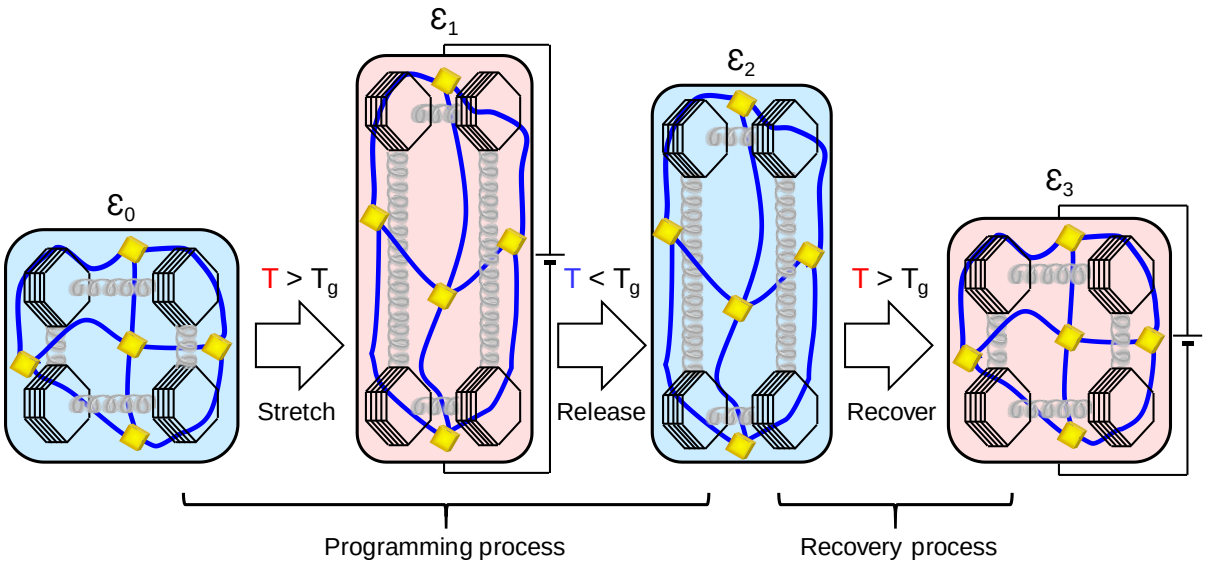

Figure 2-8 Schematic diagram of shape memory characteristics of S-PEDOT:SMP composite film.

In order to clarify the role and effect of S-PEDOT on shape memory characteristics of the SMP, dynamic mechanical analysis (DMA) was carried out to evaluate viscoelastic properties of the S-PEDOT:SMP composite films. It is seen from Figure 2-9 that the pure SMP ($W_{S\text{-}PEDOT}$ = 0 wt%) shows a steep drop of storage modulus and large tan δ peak at around 50°C, corresponding to T_g of the SMP, in which soft segments in the reversible phase of the segmented polyurethane block copolymer transfer from a glass to rubber state due to micro-Brownian motion while phase separated hard segments form hard domains by physical crosslinks through hydrogen bonding[9,34]. Interestingly, an increase of $W_{S\text{-}PEDOT}$ significantly decreases both the drop of the storage modulus and intensity of the tan δ peak whereas the T_g values are almost constant (Inset of Figure 2-9). A similar tendency was observed in the DSC measurements, where the peak of T_g around 50°C became smaller with increasing the $W_{S\text{-}PEDOT}$ and disappeared at $W_{S\text{-}PEDOT}$ = 100 wt% (Figure 2-10). This demonstrates that the shape memory characteristics of the SMP are destroyed by the S-PEDOT because of its hard and infusible nature.[19] Indeed, the shape memory characteristics of the S-PEDOT:SMP composite films disappear at $W_{S\text{-}PEDOT}$ > 30 wt%. Therefore, further investigation of the shape memory characteristics have been carried out for the S-PEDOT:SMP

composite films at $W_{S\text{-}PEDOT} \leq 30$ wt%.

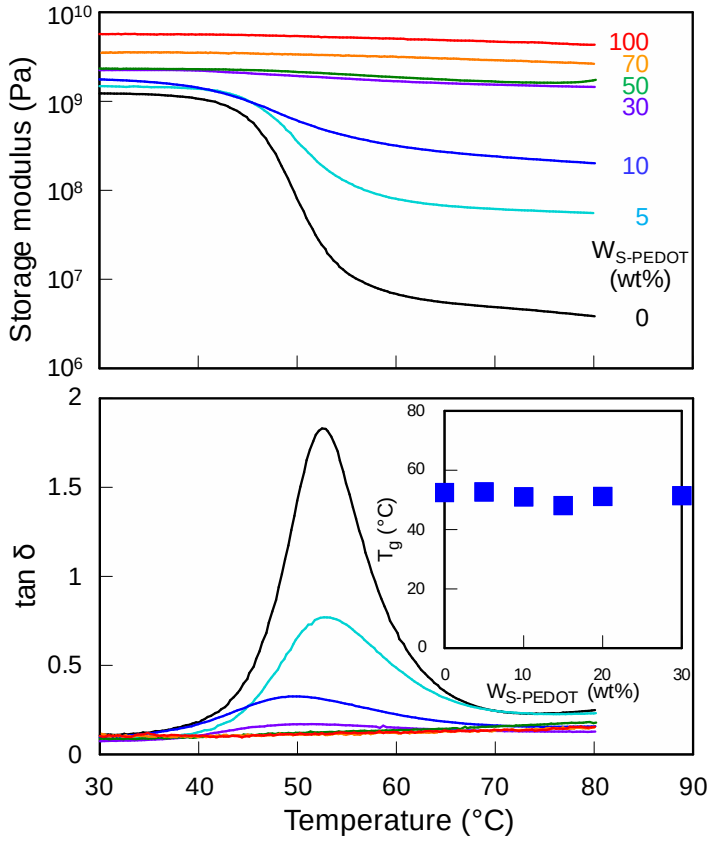

Figure 2-9 Temperature dependence of storage modulus and tan δ for various S-PEDOT:SMP composite films with different $W_{S\text{-}PEDOT}$. Inset: Relation between T_g of S-PEDOT:SMP composite films and $W_{S\text{-}PEDOT}$.

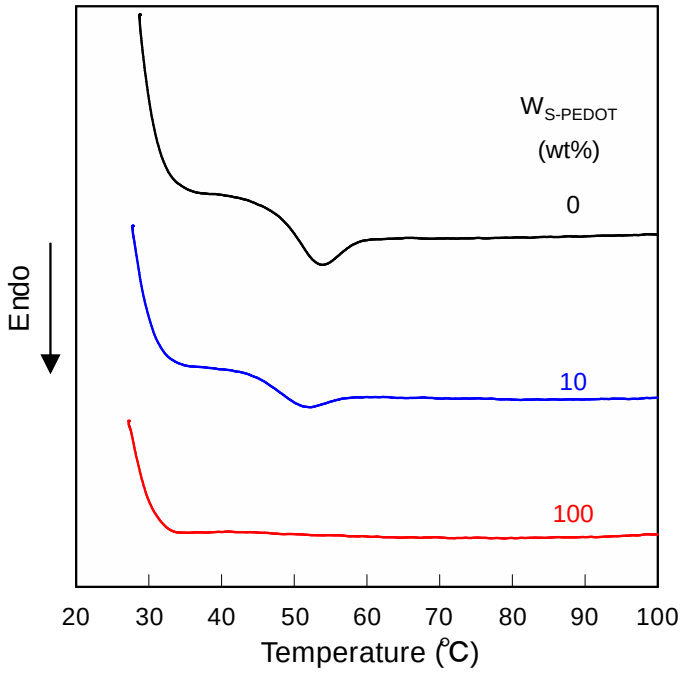

Figure 2-10 DSC thermograms of various S-PEDOT:SMP composite films with different $W_{S\text{-}PEDOT}$.

Figure 2-11 displays typical thermomechanical analysis (TMA) curves of the S-PEDOT:SMP composite film ($W_{S\text{-}PEDOT}$ = 10 wt%) for evaluating shape memory characteristics as explained in Figure 2-8. The composite film (10 mm long, 2 mm wide, and ca. 110 μm thick) was first heated to 70°C above T_g at a heating rate of 5°C min^{-1} and stretched under a constant force ca. 1.5 N, corresponding to 7 MPa, then cooled down to 30°C to fix the shape with a temporary strain of ε_1. After releasing the force, the composite film slightly relaxed with a fixed strain of ε_2. Finally, the composite film recovered from it temporary to the original shape with a recovery strain of ε_3 by heating again from 30°C to 70°C.

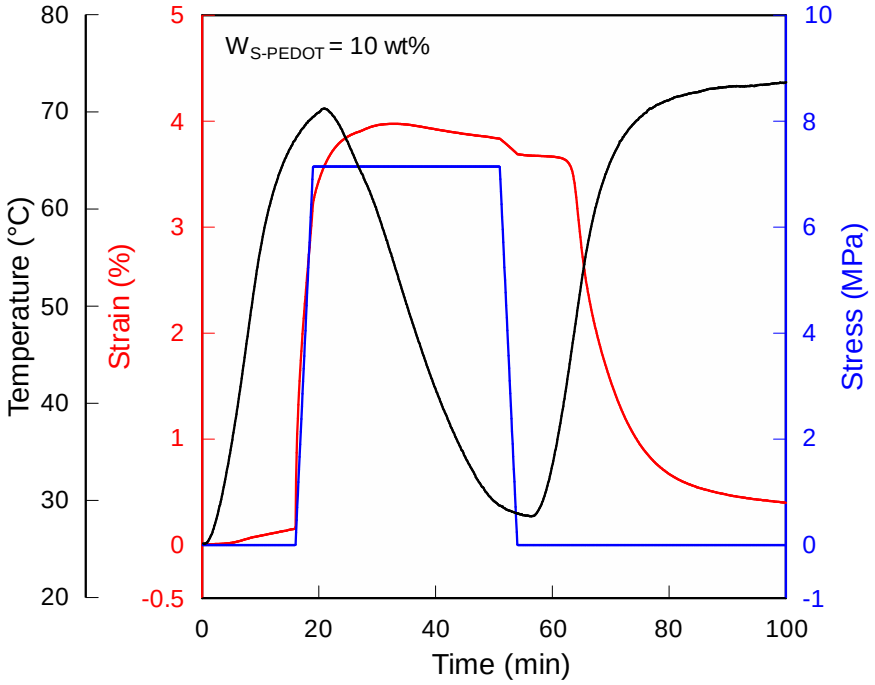

Figure 2-11 TMA curves of S-PEDOT:SMP composite film ($W_{S\text{-}PEDOT}$ = 10 wt%).

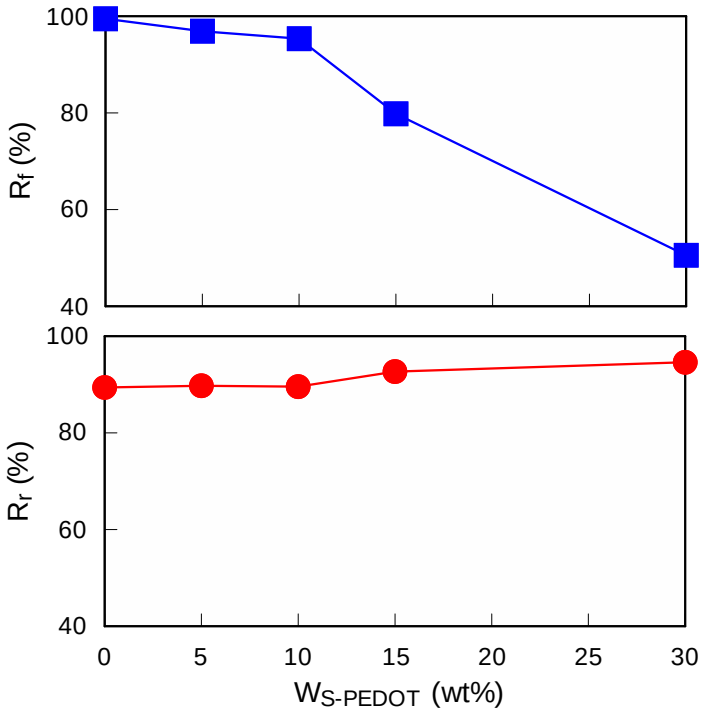

Figure 2-12 Changes in shape fixing ratio (R_f) and shape recovery ratio (R_r) of S-PEDOT:SMP composite films on $W_{S\text{-}PEDOT}$.

The shape fixing ratio (R_f) and shape recovery ratio (R_r) of the S-PEDOT:SMP composite films were calculated as follows

$$R_f\,(\%) = \varepsilon_2 / \varepsilon_1 \times 100 \quad (3)$$

$$R_r\,(\%) = (\varepsilon_2 - \varepsilon_3) / \varepsilon_2 \times 100 \quad (4)$$

where TMA curves of various S-PEDOT:SMP composite films with different $W_{S\text{-}PEDOT}$ are shown in Figure 2-13.

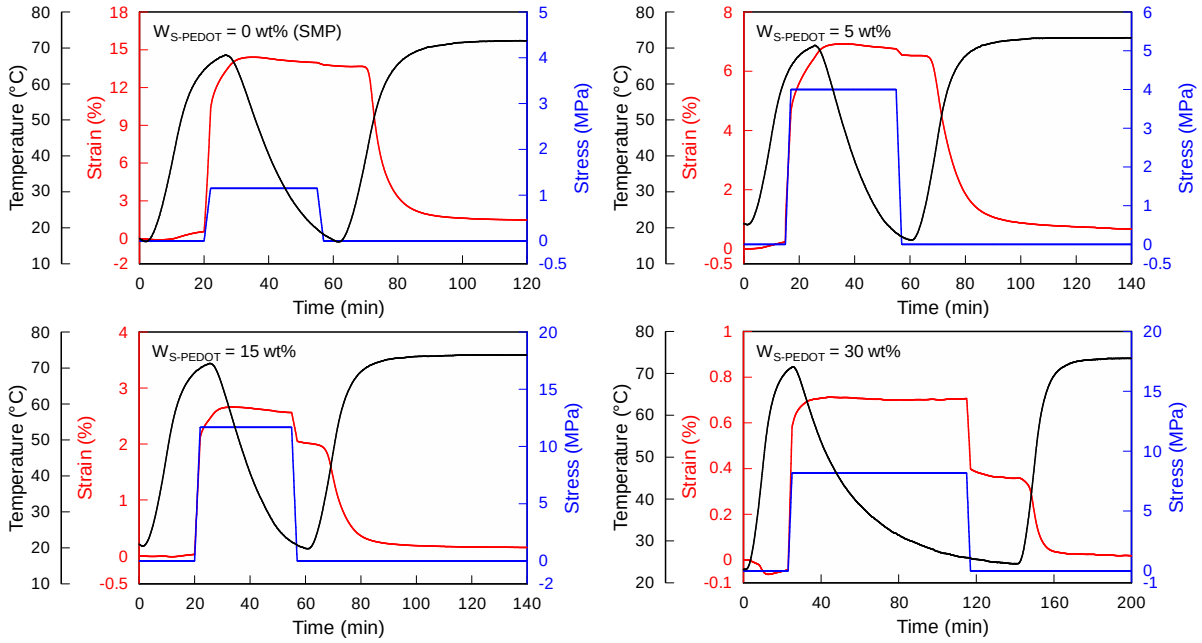

Figure 2-13 TMA curves of various S-PEDOT:SMP composite films with different $W_{S\text{-}PEDOT}$.

As shown in Figure 2-12, the values of R_f and R_r for pure SMP ($W_{S\text{-}PEDOT}$ = 0 wt%) were 100% and 90%, respectively. It was found that the increase of S-PEDOT resulted in a decrease of R_f (51% at $W_{S\text{-}PEDOT}$ = 30 wt%), while the R_r was kept almost constant (ca. 90% at $W_{S\text{-}PEDOT}$ = 0 ~ 30 wt%). These results indicate that the soft segments in the reversible phase of the SMP in the composite film play a predominant role in fixing the temporary shape. In contrast, physical crosslinks formed by hard segments of the SMP and/or network structure formed by S-PEDOT fibrils (in Figure 2-6) are crucially important for the recovery from the temporary to original shape. Furthermore, cycle test clearly demonstrates high reproducibility of TMA curves and constant values of R_f and R_r during four cycles (Figure 2-14). Based on the electrical conductivity and shape memory characteristics, the S-PEDOT:SMP composite film at $W_{S\text{-}PEDOT}$ = 10 wt%, exhibiting σ = 29 S cm^{-1}, R_f = 95.4%, and R_r = 90.1%, was determined to be the optimal, which has superior

performance compared with other composites such as CB:SMP composite (σ = 0.03 S cm^{-1}, R_f = 89.6%, and R_r = 85.9%),[35] CNT:SMP composites (σ = 0.2 S cm^{-1}, R_f = ~95%, and R_r = 85%)[36] and (σ = 0.1 S cm^{-1}, R_f = 91.7%, and R_r = 86.5%).[37]

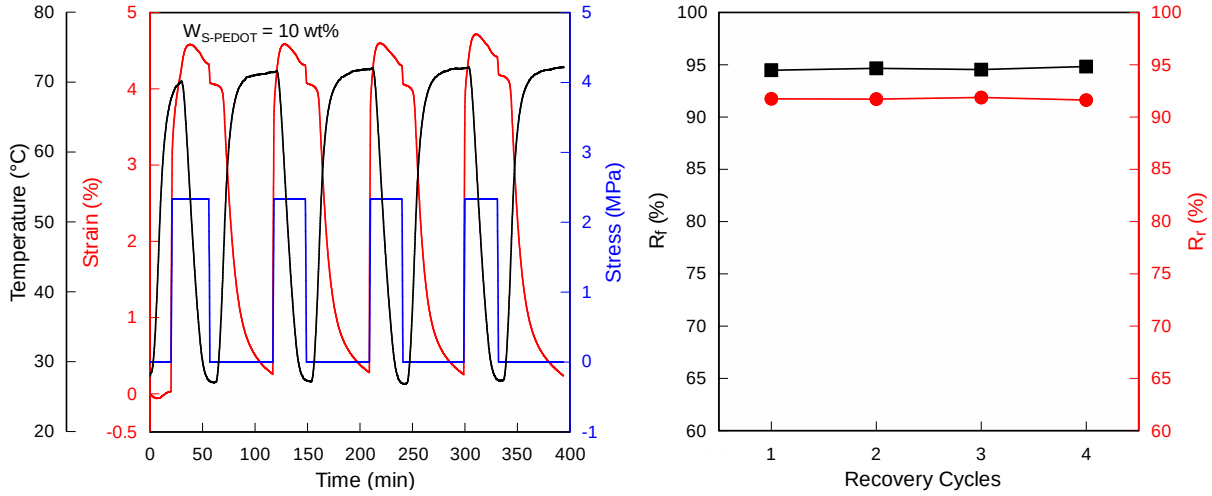

Figure 2-14 Cycle test of TMA measurement for S-PEDOT:SMP composite film ($W_{S\text{-}PEDOT}$ = 10 wt%).

2.3.4 Electro-active SMP soft actuator

The mechanism of the electro-active SMP composite is similar to the thermo-responsive SMP, where the temperature rise is caused by Joule heating. It is seen from Figure 2-15, an electro-active SMP soft actuator was fabricated by cutting the S-PEDOT:SMP composite film ($W_{S\text{-}PEDOT}$ = 10 wt%, 175 µm thick) into a U-shape. The actuator was wound around a small cylinder (10 mm in diameter), with a bending angle (θ) of 11°, and then cooled down to room temperature to fix the bent shape (programming process). Upon application of 6 V through both ends with a DC power source, the electro-active SMP soft actuator quickly recovered from temporary bent shape (θ = 11°) to its original open shape (θ = 161°) within 5 s. Furthermore, time profiles of bending angle, maximum surface temperature, and thermographic images are shown in Figure 2-16. One can see that the maximum surface temperature linearly rises from 28°C to 92°C within 7 s, which can be associated with a large electric current (142 mA) due to the high electrical conductivity and small specific heat of the S-PEDOT:SMP composite film. It should be noted here, the electro-active SMP soft actuator was suddenly driven at 2 s after application of voltage because the maximum surface temperature exceeded the T_g of the composite (~50°C), and almost finished after 5 s. The recovery response and driving voltage of the S-PEDOT:SMP composite films are superior to other electro-

active SMP soft actuators such as MWCNT:SMP (10 s at 40 V)[16] and CNT:SMP (15 s at 40 V).[18] In the bent state, the soft actuator (175 μm thick) rapidly generates a recovery force of 21 mN, corresponding to 2.2 gf, subsequently drops to ca. 7 mN because the actuator becomes soft above the T_g by the Joule heating (Figure 2-17). After voltage removal, no recovery force was seen since the actuator became hard below the T_g. Here, the maximum recovery force increases in proportion to the film thickness and the value attains 45 mN at 305 μm, which is possibly due to the increase of cross section and/or strain difference on both sides of the film.

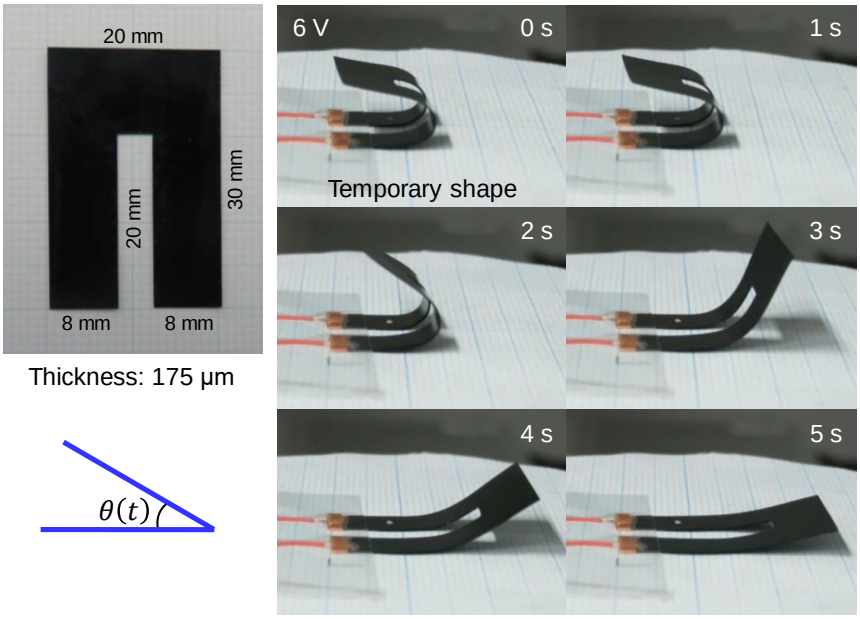

Figure 2-15 Photograph and time profiles of electro-active SMP soft actuator in action under 6 V.

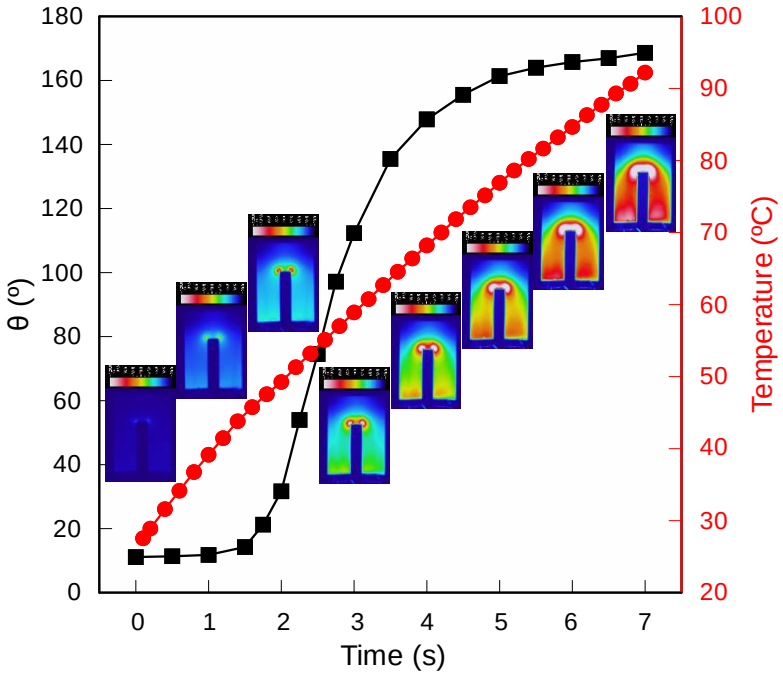

Figure 2-16 Time profiles of bending angle (θ), maximum surface temperature, and thermographic images of electro-active SMP soft actuator driven by 6 V.

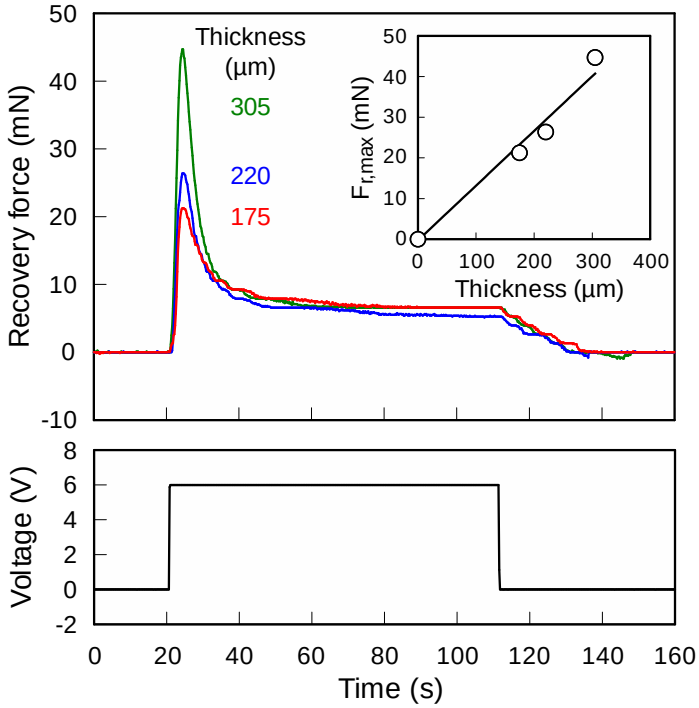

Figure 2-17 Time profiles of recovery force generated in the S-PEDOT:SMP composite actuators ($W_{S\text{-}PEDOT}$ = 10 wt%) with different thicknesses measured at 6 V. Inset: Relation between thickness and maximum recovery force ($F_{r,max}$).

2.4 Conclusion

In conclusion, we fabricated highly conductive S-PEDOT:SMP composite films by the facile solution mixing method of SMP and S-PEDOT in DMSO. The XRD and AFM analyses showed that the crystalline S-PEDOT formed conductive networks in the SMP matrices due to the phase separation, leading to the extremely low ϕ_c (0.38 vol%) and high electrical conductivity (29 S cm^{-1} at $W_{S\text{-}PEDOT}$ = 10 wt%). The DMA measurement revealed that the T_g of the S-PEDOT:SMP composite films was ~50°C at $W_{S\text{-}PEDOT} \leq 30$ wt%. It should be noted that the electro-active SMP soft actuator made of S-PEDOT:SMP composite film ($W_{S\text{-}PEDOT}$ = 10 wt%), with excellent shape memory properties of R_f = 95.4% and R_r = 90.1%, quickly recovered from temporary bent shape to its original open shape within 5 s under 6 V driven by the Joule heating.

2.5 References

1) Y. Osada, H. Okuzaki and H. Hori, A polymer gel with electrically driven motility. Nature. **355**, 242, 1992.
2) E. Smela, O. Inganäs, and I. Lundström, Controlled folding of micrometer-size structures. Science. **268**, 1735, 1995.
3) K. Asaka, H. Okuzaki, *Soft Actuators-Materials, Modeling, Applications, and Future Perspectives* (Springer, Berlin, 2019) 2nd ed., p. 245.
4) M. Shahinpoor, Ionic Polymer Metal Composites (IPMCs): Smart Multi-Functional Materials and Artificial Muscles (Vol. 1) (Royal Society of Chemistry, London, 2015).
5) C. Jo, D. Pugal, I. K. Oh, K. J. Kim, and K. Asaka, Recent advances in ionic polymer-metal composite actuators and their modeling and applications. Prog. Polym. Sci. **38**, 1037, 2013.
6) H. Okuzaki, T. Kuwabara, K. Funasaka, and T. Saido, Humidity-sensitive polypyrrole films for electro‐active polymer actuators. Adv. Funct. Mater. **23**, 4400, 2013.
7) R. H. Baughman, L. W. Shacklette, R. L. Elsenbaumer, E. Plichta, and C. Becht, *Conducting polymer electromechanical actuators.* (Springer, Dordrecht, 1990), p. 559.
8) H. Okuzaki, H. Suzuki, and T. Ito, Electromechanical properties of poly (3,4-ethylenedioxythiophene)/poly (4-styrene sulfonate) films. J. Phys. Chem. B. **113**, 11378, 2009.
9) A. Lendlein, and S. Kelch, Shape-memory polymers. Angew. Chem. Int. Ed. **41**, 2034, 2002.

10) J. Hu, Y. Zhu, H. Huang, and J. Lu, Recent advances in shape-memory polymers: Structure, mechanism, functionality, modeling and applications. Prog. Polym. Sci. **37**, 1720, 2012.
11) Q. Zhao, H. Qi, and T. Xie, Recent progress in shape memory polymer: New behavior, enabling materials, and mechanistic understanding. Prog. Polym. Sci. **49**, 79, 2015.
12) T. Xie, Recent advances in polymer shape memory. Polymer. 52, 4985, 2011.
13) J. Leng, X. Lan, Y. Liu, and S. Du, Shape-memory polymers and their composites: stimulus methods and applications. Prog. Mater. Sci. 56, 1077, 2011.
14) W. Wang, Y. Liu and J. Leng, Recent developments in shape memory polymer nanocomposites: Actuation methods and mechanisms. Coord. Chem. Rev. **320**, 38, 2016.
15) J. Leng, X. Lan, Y. Liu, and S. Du, Electroactive thermoset shape memory polymer nanocomposite filled with nanocarbon powders. Smart Mater. Struct. **18**, 074003, 2009.
16) J. W. Cho, J. W. Kim, Y. C. Jung, and N. S. Goo, Electroactive shape-memory polyurethane composites incorporating carbon nanotubes. Macromol. Rapid Commun. **26**, 412, 2005.
17) J. T. Kim, H. J. Jeong, H. C. Park, H. M. Jeong, S. Y. Bae, and B. K. Kim, Electroactive shape memory performance of polyurethane/graphene nanocomposites. React. Funct. Polym. **88**, 1, 2015.
18) M. Raja, S. H. Ryu, and A. M. Shanmugharaj, Thermal, mechanical and electroactive shape memory properties of polyurethane (PU)/poly (lactic acid)(PLA)/CNT nanocomposites. Eur. Polym. J. **49**, 3492, 2013.
19) H. Yano, K. Kudo, K. Marumo, and H. Okuzaki, Fully soluble self-doped poly (3,4-ethylenedioxythiophene) with an electrical conductivity greater than 1000 S cm^{-1}. Sci. Adv. **5**, eaav9492, 2019.
20) H. Yano, M. Nishiyama, S. Hayashi, K. Kudo, and H. Okuzaki, Synthesis and Characterization of a Novel Self-Doped Water-Soluble Conducting Polymer. Kobunshi Ronbunshu, **75**, 607, 2018.
21) Homepage of SMP Technologies Inc.: [http://www.smptechno.com/index_en.html].
22) S. Hayashi and H. Fujimura, Shape memory polymer foam. U.S. Patent 5049591 (1991).
23) S. Hayashi, Shape memory polyurethane elastomer molded article. U.S. Patent 5145935, 1992.
24) D. Stauffer, and A. Aharony, *Introduction to Percolation Theory* (CRS Press, Boca Raton, FL, 1994) 2nd ed.

25) J. Leng, X. Lan, Y. Liu, and S. Du, Electroactive thermoset shape memory polymer nanocomposite filled with nanocarbon powders. Smart Mater. Struct. **18**, 074003, 2009.

26) H. Yoon, K. Kwon, K. Nagata, and K. Takahashi, Changing the percolation threshold of a carbon black/polymer composite by a coupling treatment of the black. Carbon. **42**, 1877, 2004.

27) J. Yu, K. Lu, E. Sourty, N. Grossiord, C. Koning, and J. Loos, Characterization of conductive multiwall carbon nanotube/polystyrene composites prepared by latex technology. Carbon. **45**, 2897, 2007.

28) T. Villmow, P. Pötschke, S. Pegel, L. Häussler, and B. Kretzschmar, Influence of twin-screw extrusion conditions on the dispersion of multi-walled carbon nanotubes in a poly (lactic acid) matrix. Polymer, 49, 3500, 2008.

29) E. Tkalya, M. Ghislandi, A. Alekseev, C. Koning, and J. Loos, Latex-based concept for the preparation of graphene-based polymer nanocomposites. J. Mater. Chem. **20**, 3035, 2010.

30) M. Seyedin, J. Razal, P. Innis, and G. Wallace, Strain-responsive polyurethane/PEDOT: PSS elastomeric composite Fibers with high electrical conductivity. Adv. Funct. Mater. **24**, 2957, 2014.

31) P. Li, D. Du, L. Guo, Y. Guo, and J. Ouyang, Stretchable and conductive polymer films for high-performance electromagnetic interference shielding. J. Mater. Chem. C. **4**, 6525, 2016.

32) Y. An, K. Iwashita, and H. Okuzaki, Electromechanical properties and structure of stretchable and highly conductive polymer hydrogels. Multifunct. Mater. **2**, 014001, 2018.

33) B. Dietsch, and T. Tong, A review-features and benefits of shape memory polymers (SMPs). J Adv Mater, **39**, 3, 2007.

34) B. Lee, B. Chun, Y. Chung, K. Sul, and J. Cho, Structure and thermomechanical properties of polyurethane block copolymers with shape memory effect. Macromolecules, **34**, 6431, 2001.

35) X. Qi, H. Xiu, Y. Wei, Y. Zhou, Y. Guo, R. Huang, H. Bai, and Q. Fu, Enhanced shape memory property of polylactide/thermoplastic poly(ether)urethane composites via carbon black self-networking induced co-continuous structure. Compos. Sci. Technol. **139**, 8, 2017.

36) T. Liu, R. Huang, X. Qi, P. Dong, and Q. Fu, Facile preparation of rapidly electro-active shape memory thermoplastic polyurethane/polylactide blends via phase morphology control and incorporation of conductive fillers. Polymer, **114**, 28, 2017.

37) Z. Wang, J. Zhao, M. Chen, M. Yang, L. Tang, Z. M. Dang, and X. Dong, Dually actuated triple shape memory polymers of cross-linked polycyclooctene-carbon nanotube/polyethylene nanocomposites. Appl. Mater. Interfaces. **6**, 20051, 2014.

Chapter 3 Novel Wearable High Sensitivity Acceleration and Non-Powered Displacement Sensors Based on Piezoionic Effect

3.1 Introduction

Internet of Things (IoT) is a system that connects between people and things, and between things through the Internet such as health monitoring using heart rate sensors[1)], remote control of appliances using wearable devices[2)], gait measurement using sole sensors[3)] and so on, has widely application in the areas of soft robotics, biomedical devices and wearable electronics. Flexible sensors which can detect motions as displacement, acceleration, velocity as well as vibration, play the dominant role in the field of IoT. Recently, with the rapid development of IoT has substantially increased wearable electronics demands, especially the requirement of flexible and wearable sensors. Many flexible and stretchable sensors have been developed to detecting human motions and monitoring personal health. In general, the flexible sensors can be categorized into two types, one is resistive sensor, and the other is capacitive one[4)]. The resistive sensor detects changes in resistance of conductors such as metal wires[5,6)], carbon nanotubes[7,8)] and graphene[9)]. However, electric power consumption is relatively high because electric current always flows through the conductor. On the other hand, the capacitive sensor detects changes in capacitance of a dielectric such as silicones[10,11,12)], and polyurethanes[13,14)]. But difficult to distinguish the direction of deformation, which is not suitable for a motion sensor. In order to monitor the motions, acceleration and displacement are the most important parameters in the characterization of an object's movement. Usually, the sensors which can detect acceleration and displacement are based on force sensing mechanisms has been widely applied in navigation[15)], industrial engineering[16)] and robots[17,18)]. In the view of energy consumption and precise determine the displacement and acceleration motions, piezoresistive strain sensors, piezoelectric[19,20)], triboelectric[21)] sensors and capacitive sensors are not suitable to use as motion sensors.

Ionic polymer gel is a material that exhibits electric response (such as voltage and current) under mechanical stimulate, due to the migration and redistribution of ions inside the gel matrix, so called piezoionic effect. For the piezoionic effect sensors, Kamamichi[22] et al. found that a bucky gel cantilever showed a voltage less than 0.1 mV even under a large bending displacement. Must[23)]

et al. reported a maximum voltage of about 0.37 mV for a carbon-polymer-ionic liquid composites. Wu[24] et al. fabricated a polypyrrole based ionic polymer sensor that the generated voltage was about 0.1 mV under a 4 mm deformation. Recently, Woehling[25] et al. presented a PEDOT/IPN-EMI^+TFSI^-/PEDOT trilayer sensor which the output voltage was 0.35 mV under the strain difference of 2 %. The lower generated voltage and sensitivity limited the application of those piezoionic sensors to motion sensors.

In this research, a multi-functional wearable ionic polymer sensor was fabricated using ionic liquid of EMI^+TFSI^- and shape memory polymer, PEDOT:PSS was used as flexible electrodes. The sensing performance of the piezoionic sensors was characterized in the term of generated voltages and charges under mechanical stimulates of various displacements and various accelerations. This study deals with the fabrication of multi-functional IL-SMP/PEDOT:PSS sensors and characterization of IL-SMP gels by means of AC impedance, electron probe microanalyzer (EPMA), dynamic mechanical analysis (DMA), and mechanical analysis (TMA). It was found that the IL-SMP/PEDOT:PSS composite exhibits larger acceleration sensitivity as 8.6 nA m^{-1} s^2 at W_{IL} = 30 wt%, while highest displacement sensitivity as 1.25 V m^{-1} at W_{IL} = 25 wt%. The mechanism of the piezoionce ionic SMP/PEDOT:PSS sensor can be explained by the migration and redistribution of ions under mechanical stimulation. Furthermore, the shape memory properties of the ionic SMP gels also was investigated, it was found that the ionic SMP with 10 wt% of IL exhibits good shape memory properties, as R_f = 86.9 %, R_r = 89.8 %.

3.2 Experimental section

3.2.1 Materials

A polyurethane-based shape memory polymer (SMP, MM-5520) with a nominal glass transition temperature (T_g) of 55ºC was purchased from the SMP Technologies Inc. The chemical formula of the SMP is shown in Fig. 3-1[26], inferred from the previous patents[27,28]. 1-ethyl-3-methylimidazolium bis(trifluoromethylsulfonyl)imide (EMI^+TFSI^-) purchased from Kanto Chemical Industry was used as ionic liquid (IL). N,N-dimethylacetamide (DMAc) was purchased from Kanto Chemical Co. Inc. PEDOT:PSS water dispersion (pH = 1.77) with 1.3 wt% solid content was synthesized in our laboratory by oxidative polymerization of EDOT (Aldrich) monomer in the presence of PSS (M_w = 75,000 g mol^{-1}) as the previous report[29]. Ethylene glycol (EG, Kanto Chemical) as a secondary dopant to improve the electrical conductivity of the

PEDOT:PSS was used as received. Ammonia solution (1 M, Kanto Kagaku) was used as neutralizer.

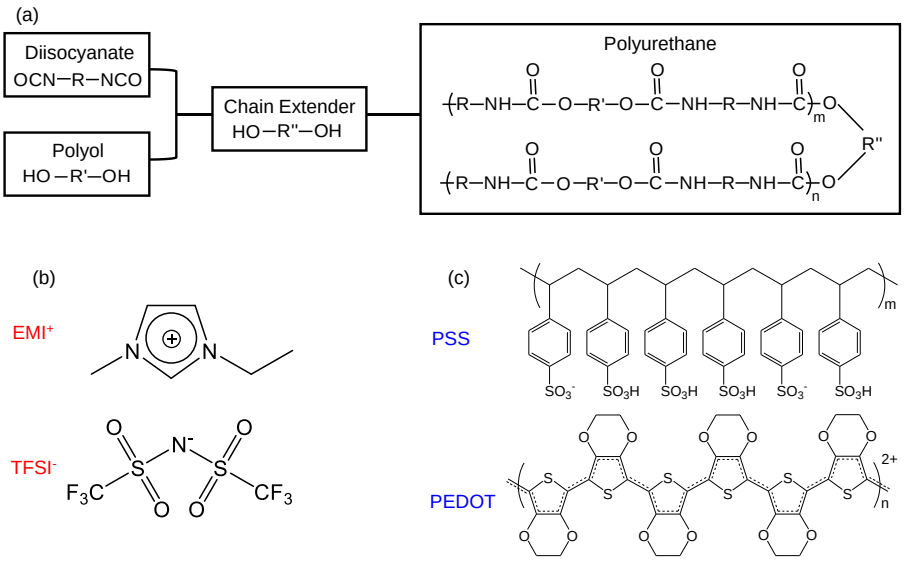

Figure 3-1 Synthetic rout of polyurethane-based SMP (a), Chemical structures of $EMI^{+}TFSI^{-}$ (b) and PEDOT:PSS (c).

3.2.2 Fabrication of the IL-SMP/PEDOT:PSS flexible sensor

SMP pellets were dissolved in DMAc with concentration of 10 wt%. Ionic liquid and SMP/DMAc solution were mixed together at different proportions, with IL content varying from 0 to 30 wt%. After vigorous stirring, the mixed solution was drop cast and dried at a Teflon dish for 2 days, using an oven set at 50ºC. Then the SMP-IL gel was dried at 140°C in vacuum for 2 hours. After the solvent was evaporated completely, the SMP-IL gel was peeled off from the Teflon dish. The SMP-IL gels with various thickness can be obtained by casting different volumes of composite solution on Teflon dish. The pristine PEDOT:PSS aqueous dispersion was strong acid dispersion with pH of 1.77. After the PEDOT:PSS dispersion was spin coated on the SMP-IL gel, the interface would be damaged due to the strong acid dispersion. Furthermore, the stability and the sensing performance of the sensors will be reduced. In this study, the PEDOT:PSS dispersion was neutralized by 1 M of ammonia solution, to obtain the dispersion with pH of 7. The pH value was measured using a pH meter (F-50, HORIBA). After that the PEDOT:PSS dispersion (pH = 7) was freeze dried with a freeze dryer (DC 400, Yamato, Japan). The PEDOT:PSS pellets were re-dispersed in deionized water, making up a dispersion with 2.5 wt% of solid content. Furthermore, 10 wt% of EG was added into the dispersion as a secondary dopant to improve the conductivity of

PEDOT:PSS electrodes. After vigorous stirring, PEDOT:PSS electrodes were deposited on SMP-IL gels by spin coating of the dispersion using a spin coater (MS-A150, Mikasa). Spin-coatings were applied at a rotational speed of 1000 rpm for 60 s under atmospheric conditions. After spin-coating, films were dried at 120ºC for 30 min with a moisture analyzer (MOC-120H, Shimadzu). Both surfaces of the SMP-IL gel were coated by PEDOT:PSS electrodes. At last, the sandwich IL-SMP/PEDOT:PSS strips were trimmed to a rectangular shape of 15 mm × 5 mm with a blade. Fig. 3-2 demonstrates the fabrication of the ionic SMP/PEDOT:PSS composites.

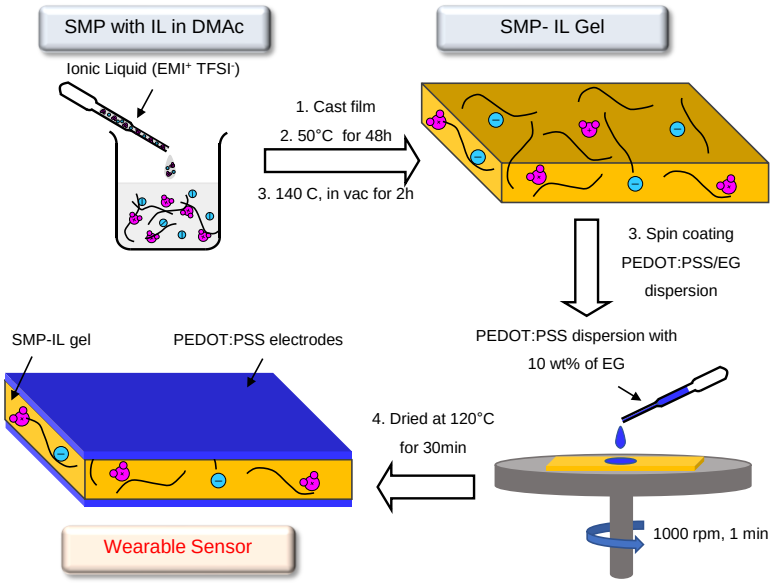

Figure 3-2 Fabrication of IL-SMP/PEDOT:PSS sensors.

3.2.3 Characterization of ionic SMP gel

The distribution of oxygen, nitrogen, and sulfur elements in the ionic SMP gel was observed with an electron probe microanalyzer (EPMA) (JXA-8200, JEOL) at an accelerating voltage of 10 kV. The electrical properties of the dish-like SMP-IL gels (300 μm thick and 10 mm in diameter) were measured at 0.1-10^6 Hz by an AC impedance technique with a frequency response analyzer (1255WB, Solartron) equipped with a sample holder (SH 1-Z, Toyo). The analyses of Cole-Cole plots and equivalent circuits were carried out using a ZView (Solartron) software. The dynamic mechanical analysis (DMA) of the ionic SMP gels (10 mm long, 2 mm wide, and ca. 300 μm thick) was carried out using TMA/SS6200 (Hitachi High-Tech) under a constant tension measured from 5 to 80°C at a heating rate of 2°C min^{-1} and a frequency of 0.1 Hz. The cyclic voltammograms

were measured in a sweeping range of 0 - 1 V and sweeping rate of 10 mV s^{-1}, with electrochemical impedance system (1255WB, Solartron). Furthermore, the capacitance was evaluated by CorrView software (Solartron).

3.2.4 Sensing characterization of ionic SMP sensor

The sensing performance of the flexible sensors was evaluated by generated voltage and electric charge under bending deformation. The bending deformation which was caused by mechanical perturbation was introduced by a tensile tester (EZ-TEST, Shimadzu) in compression mode at various displacements (3, 5 and 7 mm) and velocity (50, 100 and 200 mm min^{-1}). The acceleration of the mechanical stimulation was measured by an acceleration sensor (AS-1GB, KYOWA). The mechanical induced output signals included of electric charges and voltages were collected by the analyzer units (NR-500, NR-CA04 and NR-HA08, Keyence). Fig. 3-3a and b demonstrate the sensor at initial and bending states. The sensor strip was located on a sample holder. One end of the strip was fixed on the sample holder with two gold electrodes to allow independent electric contacts with the PEDOT:PSS electrodes. The free length of the strip was set at 10 mm. The displacement of the mechanical stimulation is corresponded to the strain difference between the electrodes, while the velocity is expressed as the acceleration of the mechanical stimulation. After the sensor strip was bended, the generated strain difference (ε) between the electrodes can be calculated by the equation:[25)]

$$\varepsilon = \frac{2d\delta}{L^2+\delta^2} \times 100\% \quad (3\text{-}1)$$

where d (300 μm) is the thickness of the ionic SMP gel, L (10 mm) is the free length of the sensor, δ is the displacement of the bending deformation, respectively. The strain difference of the sensor strip at various bending displacement is shown in Fig. 3-3c. On the other hand, the velocity of the mechanical stimulation is correlated to the acceleration. As shown in Fig. 3-3d, the acceleration increases linearly with the velocity.

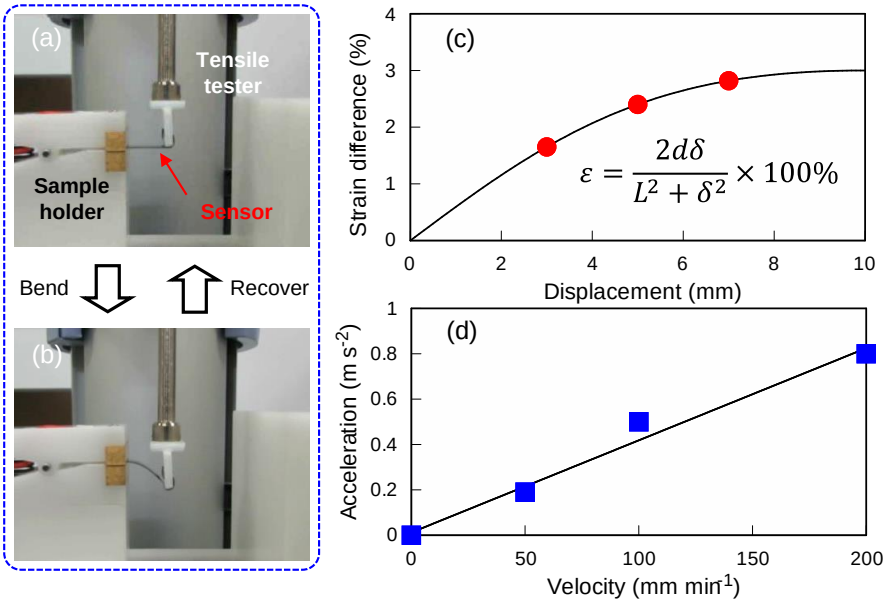

Figure 3-3. Experimental setup of the bending mechanical stimulation for sensor characterization (a, b). The generated strain difference of the sensors at different bending displacements (c). The relationship between bending velocity and acceleration of the mechanical stimulation (d).

3.3 Results and Discussion

3.3.1 Miscibility and ionic conductivity of SMP-IL Gels

Fig. 3-4a illustrates the ionic SMP gels composing of EMI^+TFSI^- and SMP, while Fig. 3-4b shows element mapping images of the ionic SMP gel (W_{IL} = 30 wt%, cross section) measured by EPMA. It was found that sulfur, nitrogen, and oxygen originated from EMI^+TFSI^-, both SMP and EMI^+TFSI^-, distributed homogeneously in the ionic SMP gel. This clearly indicates the good miscibility between EMI^+TFSI^- and SMP.

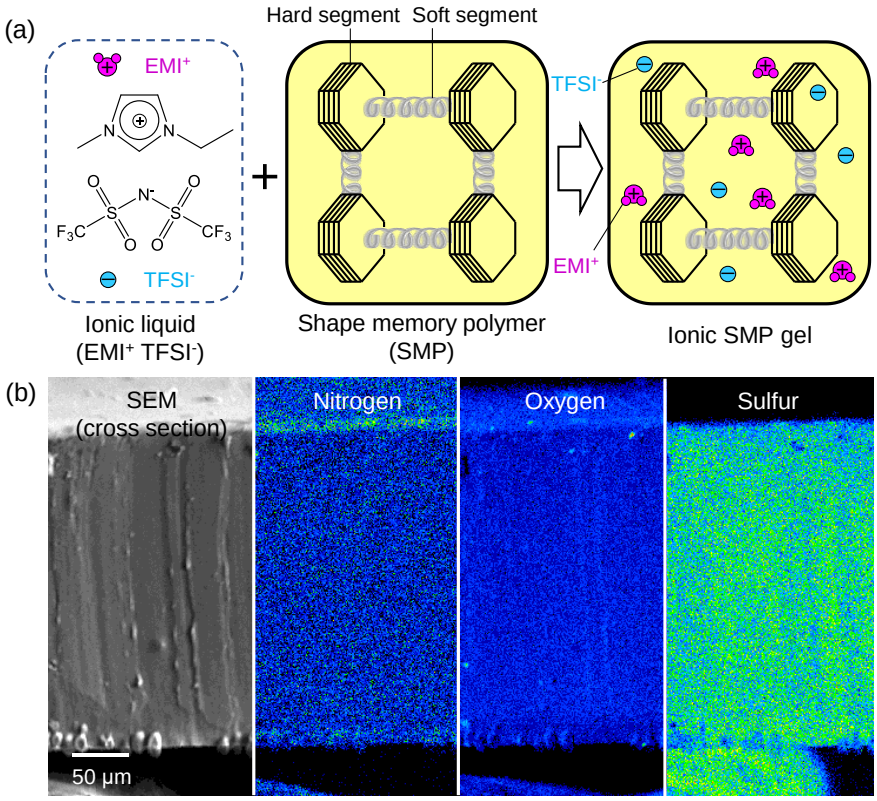

Figure 3-4. Schematic illustration of ionic shape memory polymer (SMP) composing of EMI^+TFSI^- and SMP (a). EPMA element mapping images of ionic SMP gel (cross section) at W_{IL} = 30 wt% (b).

The electrical properties of the ionic SMP gels is shown in Fig. 3-5. A clear indication of the importance of IL on electrical properties is seen in the AC impedance analysis. The Cole-Cole plots of the ionic SMP gels are shown in Fig. 3-5a, a semicircle at higher frequencies with a straight line at lower frequencies, which can be expressed by a Randles equivalent circuit[30,31] consisting of a gel resistant (R_{gel}) in series with the parallel combination of a constant phase element (CPE) and an impedance of a faradic reaction composed of charge transfer resistance (R_{ct}) and a Warburg impedance (Z_w) representing the diffusion of ions as shown in the inset of Fig. 3-5b. One can see that the semicircle in the Cole-Cole plot becomes smaller and slightly shifts toward lower resistance with increasing the IL content from 10 wt% to 30 wt%, indicative of changes in the parameters of the equivalent circuit. As shown in Fig. 3-5b, a rise in the IL content brings about a decrease of the R_{gel} owing to the increase of ionic conductivity (σ) calculated as follow equation (3-2):

$$\sigma = \frac{d}{R_{gel}\, S} \tag{3-2}$$

where d (300 μm) and S (0.785 cm^2) are the thickness of the ionic SMP gel and the electrode surface area of the sample holder, respectively. The ionic conductivity of the ionic SMP gels increases in proportion to the IL content. The values attains as high as 1.85×10^{-5} S cm^{-1} at W_{IL} = 30 wt%, which is comparable to that of poly (ethylene glycol) diacrylate (PEGDA) with EMI^+TFSI^- composites polymer electrolyte membranes[32] and polyurethane (PU) with EMI^+TFSI^- composite gels[14] at the same IL content.

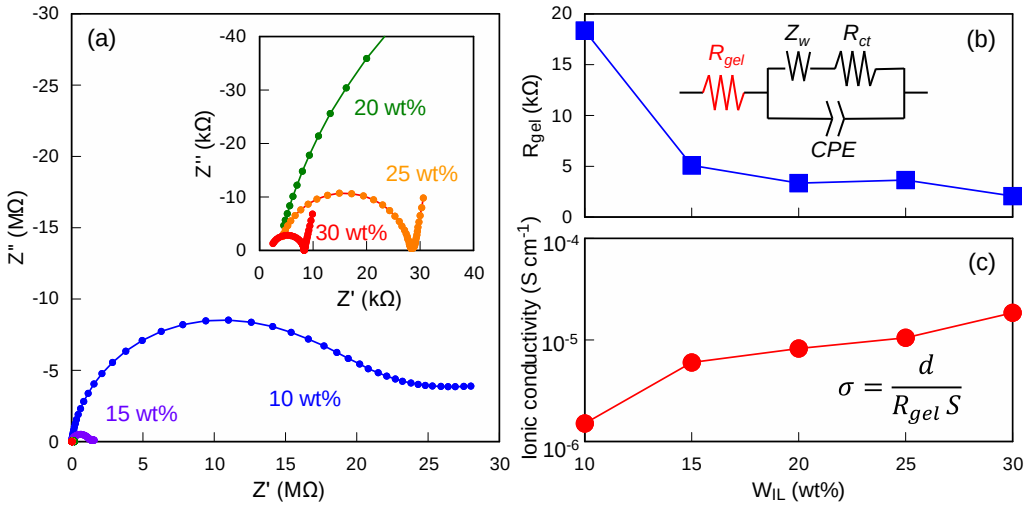

Figure 3-5 Cole-Cole plots of ionic SMP gels with various IL contents (a). Changes in gel resistance (R_{gel}) (b) and ionic conductivity (σ) (c) of ionic SMP gels on IL content. Inset: equivalent circuit model of the ionic SMP gels.

3.3.2 Thermo mechanical properties

Dynamic mechanical analysis (DMA) was carried out to evaluate the viscoelastic properties of the ionic SMP gels. It is seen from Fig. 3-6a that the pure SMP (W_{IL} =0 wt%) shows a steep drop of storage modulus and large tan δ peak at around 50ºC, corresponding to the glass transition temperature (T_g) of the SMP, in which soft segments in the reversible phase of the segmented polyurethane block copolymer transfer from a glass to rubber state due to micro-Brownian motion while phase separated hard segments from hard domains by physical crosslinks through hydrogen bonding[33]. Notably, an increase of W_{IL} significantly decreases both the storage modulus at room temperature (Fig. 3-6c) and the drop of the storage modulus (Fig. 3-6a), which indicates the rigid SMP network was soften by IL. Moreover, the peak of the tan δ which correlated to T_g of the ionic

SMP gels shifts to lower temperature with increasing W_{IL} (Fig. 3-6d), due to the IL works as plasticizer in the ionic SMP gels[32].

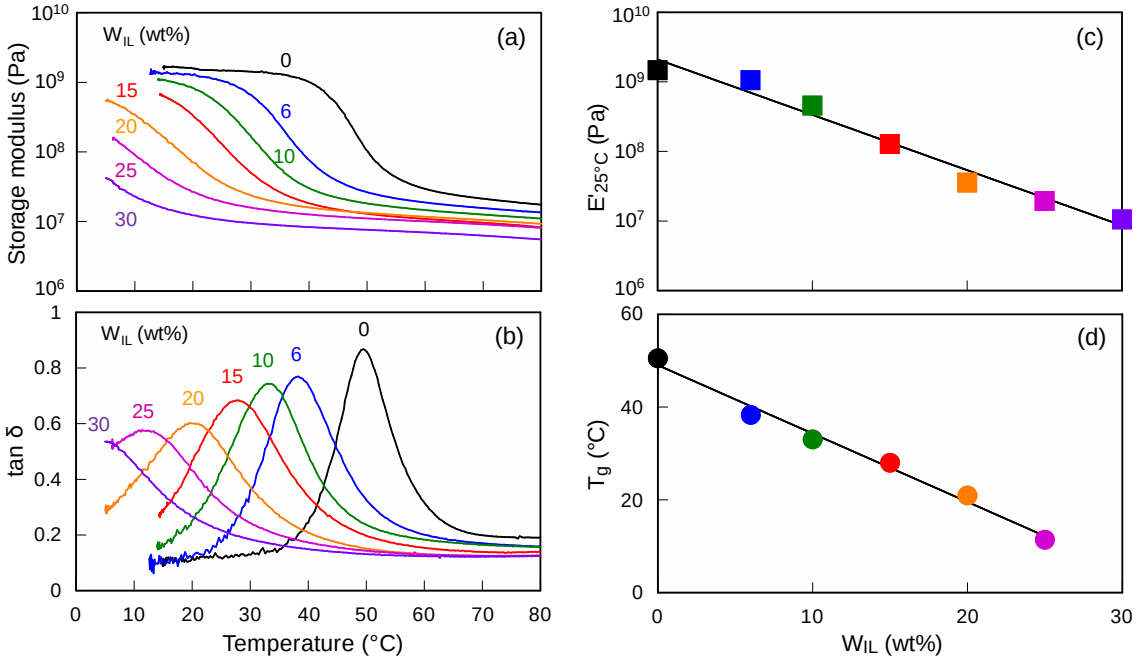

Figure 3-6 Temperature dependence of storage modulus (a) and tan δ (b) for ionic SMP gels with various W_{IL}. Relation between the storage modulus at 25ºC (c), T_g (d) of ionic SMP gels and W_{IL}.

3.3.3 Sensing behavior of ionic SMP/PEDOT:PSS composite

In order to evaluate the sensing performance of the ionic SMP sensors, mechanical stimulation with various displacement, velocity, as well as acceleration was applied on the sensors. Fig. 3-7a, b, c display the input mechanical stimulation with displacement of 7 mm, velocity of 50, 100 and 200 mm min^{-1}, while the correlated acceleration of 0.19, 0.5 and 0.8 m s^{-2}, respectively. It can be seen that voltage, electric charge and current were induced, once the mechanical bending was applied on the ionic SMP/PEDOT:PSS composite (W_{IL} = 30 wt%), as shown in Fig. 3-7d, e and f. Notably, the output voltage, electric charge and current show highly agreement with the input mechanical stimulation of displacement, velocity and acceleration, respectively. The open circuit voltage responses are presented in Fig 3-7d. They show similar behavior with the input displacement (Fig. 3-7a). The induced electric charges are shown in Fig. 3-7e, they behave similar shape with the input velocity (Fig. 3-7b). It can be seen that, positive charge was rapid generated while the velocity increased from 0 to desired value, which can be explained by the migration of EMI^+ cations. Once the bending deformation attained equilibrium state, the velocity decreased to

0, small amount of negative charges was generated, related to the movement of $TFSI^-$ anions that will be discussed later. The opposite phenomenon was observed when the bending deformation was released. Furthermore the acceleration of the mechanical stimulation which was corresponded to the velocity is shown in Fig. 3-7c. On the other hand, the mechanical bending induced electric current was calculated by differentiating the charge with time (Eq. 3-3), was shown in Fig. 3-7f.

$$I = \frac{dQ}{dt} \tag{3-3}$$

The electric current increased sharply once the mechanical stimulation was applied, similar with the acceleration. Notably, it was found that the induced peak current increases while the acceleration increases from 0.19 to 0.8 m s^{-2}. This clearly indicates the ionic SMP/PEDOT:PSS composite behaves as an acceleration sensor.

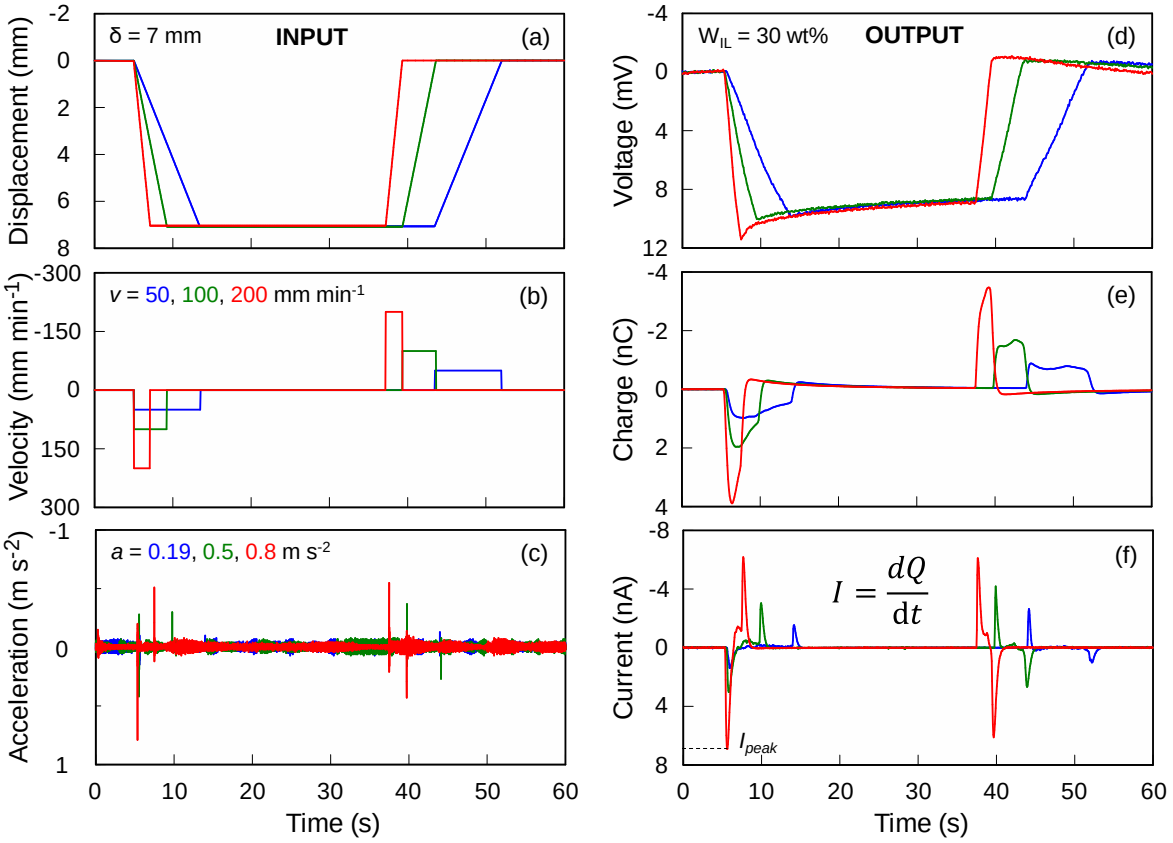

Figure 3-7 Applied mechanical stimulation with displacement of 7 mm (a), velocity of 50, 100 and 200 mm min^{-1} (b) and the correlated accelerations of 0.19, 0.5 and 0.8 m s^{-2} (c). Mechanical induced voltage (d), electric charge (e) and current (f) of the ionic SMP composite with 30 wt% of EMI^+ $TFSI^-$.

In order to clarify the acceleration sensing performance in more detail, the measurements were carried out at various acceleration (0.19, 0.5, 0.8 m s^{-2}) and bending displacement (3, 5, 7 mm), while the ionic SMP/PEDOT:PSS composite with IL of 30 wt%. Fig. 3-10a and b show the profile of mechanical induced current on time. It can be found that the peak current increases in proportion to the acceleration. On the other hand, the peak current almost keep constant at different bending displacements. Fig. 3-10c displays the plot of peak current (I_{peak}) versus acceleration, while the displacements are 3, 5 and 7 mm, respectively. I_{peak} exhibits linearly varying trends while less dependent on displacements. The acceleration sensitivity can be evaluated from the slopes of these straight lines. It was found that the ionic SMP/PEDOT:PSS composite exhibits acceleration sensitivity of 8.6 nA m^{-1} s^2. Furthermore, the dependence of acceleration sensitivity on IL content was examined. Fig. 3-8 and 3-9 display the mechanical bending induced electric charge and current of the ionic SMP/PEDOT:PSS composites (W_{IL} = 15 ~30 wt%) at various mechanical stimulation, respectively. The acceleration sensitivity of these composites was evaluated and displayed in Fig. 3-10d. It was found that the ionic SMP/PEDOT:PSS composites hardly exhibit acceleration sensing performance at lower IL content, which can be explained by the poor ion mobility (Fig. 3-5c) in the rigid polymer network (Fig. 3-6c). Once W_{IL} is higher than 15 wt%, the rigidity of the ionic SMP gels declines and the ionic conductivity increases, much more mobile ions can move freely in the ionic SMP gels, leading to the increasing of the mechanical induced charges and current. As the result, the acceleration sensitivity increases drastically when IL content is higher than 15 wt%, attained the highest at W_{IL} = 30 wt%, as high as 8.6 nA m^{-1} s^2.

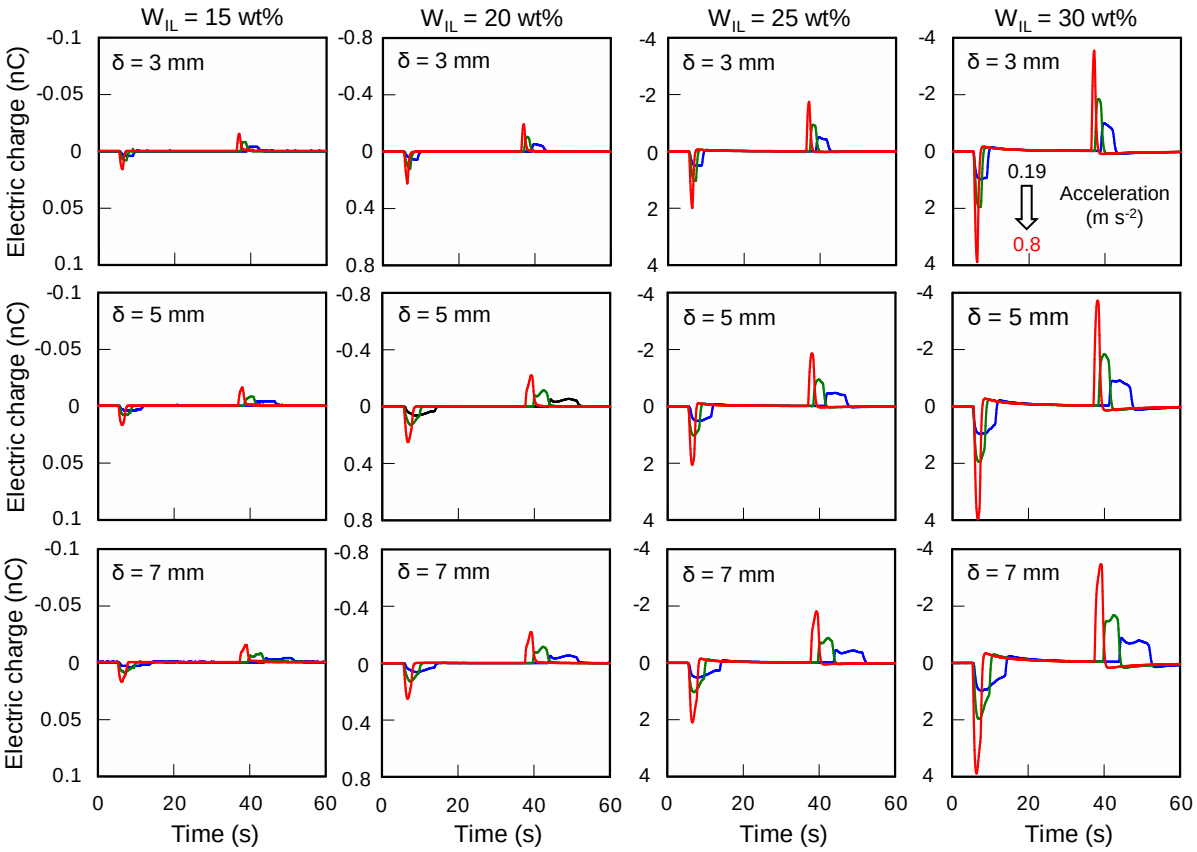

Figure 3-8 Mechanical bending induced electric charge of the ionic SMP gel sensors with various IL contents at different bending displacements (3, 5 and 7 mm) and accelerations (0.19, 0.5 and 0.8 m s^{-2}).

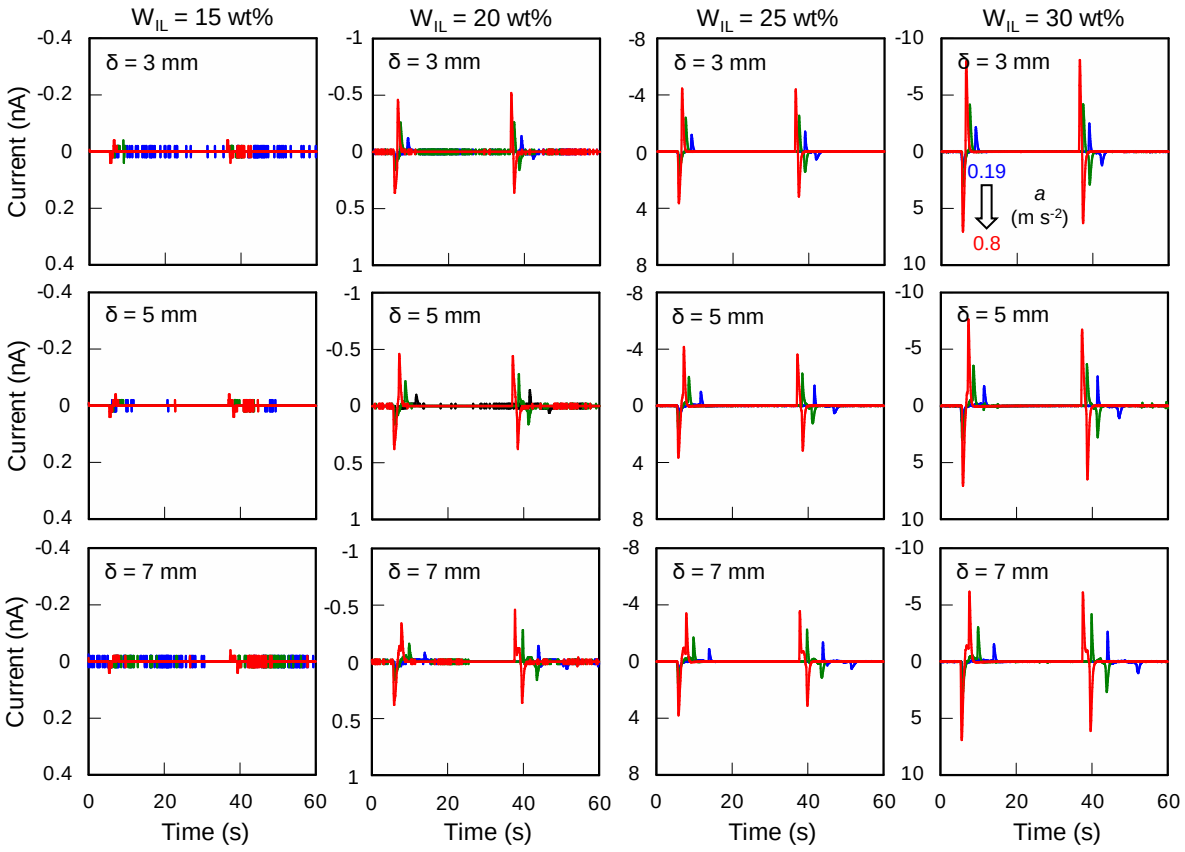

Figure 3-9 Mechanical bending induced electric current of the ionic SMP gel sensors with various IL contents at different bending displacements (3, 5 and 7 mm) and accelerations (0.19, 0.5 and 0.8 m s^{-2}).

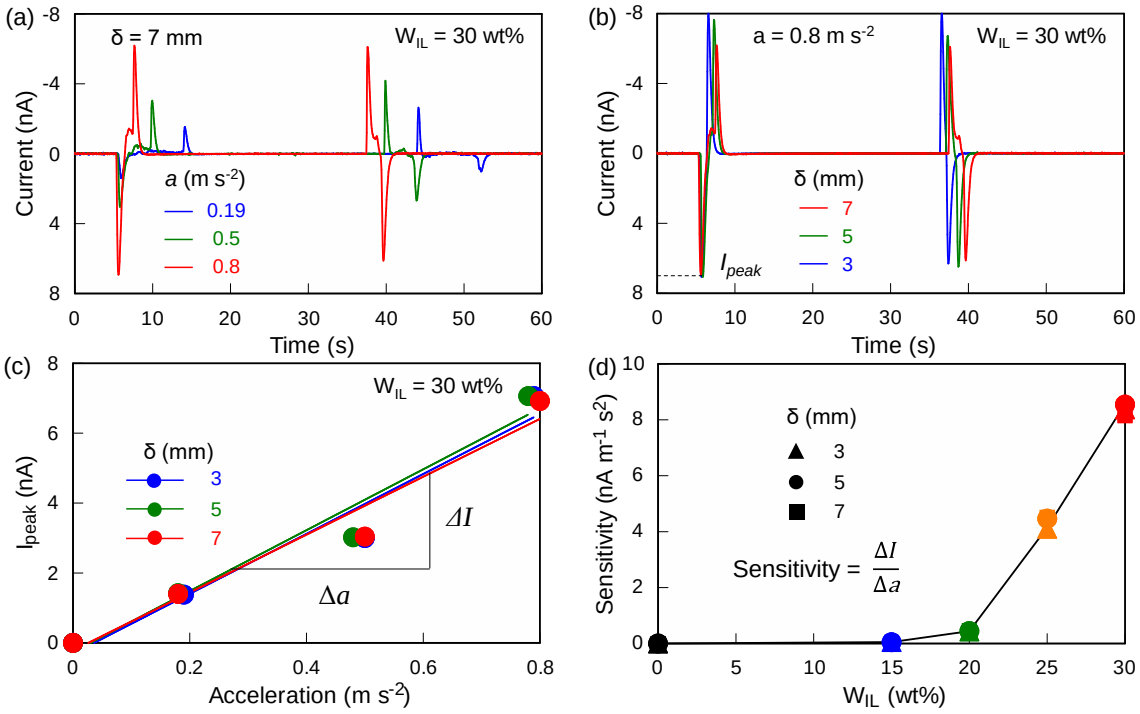

Figure 3-10 Generated peak current of the ionic SMP sensors with various IL contents versus acceleration (a). Relation between acceleration sensitivity of the ionic SMP sensors and IL content (b).

It should be noted that, voltage also was induced once mechanical stimulation was applied on the ionic SMP/PEDOT:PSS composite. The induced voltage exhibits similar behavior with input displacement, as shown in Fig. 3-7a and d. In order to clarify the relation between input displacement and induced voltage of the ionic SMP/PEDOT:PSS composite, the measurements were performed at various displacements and acceleration. Fig. 3-12a and b present the mechanical induced voltage of the ionic SMP/PEDOT:PSS composite (W_{IL} = 30 wt%) at various displacement and acceleration, respectively. It can be seen that the mechanical induced voltage increases with increasing the bending displacements, while keeps constant at various acceleration. Due to the higher strain difference between the electrodes at larger bending displacement (Fig. 3-3), which will be discussed later. It is surprising to notice that the mechanical induced voltage linearly increases in proportion to the input displacement, while less dependent on the acceleration, as shown in Fig. 3-12c. The slope of these straight lines corresponded to the displacement sensitivity is 1.17 V m^{-1}, slightly higher than ionic polymer metal composites (IPMC) sensor with displacement sensitivity of 1 V m^{-1}[134]. Due to the generation of the electric signals is based on the

mechanical induced migration of the ions, the generated voltage should affect by the IL content in the ionic SMP gels. The mechanical induced voltage of ionic SMP/PEDOT:PSS composites with various IL contents was examined (Fig. 3-11). In fact, the mechanical induced voltage increases in proportion to the IL content. Furthermore, the dependence of displacement sensitivity on IL content of ionic SMP/PEDOT:PSS composites is displayed in Fig. 8d. It can be found that the sensitivity increases rapidly once W_{IL} is higher than 15 wt%. The highest displacement sensitivity is attained at W_{IL} = 25 wt%, as high as 1.25 V m^{-1}. After that, it decreases slightly at W_{IL} = 30 wt%.

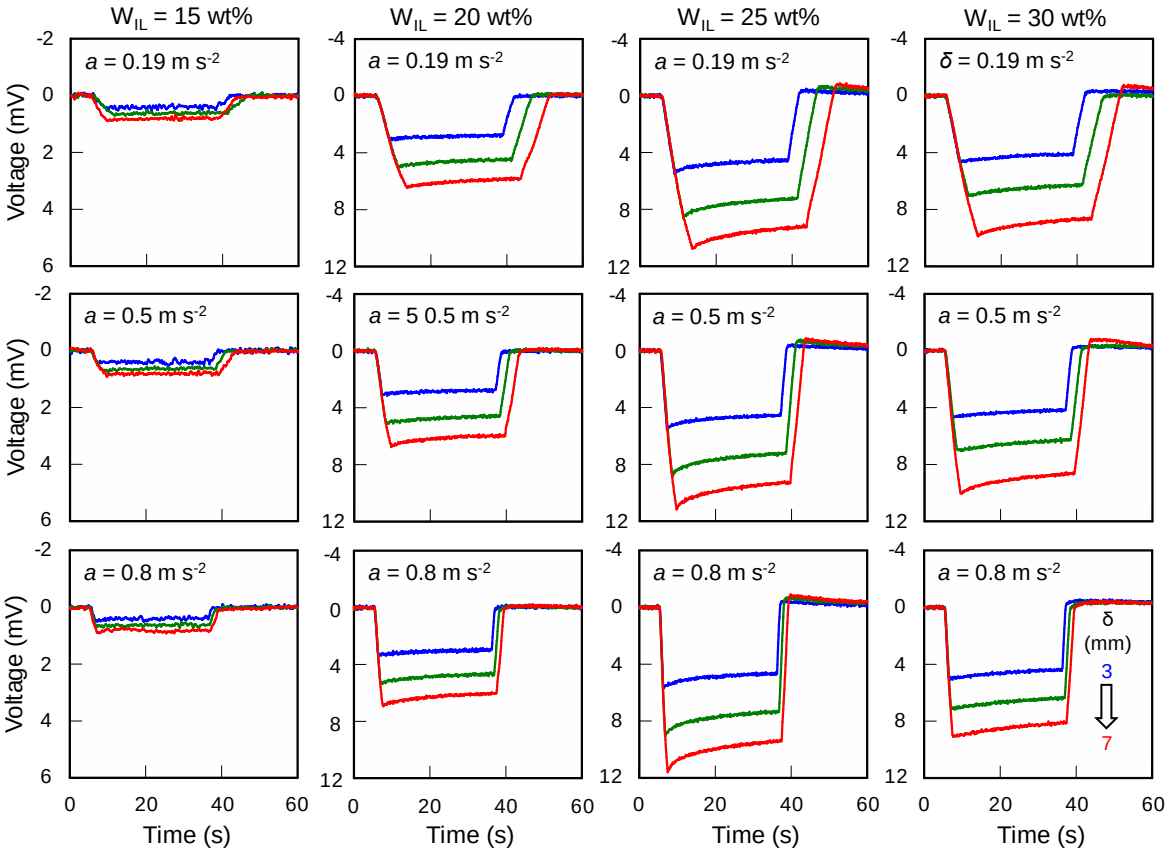

Figure 3-11 Mechanical bending induced voltage of the ionic SMP gel sensors with various IL contents at different bending displacements (3, 5 and 7 mm) and accelerations (0.19, 0.5 and 0.8 m s^{-2}).

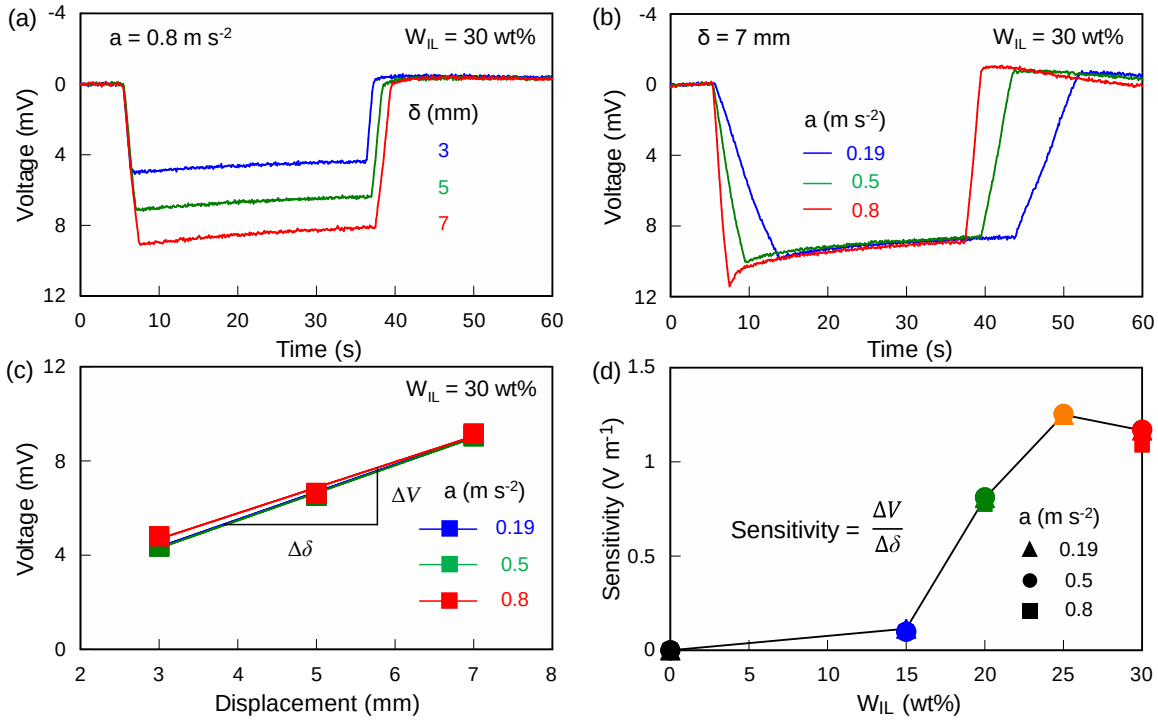

Figure 3-12 Applied bending deformation at various displacements of 3, 5 and 7 mm (a) and the corelated velocity (b) and accelerations (c). Voltage (d), electric charge (e) and current (f) responses corresponding to bending displacement.

On the other hand, it is surprising to notice that the ionic SMP/PEDOT:PSS composite (W_{IL} = 25 wt%) exhibits highest mechanical induced voltage of 9.81 mV under a displacement of 7 mm (corresponded strain difference of 2.8 %), which is much higher than other trilayer ionic polymer sensors[35,36], as listed in Tab. 1.

Table 1. Mechanical induced voltage of trilayer ionic polymer sensors

Sensor composition	Strain difference (%)	Generated voltage (mV)	Ref
Pt/Nafion-H_2O/Pt	-	2	[37]
Ppy/PVDF-BMI PF_6/Ppy	1	0.07	[38]
Au/Nafion-Na^+/Au	0.77	~1	[39]
Au/TPU-EMI TFSI/Au	1.3	1.8	[14]
PEDOT:PSS/PEO-EMI TFSI/PEDOT:PSS	0.5	0.4	[40]
PEDOT/IPN-EMI TFSI/PEDOT	1.8	1.3	[41]
PEDOT:PSS/SMP-EMI TFSI/PEDOT:PSS	2.8	9.8	This work

The generation of electric signals in the curved ionic SMP/PEDOT:PSS composites can be explained by piezoionic effect[39]. In the initial state of the ionic polymer gel, both cations and anions distribute homogenously. Upon bending the ionic polymer gel strip, the dissociated cations and anions would migrate from compressed side to expended side because of the pressure gradient in the curved ionic polymer gel strip. As the result, positive and negative charges can be generated. On the other hand, once the transferred cations are not equal with anions in the curved gel strip, voltage will be induced between the electrodes. It is well knew that, in neat EMI^+TFSI^-, the molar ionic conductivity of EMI^+ cation (λ_+ = 1.45 S cm mol^{-1}) is much higher than $TFSI^-$ anion (λ_- = 0.63 S cm mol^{-1}). Furthermore, the EMI^+ cation exhibits larger transfer number (t_+ = 0.63) than $TFSI^-$ anion (t_- = 0.37)[42]. Fig. 3-14 displays the plausible mechanism of the piezoionic effect in the ionic SMP/PEDOT:PSS composite. Once the mechanical stimulation was applied on the sensor strip, the EMI^+ cations with higher molar ionic conductivity (λ_+) moved rapidly toward the expanded outer-surface. As the result, positive electric charges (Q+) were generated. Then small amount of $TFSI^-$ anions with lower molar ionic conductivity (λ_-) followed afterwards, generating the negative electric charges (Q-). On the other hand, the generation of charges in the recovery motion can be explained in the same manner. In the bending state, due to the difference of molar ionic conductivity between EMI^+ cation and $TFSI^-$ anion, EMI^+ cations will transfer to the expanded side of the ionic SMP gel much faster than $TFSI^-$ anions. Once the transferred EMI^+

cations are not equal to $TFSI^-$ anions, ΔQ will store in the bended ionic SMP/PEDOT:PSS composites strip. As the result, voltage will be induced under the mechanical bending stimulation. The mechanical bending induced voltage should be strongly dependent on the electric charges (ΔQ) which were stored in the bended sensor strips. The transferred EMI^+ cations are evaluated by integrating the positive charges with time, as well as the transferred $TFSI^-$ anions are evaluated by integrating the negative charges with time, as shown in the inset of Fig. 3-13c. Furthermore, the total transferred electric charges (ΔQ) were evaluated by Q+ and Q-,

$$\Delta Q = Q_+ - Q_- \tag{3-4}$$

The relationship between mechanical bending induced voltage, electric charge, as well as capacitance and IL content in the ionic SMP/PEDOT:PSS composites are displayed in Fig. 3-13a, b and c. In general, higher voltage was generated at larger ΔQ. It can be seen that, the mechanical induced electric charges (ΔQ) in the bended sensor strips increase in proportion to the IL content, as well as the mechanical induced voltage increases at first and then decreases slightly at W_{IL} = 30 wt%. On the other hand, the capacitance (C) increases with increasing the IL content in the ionic SMP/PEDOT:PSS composites. Fig. 3-13d shows the magnitude of voltage (V) multiplied by capacitance (C) as a function of the stored charge (ΔQ) calculated by eq 3-5. It is surprising to notice that, after V is multiplied by C, the results exhibiting linearly varying trends with ΔQ, which are regardless with bending displacement, acceleration, as well as IL content (Fig. 3-13d). Furthermore, it is found that the values of C·V equal to ΔQ,

$$\Delta Q = CV \tag{3-5}$$

This equation is well knew in the field of electric double layer capacitor. It clearly indicates that the piezoionic effect sensors show double layer capacitive. This is the first time to clarify the generation of voltage by electric charge and capacitance, in the piezoionic effect sensors. The mechanical bending induced voltage is not only dependent on the charge, but also the capacitance of the ionic polymer sensor.

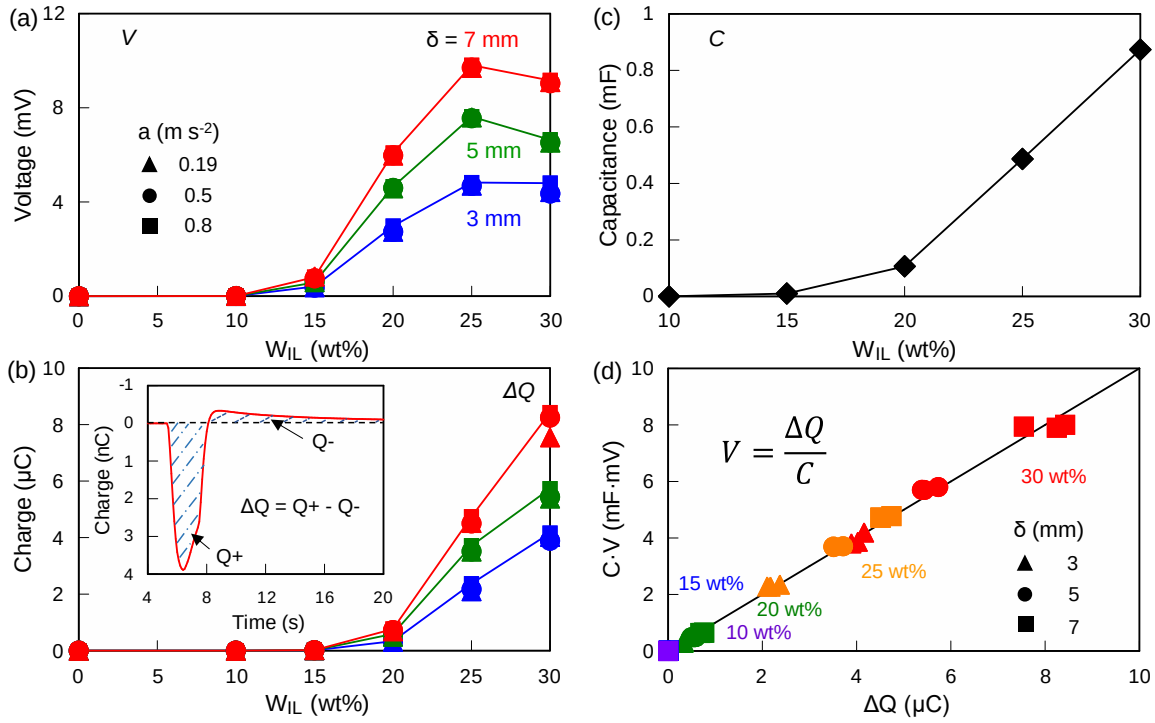

Figure 3-13 Dependence of mechanical bending induced voltage (a), electric charge (b), as well as capacitance (c) of the ionic SMP/PEDOT:PSS composites on IL content. Relation between V, C and ΔQ of the piezoionic effect ionic SMP/PEDOT:PSS sensors.

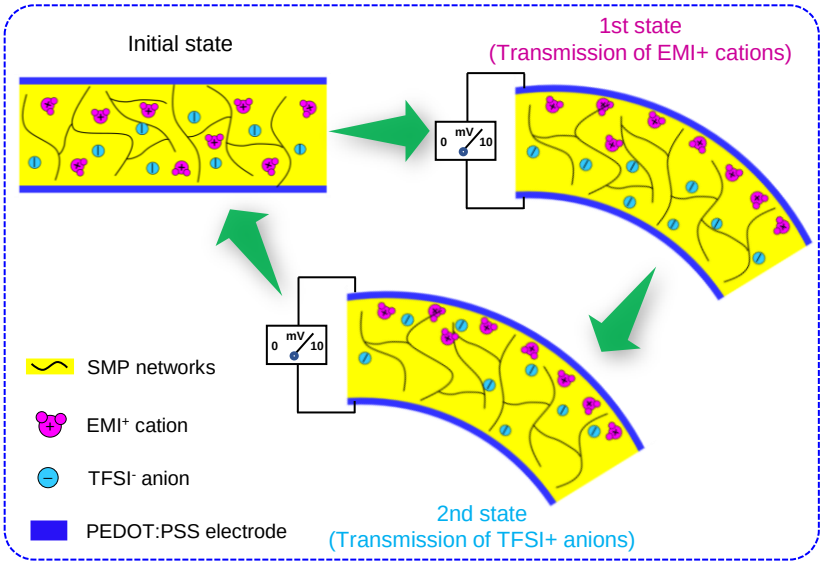

Figure 3-14 Schematic illustration of the plausible mechanism of the piezoionic effect in the IL-SMP/PEDOT:PSS sensor.

In general, the generated electric current of the IL-SMP/PEDOT:PSS sensor is strongly dependent

on the acceleration of the mechanical stimulation while less affected by the bending displacement. On the other hand, the generated voltage of the sensor increases linearly with the bending displacement, as less dependent on the acceleration of the mechanical stimulation. It can works as flexible sensor to detect the acceleration and bending displacement of human motions.

3.3.4 Shape memory properties of the ionic SMP gel

In general, thermally induced shape memory characteristics of the SMP consist of two processes as shown in Fig. 3-15. One is the programing process where the SMP heated above T_g is deformed by an external force (strain changes from ε_0 to ε_1), and then cooled down below T_g to fix the temporary shape (strain relaxes from ε_1 to ε_2). The other is the recovery process where the heating of the deformed SMP above the T_g will release the accumulated stress, which results in a recovery of the SMP from the temporary to its original shape (strain recovers from ε_2 to ε_3) [43].

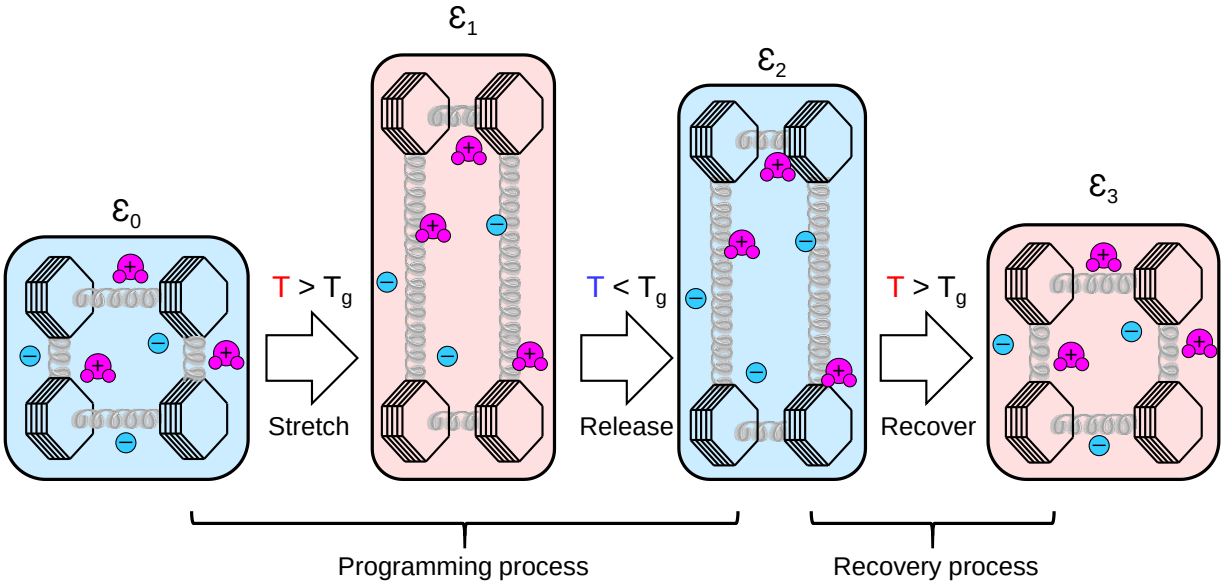

Figure 3-15 Schematic diagram of shape memory characteristics of IL-SMP gels.

Figure 3-16 displays typical thermomechanical analysis (TMA) curves of the IL-SMP gels for evaluating shape memory characteristics as explained in Fig. 3-15. The IL-SMP gel was first heated to 70 °C above T_g at a heating rate of 5°C min^{-1} and stretched under a constant stress of 1 MPa, then cooled down to room temperature (~20°C) to fix the shape with a temporary strain of ε_1. After releasing the force, the composite gel slightly relaxed with a fixed strain of ε_2. Finally, the composite gel recovered from its temporary shape to the original shape with a recovery strain

of ε_3 by heating again from RT to 70°C.

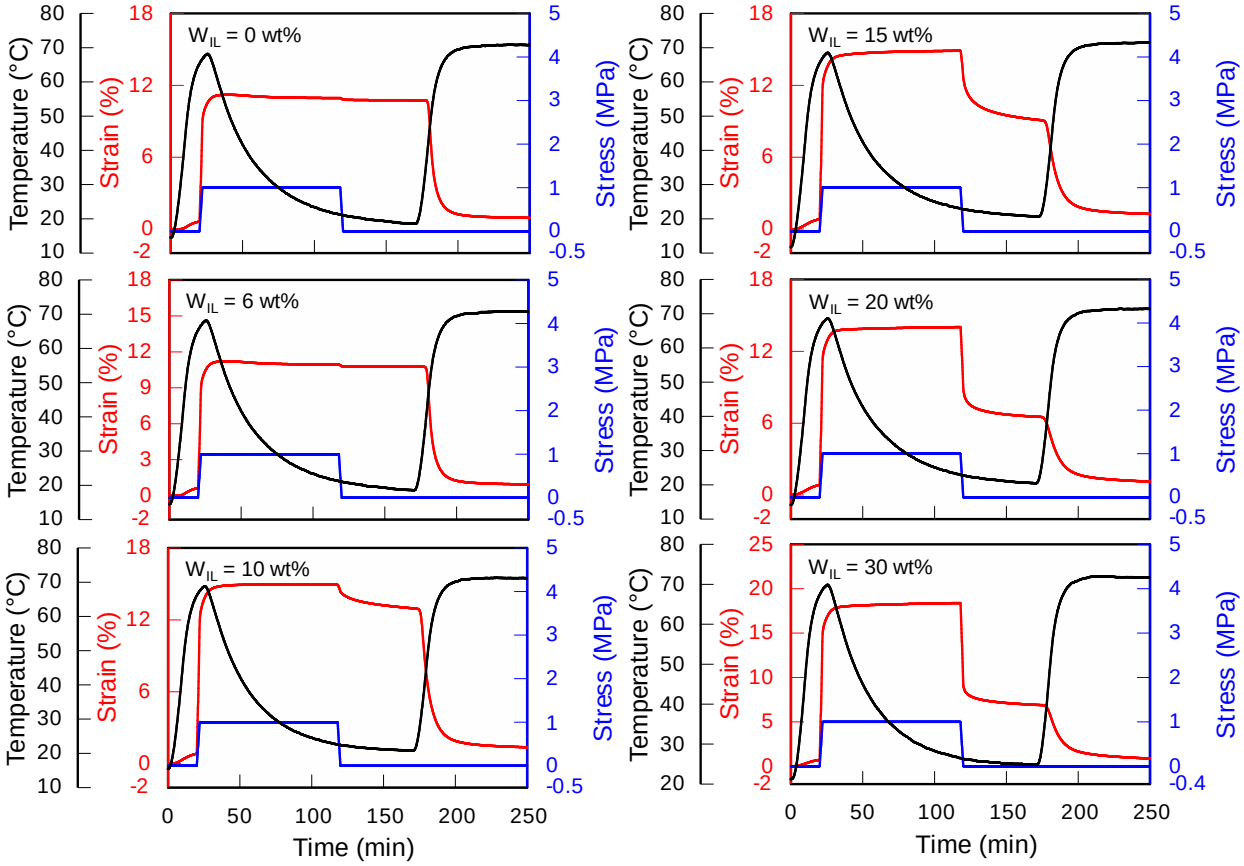

Figure 3-16 TMA curves of IL-SMP gels with various IL contents.

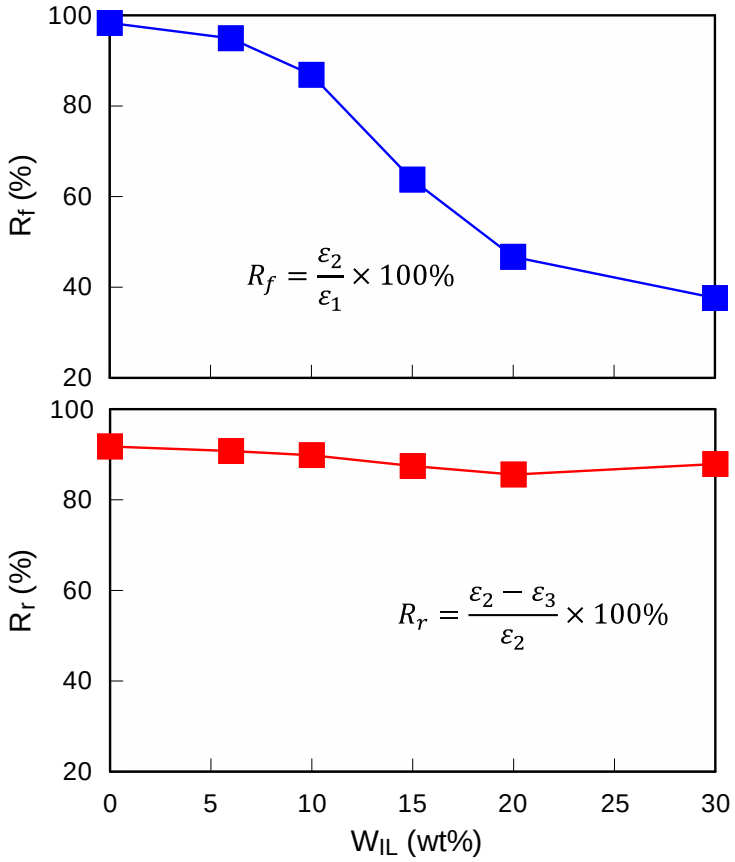

Figure 3-17 Changes in shape fixing ratio (R_f) and shape recovery ratio (R_r) of IL-SMP gels on W_{IL}.

The shape fixing ratio (R_f) and shape recovery ratio (R_r) of the IL-SMP gels were calculated as follows

$$R_f(\%) = \varepsilon_2 \,/\, \varepsilon_1 \times 100 \tag{3-6}$$

$$R_r(\%) = (\varepsilon_2 - \varepsilon_3) \,/\, \varepsilon_2 \times 100 \tag{3-7}$$

As shown in Fig. 3-17, the values of R_f and R_r for pure SMP were 100% and 90%, respectively[44]. It was found that the increase of S-PEDOT resulted in a decrease of R_f (37.6% at W_{IL} = 30 wt%), while the R_r was kept almost constant (ca. 90 % at W_{IL} = 0 ~ 30 wt%).

Furthermore, the dependence of voltages and charges response to mechanical stimulate on temperature was investigated (W_{IL} = 10 wt%) (Fig. 3-18). Fig. 3-19 displays the plots of V, Q+, Q-, ΔQ and C versus temperature of the IL-SMP/PEDOT:PSS sensor under bending displacement, acceleration of 7 mm, 0.28 m s^{-2}. Smaller V, Q+, Q- and ΔQ are generated at the temperature range of 20 to 30ºC. Then the V drastically increases while the temperature is higher than 30ºC, achieves

the maximum at 50ºC, then it becomes constant at the temperature range of 50 to 60ºC, exhibits less depend on the temperature behavior. On the other hand, both the electric charges (Q+, Q-, ΔQ) and capacitance (C) increase drastically while the ambient temperature is higher than 30ºC. From the DMA measurements (Fig. 3-3), the IL-SMP gel with 10 wt% of IL exhibits T_g of 33ºC. When the ambient temperature below T_g, the IL-SMP gel exhibits rigid polymer network, the mobility of the ions is limited, only few cations and anions can move freely in the gel. Extremely low Q+, Q- and ΔQ can be generated under mechanical stimulate. As the result, the potential between the two electrodes is lower. Once the temperature increases around T_g, the polymer network will transfer from glass state to rubber state, the polymer chains becomes soft, exhibits a drop of storage modulus, both the movement of polymer chains and the ions in the polymer networks can be improved. On the other hand, the mobility of ions also will be enhanced by increasing the temperature, according to the Arrhenius principle. The transferred charges ΔQ increases drastically in proportion to the temperature. At the same time, the capacitance of the IL-SMP gel increases slightly. As the result, V increases drastically in proportion to temperature (30 to 50ºC). When the temperature is higher than 50ºC, the V exhibits less dependent on temperature, due to the drastically increase of both electric charge (ΔQ) and capacitance (C). The generated voltage of the IL-SMP/PEDOT:PSS sensors exhibits transition behavior corelated to the thermo mechanical transition behavior. Furthermore, the measured V is highly agreed with the calculated V by equation (3-5).

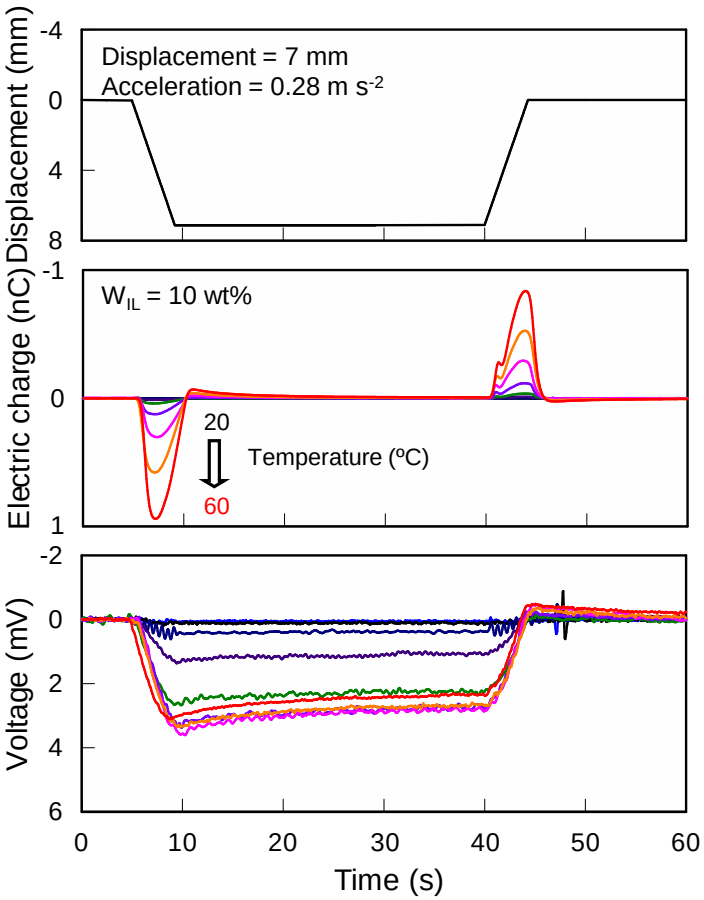

Figure 3-18 Applied mechanical stimulate at a constant displacement and acceleration (7 mm and 0.28 m s^{-2}) and electric charge and voltage response behavior versus time of the IL-SMP/PEDOT:PSS sensor (W_{IL} = 10 wt%) at various temperature.

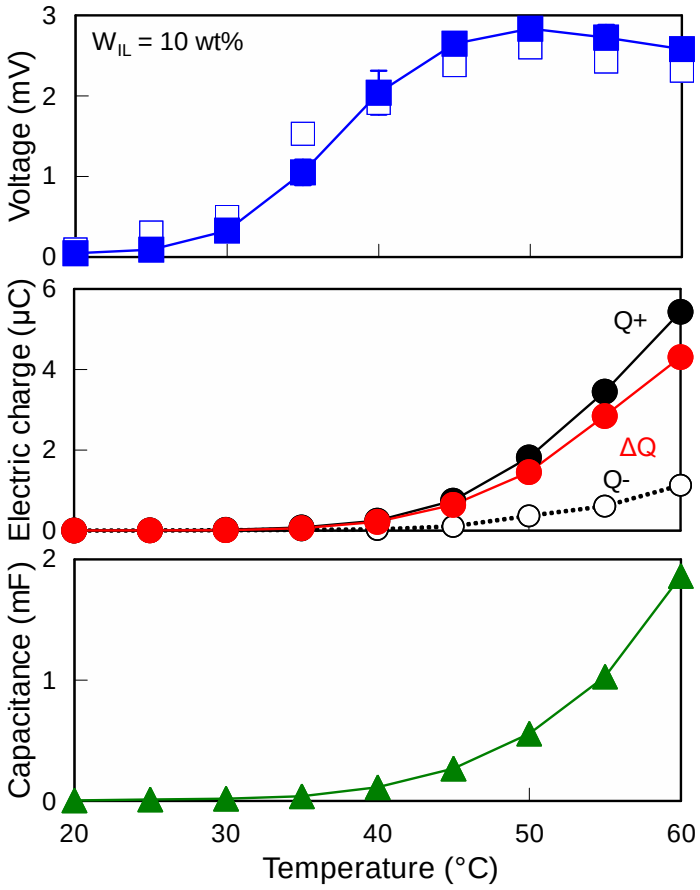

Figure 3-19 The generated voltages, calculated voltages and electric charges under mechanical stimulate (7 mm and 0.28 m s^{-2}) and the capacitances of the IL-SMP/PEDOT:PSS composites at various temperature.

3.4 Conclusion

A novel multi-functional flexible sensor based on piezoionic effect was fabricated using $EMI^{+}TFSI^{-}$, SMP and PEDOT:PSS. It exhibits excellent acceleration sensitivity, as high as 8.6 nA m^{-1} s^{2}. It also shows good displacement sensing performance, the highest generated voltage is 9.8 mV at displacement of 7 mm. And the displacement sensitivity attains 1.2 V m^{-1} at W_{IL} = 25 wt%. The generation of electric signals can be explained by the piezoionic effect. Under the mechanical stimulation, the generation of electric charge is originated from the migration of the ions in the ionic SMP gel. Due to the difference of molar ionic conductivity between EMI^{+} cations and $TFSI^{-}$ anions, the total transferred electric charge was different in the bending state of the ionic SMP gel. Due to the inhomogeneous distribution of the ions, voltage can be generated Notably, the generated

voltage can be calculated by the combination of total transferred electric charge and capacitance of the sensor. And the calculated voltage shows highly agreement with the measurement data. This remarkable finding provides a strategy to improve the generated voltage of the ionic polymer gel sensors: 1. increasing the total transferred electric charges by selecting the IL with larger difference of molar ionic conductivity between the cations and anions; 2. decreasing the capacitance of the ionic polymer gel sensor by selecting the support polymer with lower dielectric constant. Furthermore, the IL-SMP/PEDOT:PSS composites can work as monitor sensor to detect human motionsThe generated voltage of the IL-SMP/PEDOT:PSS sensor (W_{IL} = 10 wt%) shows transition behavior while the ambient temperature is around T_g. The TMA measurement revealed that the IL-SMP gels exhibit acceptable shape memory property while $W_{IL} \leq 10$ wt%, R_f = 86.9 %, R_r = 89.8 % at W_{IL} = 10 wt%.

3.5 References

1) C. Boutry, A. Nguyen, Q. Lawal, A. Chortos, S. Gagné and Z. Bao. A sensitive and biodegradable pressure sensor array for cardiovascular monitoring. Adv. Mater. **18**, 6954, 2015.
2) S. Mallineni, Y. Dong, H. Behlow, A. Rao and R. Podila. A wireless triboelectric nanogenerator. Adv. Energy Mater. **8**, 1702736, 2018.
3) S. Chen, T. Huang, H. Zuo, S. Qian, Y. Guo, L. Sun, D. Lei, Q. Wu, B. Zhu, C. He, X. Mo, E. Jeffries, H. Yu, Z. You. A single integrated 3D-printing process customizes elastic and sustainable triboelectric nanogenerators for wearable electronics. Adv. Funct. Mater. **14**, 1805108, 2018.
4) X. Liao, Q. Liao, X. Yan, Q. Liang, H. Si, M. Li, H. Wu, S. Cao and Y. Zhang. Flexible and Highly Sensitive Strain Sensors Fabricated by Pencil Drawn for Wearable Monitor. Adv. Funct. Mater. **25**, 2395, 2015.
5) S. Gong, W. Schwalb, Y. Wang, Y. Chen, Y. Tang, J. Si, B. Shirinzadeh, and W. Cheng. A wearable and highly sensitive pressure sensor with ultrathin gold nanowires. Nat. Commun. **5**, 1, 2014.
6) M. Amjadi, A. Pichitpajongkit, S. Lee, S. Ryu, I. Park. Highly stretchable and sensitive strain sensor based on silver nanowire-elastomer nanocomposite. ACS Nano. **8**, 5154, 2014.

7) T. Yamada, Y. Hayamizu, Y. Yamamoto, Y. Yomogida, A. Najafabadi, D. Ftaba and K. Hata. A stretchable carbon nanotube strain sensor for human-motion detection. Nat. Nanotechnol. **6**, 296, 2011.

8) D. Lipomi, M. Vosgueritchian, B. Tee, S. Hellstrom, J. Lee, C. Fox, and Z. Bao, Skin-like pressure and strain sensors based on transparent elastic films of carbon nanotubes. Nat. Nanotechnol. **6**, 788, 2011.

9) T. Yang, X. Jiang, Y. Zhong, X. Zhao, S. Lin, J. Li, X. Li, J. Xu, Z. Li and H. Zhu. A wearable and highly sensitive graphene strain sensor for precise home-based pulse wave monitoring. ACS Sens. **2**, 967, 2017.

10) X. Wang, T. Li, J. Adams and J. Yang. Transparent, stretchable, carbon-nanotube-inlaid conductors enabled by standard replication technology for capacitive pressure, strain and touch sensors. J. Mater. Chem. A. **1**, 3580, 2013.

11) S. Yao and Y. Zhu. Wearable multifunctional sensors using printed stretchable conductors made of silver nanowires. Nanoscale, **6**, 2345, 2014.

12) S. Kim, S. Park, H. Park, D. Park, Y. Jeong and D. Kim. Highly sensitive and multimodal all-carbon skin sensors capable of simultaneously detecting tactile and biological stimuli. Adv. Mater. **27**, 4178, 2015.

13) S. Mirza, Y. Dobashi, E. Glitz, M. Farajollahi, S. Mirabbasi, S. Naficy, G. Spinks, J. Madden. Transparent and conformal 'piezoionic' touch sensor. Electroactive Polymer Actuators and Devices (EAPAD). **9430**, 943026, 2015.

14) Y. Liu, Y. Hu, J. Zhao, G. Wu, X. Tao and W. Chen. Self-powered piezoionic strain sensor toward the monitoring of human activities. Small. **12**, 5074, 2016.

15) C. Xiang, C. Liu, C. Hao, Z. Wang, L. Che and X. Zhou. A self-powered acceleration sensor with flexible materials based on triboelectric effect. Nano Energy. **31**, 469, 2017.

16) D. Lee, H. Hong, M. Lee, C. Park, and N. Min. A prototype high sensitivity load cell using single walled carbon nanotube strain gauges. Sens. Actuators, A. **180**, 120, 2012.

17) T. Someya, T. Sekitani, S. Iba, Y. Kato, H. Kawaguchi, and T. Sakurai. A large-area, flexible pressure sensor matrix with organic field-effect transistors for artificial skin applications. Proc. Natl Acad. Sci. USA. **101**, 9966, 2004.

18) M. Cheng, X. Huang, C. Ma and Y. Yang. A flexible capacitive tactile sensing array with floating electrodes. J. Micromech. Microeng. **19**, 115001, 2009.

19) Z. Wang and J. Song. Piezoelectric nanogenerators based on zinc oxide nanowire arrays. Science. **312**, 14, 2006.

20) S. Lim, D. Son, J. Kim, Y. Lee, J. Song, S. Choi, D. Lee, J. Kim, M. Lee, T. Hyeon and D. Kim. Transparent and stretchable interactive human machine interface based on patterned graphene heterostructures. Adv. Funct. Mater. **25**, 375, 2015.

21) H. Zhang, Y. Yang, Y. Su, J. Chen, K, Adams, S. Lee, C. Hu and Z. Wang. Triboelectric nanogenerator for harvesting vibration energy in full space and as self-powered acceleration sensor. Adv. Funct. Mater. **24**, 1401, 2014.

22) N. Kamamichi, M. Yamakita, K. Asaka, Z. Luo and T. Mukai, Sensor property of a novel EAP device with ionic-liquid-based bucky gel, Sensors, IEEE, Atlanta, GA, 221, 2007.

23) I. Must, F. Kaasik, I. Põldsalu, U. Johanson, A. Punning, and A. Aabloo, A carbide-derived carbon laminate used as a mechanoelectrical sensor, Carbon, **50**, 535, 2012.

24) Y. Wu, G. Alici, J. D. W. Madden, G. M. Spinks, and G. G. Wallace, Soft mechanical sensors through reverse actuation in polypyrrole, Adv. Funct. Mater. **17**, 3216, 2007.

25) V. Woehling, G. Nguyen, C. Plesse, Y. Petel, Y. Dobashi, J. Madden, C. Michal and F. Vidal, Study of the piezoionic effect and influence of electrolyte in conducting polymer based soft strain sensors. ACS Sensors. **2**, 045002, 2019.

26) Homepage of SMP Technologies Inc.: [www.smptechno.com/index_en.html]

27) S. Hayashi and H. Fujimura, U.S. Patent 5049591, 1991.

28) S. Hayashi, U.S. Patent 5145935, 1992.

29) T. Horii, H. Hikawa, M. Katsunuma and H. Okuzaki. Synthesis of highly conductive PEDOT:PSS and correlation with hierarchical structure. Polymer. **140**, 33, 2018.

30) J. Randles. Discussions of the Faraday Society, 1, 11-19, 1947.

31) H. Okuzaki, S. Takagi, F. Hishiki and R. Tanigawa. Ionic liquid/polyurethane/PEDOT:PSS composites for electro-active polymer actuators. Sens. Actuators B Chem. **194**, 59, 2014.

32) C. Piedrahita, P. Yue, J. Cao, H. Lee, C. Rajapaksha, C. Feng, A. Jákli and T Kyu. Flexoelectricity in flexoionic polymer electrolyte membranes: effect of thiosiloxane modification on poly(ethylene glycol) diacrylate and ionic liquid electrolyte composites. ACS Appl. Mater. Interfaces 2020, 12, 16978-16986.

33) B. Lee, B. Chun, Y. Chung, K. Sul, and J. Cho. Structure and thermomechanical properties of polyurethane block copolymers with shape memory effect. Macromolecules. **34**, 6431, 2001.

34) Jin W, Chunye X, Minoru T and Yasuo K 2007 Design and fabrication of tactile sensors based on electroactive polymer composites. Proc. SPIE 6524 65241K.

35) Z. Zhu, L. Chang, T. Horiuchi, K. Takagi, A. Aabloo and K. Asaka. Multi-physical model of cation and water transport in ionic polymer-metal composite sensors. J. Appl. Phys. **119**, 124901, 2016.

36) M. Shahinpoor, Y. Bar-Cohen, T. Xue, J. S. Harrison, and J. G. Smith. Some experimental results on ionic polymer-metal composites (IPMC) as biomimetic sensors and actuators. Proc. SPIE. **3324**, 251, 1998.

37) M Shahinpoor and K Kim. Ionic polymer-metal composites: I. Fundamentals. Smart Mater. Struct. **10**, 819, 2001.

38) Y Wu, G Alici, J Madden, G Spinks and G Wallace. Soft mechanical sensors through reverse actuation in polypyrrole. Adv. Funct. Mater. **17**, 3216, 2007.

39) Z Zhu, T Horiuchi, K Takagi, J Takeda, L Chang and K Asaka. 2016 Effects of cation on electrical responses of ionic polymer-metal composite sensors at various ambient humidities. J. Appl. Phys. **120**, 084906, 2016.

40) K Rohtlaid, G Nguyen, C Soyer, E Cattan, F Vidal, C Plesse. Poly(3,4-ethylenedioxythiophene):poly(styrene sulfonate)/polyethylene oxide electrodes with improved electrical and electrochemical properties for soft microactuators and microsensors. Adv. Electron. Mater. **5**, 1800948, 2019.

41) V Woehling, G Nguyen, C Plesse, Y Petel, Y Dobashi, J Madden, C Michal and F Vidal. Study of the piezoionic effect and influence of electrolyte in conducting polymer based soft strain sensors. Multifunct. Mater. **2**, 045002, 2019.

42) IEEJ Ed., Handbook of Electrochemistry 6th Ed., Maruzen Pub., p.251, 2013.

43) A. Lendlein and S. Kelch. Shape-memory polymers. Angew. Chem. Int. Ed. 41. 2034, 2002.

44) Y. An and H. Okuzaki. Novel electro-active shape memory polymers for soft actuators. Jpn. J. Appl. Phys. **59**, 061002, 2020.

Chapter 4 3D Printable Electric and Ionic Shape Memory Polymer (SMP) and Future Prospective

4.1 Introduction

3-dimensional (3D) printing technology, also was called as additive manufacturing, has been attracted extensively attention from viewpoints of academic and technologic aspects[1-6], due to it has many advantages compared with traditional manufacturing technology, as rapid prototyping, lower cost, flexibility, risk reduction, sustainability and so on[7]. Many different types of commercial 3D technology has been developed, like stereolithography (SLA)[8], selective laser sintering (SLS)[9], 3D plotting/direct-write (3DP)[10] and fused deposition modeling (FDM)[11]. Some research groups had tried to fabricate smart devices using 3D printing technology. Leigh et al[12] had printed electric circuits using carbon black (CB)/polycaprolactone (PCL) composite and the 3D printed composites can work as monitor sensor to detect human motions. Odent et al[13] had successfully 3D printed transparence, stretchable and ionic conductive hydrogel. In this dissertation, novel electric and ionic SMP which can work as electroactive actuator and multi-functional sensor have been developed. Due to the novel electric SMP in chapter 2 and ionic SMP in chapter 3 exhibit T_g at ca. 50 and lower 50 ºC, these novel SMPs have the potential to apply to FDM 3D printing technology. In this chapter, the 3D printability of the novel electric SMP and ionic SMP was investigated. Furthermore, electroactive soft actuators and ionic SMP gel with shape memory properties were fabricated using 3D printing technology.

Figure 4-1 various types 3-dimenssional printers and 3D printed smart devices.

4.2 Experimental methodologies

As described in chapter 2, the S-PEDOT water solution was freeze dried using a freeze dryer (DC400, Yamato Scientific). The S-PEDOT powder and SMP pellets were dissolved in DMSO with concentrations of 1 and 10 wt%, respectively, and both solutions were mixed together with S-PEDOT concentration of 10 wt%. After vigorous stirring, the S-PEDOT/SMP composites was evaluated using coagulation bath (non-solvents) which isopropanol (IPA) was used as the non-solvent. After S-PEDOT/SMP composite was coagulated, the pellets were dried at 80 ºC overnight and 200 ºC in vacuum for 1h. Then the dried S-PEDOT/SMP pellets were poured in to an extruder to fabricate the filament with diameter of 1.75 mm. Finally, U shape electroactive actuators were fabricated by FDM 3D printer, using conductive S-PEDOT/SMP filament. Fig. 4-2 shows the fabrication process of the electric SMP filament.

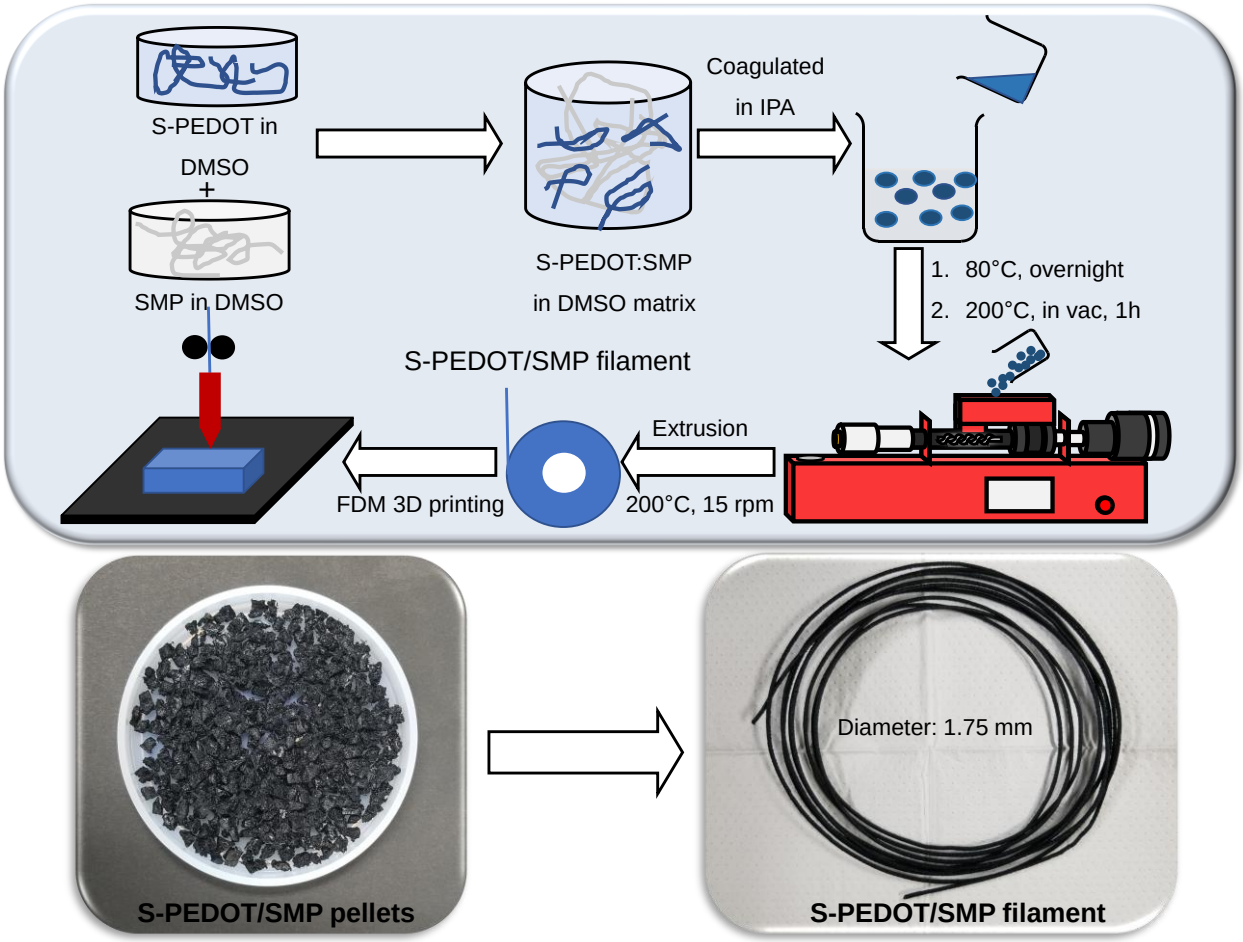

Figure 4-2 Fabrication of conductive S-PEDOT/SMP filament ($W_{S\text{-}PEDOT}$ = 10 wt%).

The ionic SMP filament was fabricated using ionic SMP gel which were developed in chapter 3. IL (EMI^+TFSI^-) was mixed with SMP in DMAc solution with IL concentration of 10 wt%. After vigorous stirring, the IL-SMP composite solution was poured into Teflon dish and dried at 50 ºC to evaporate DMAc solvent. After that, the ionic SMP gel was dried at 140 ºC in vacuum for 2h. Then the dried ionic SMP gel was pushed into the extruder to fabricate ionic SMP filament. At last, the ionic SMP filament was used for FDM 3D printing. The fabrication process of ionic SMP filament was described in Fig. 4-3.

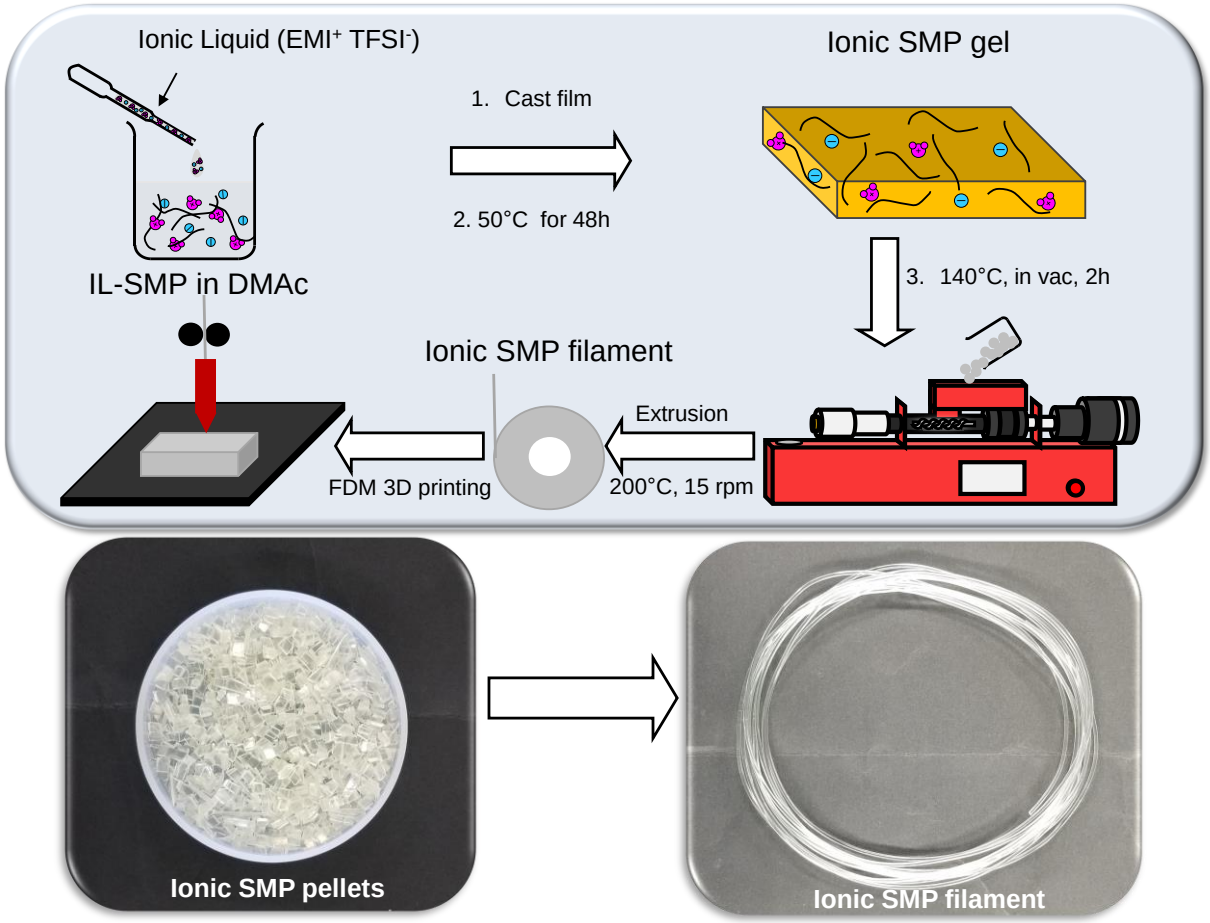

Figure 4-3 Fabrication of ionic SMP filament (W_{IL} = 10 wt%).

4.3 Performance of the 3D printed electric and ionic SMP

A 'U' shape objective (Fig. 4-4a) was printed using electric SMP filament. Then it was programed to a temporary shape (Fig. 4-4b) It can be found that the 3D printed electric SMP recovered gradually to its initial shape (Fig. 4-4c-f), once voltage (25V) was applied on. On the other hand, it was found that the temperature of the 3D printed electroactive actuator increased above T_g (ca. 50 ºC) by electricity Joule heating.

On the other hand, a semi-cycle objective was printed by FDM 3D printer, using ionic SMP filament, as shown in Fig. 4-5. It was hard and the shape was kept at room temperature (Fig. 4-6a). Once it was heated above T_g (ca. 45 ºC), it became soft and flexible (Fig. 4-6b). Furthermore, it could be programmed to any kinds of shape (Fig. 4-6c). When the temperature of the 3D printed ionic SMP gel was cooling down below T_g, the temporary shape was fixed (Fig. 4-6d)). After it was heated above T_g again, it was seen that the ionic SMP recovered to its initial shape immediately.

Fig. 4-6 clearly shows that the 3D printed SMP exhibits good shape memory properties, indicates that the 3D printed SMP gel is possible to adjust to human body and works as motion sensor.

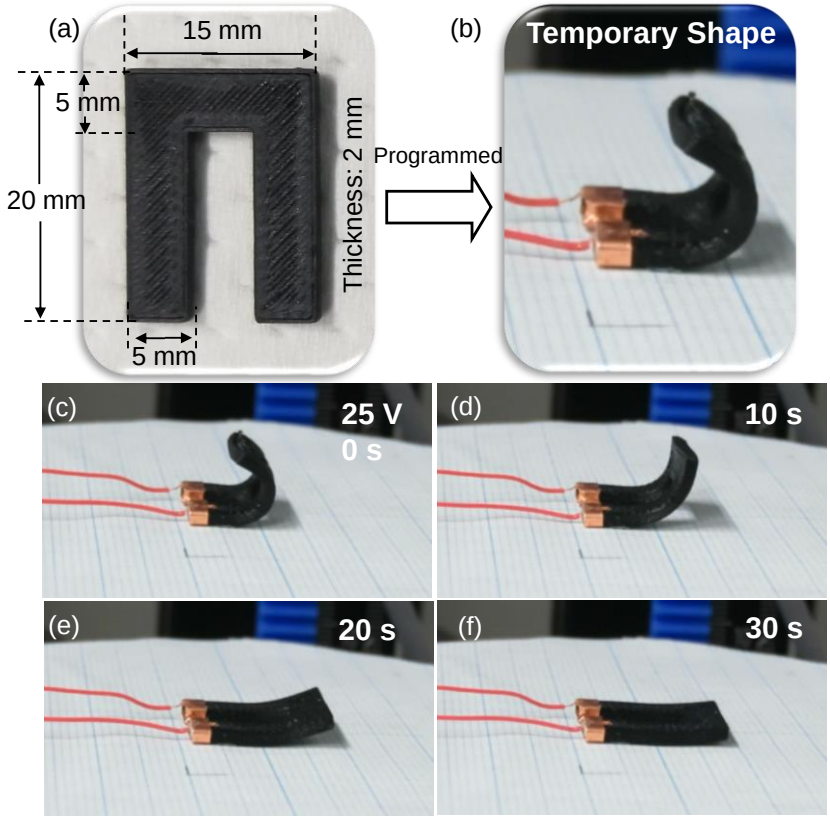

Figure 4-4 3D printed electroactive actuator. And the actuation process of the 3D printed electric SMP actuator driven by Joule heating.

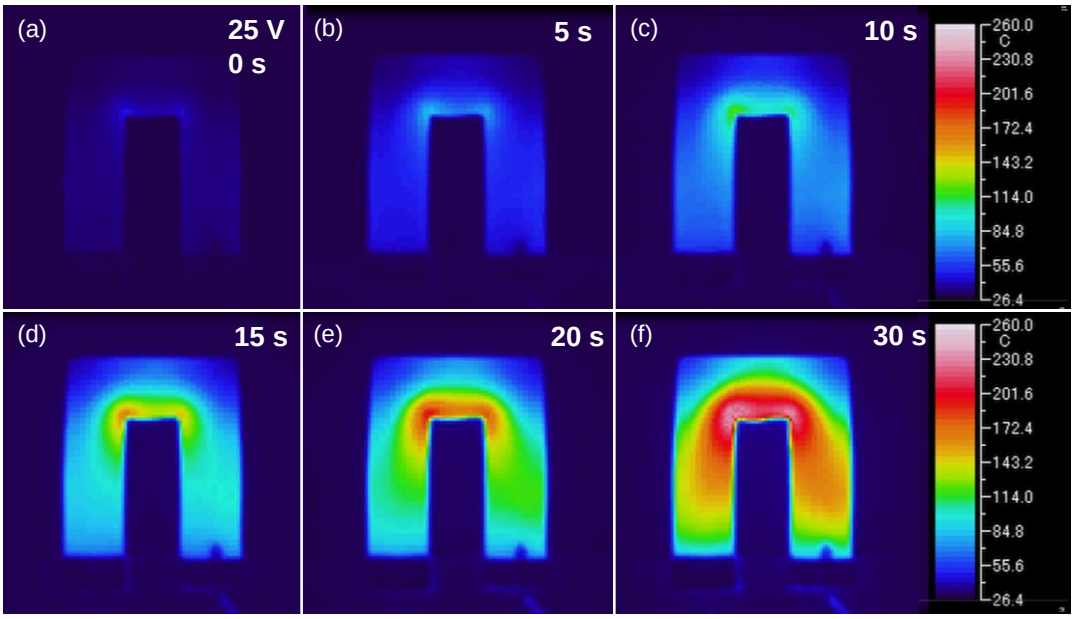

Figure 4-5 Thermographic images of 3D printed electric SMP actuator.

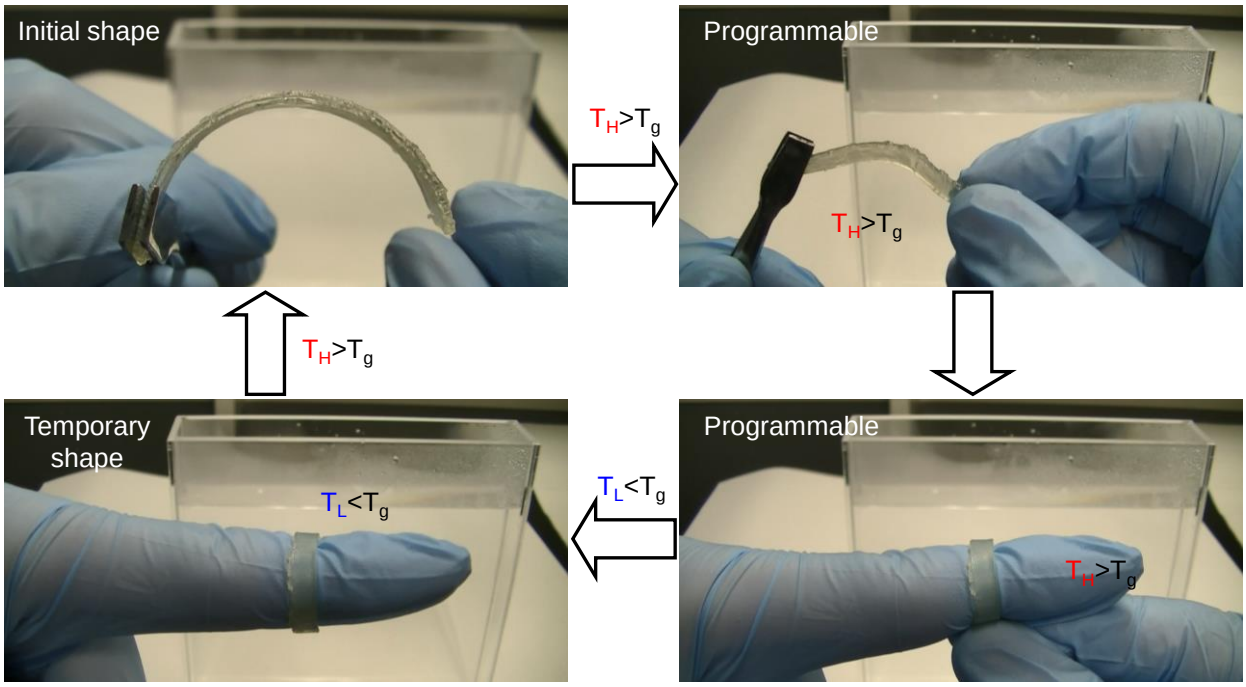

Figure 4-6 Shape memory effect of 3D printed ionic SMP gel.

4.4 Future prospective

In this chapter, 3D printable electric and ionic SMP filament was developed. And electroactive actuator can be driven Joule heating, as well as ionic SMP with good shape memory properties were printed by FDM 3D printing technology.

As I descripted in chapter 1, robot system will plays very important roles in future with the aged population increases. Many researchers have paid many attentions on the development of robot. As shown in Fig. 4-7, a 3D printed robots has been developed. In this robot system, the white body was printed by normal polylactic acid (PLA). The black parts which worked as nerve and joints or muscle to detect motions and provide force are traditional hard machines (motion sensors and electricity motors). It should be noted that only the white body is 3D printable in this robot system. And it will limit the partial applications of this 3D printed robot. In this dissertation, novel electric and ionic SMP were developed, they can work as electroactive actuator and flexible motion sensors, respectively. And both of them are 3D printable. This provide a strategy to develop intelligent soft robots. As a 3D printable intelligent soft robot can be fabricated by 3D printing electric SMP as soft actuators and ionic SMP as multi-functional flexible sensors, as shown in Fig. 4-7.

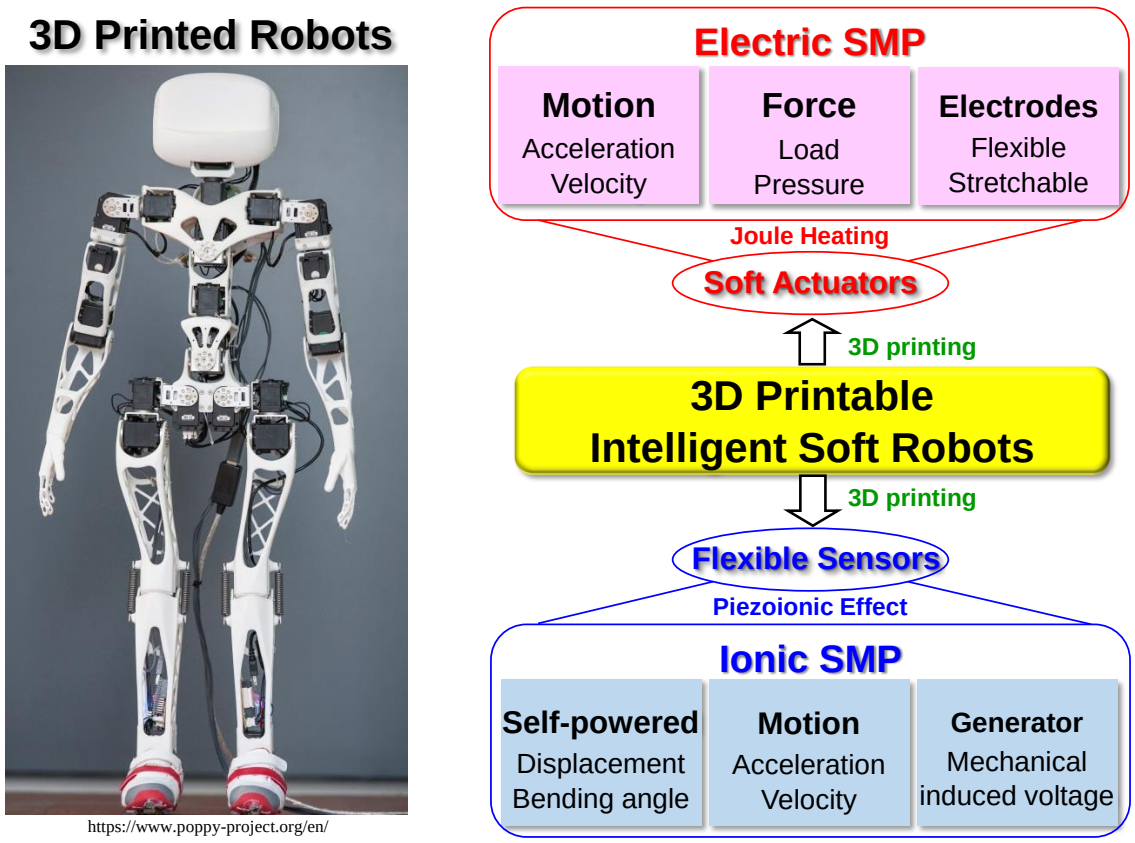

Figure 4-7 3D printed robot system. The possible 3D printable intelligent soft robot system fabricated by electric and ionic SMP as soft actuators and flexible sensors, respectively.

4.5 References

1) X Xu, P Martineza, C Madla, F Joubert, A Goyanes, A Basit and S Gaisford. Stereolithography (SLA) 3D printing of an antihypertensive polyprintlet: Case study of an unexpected photopolymer-drug reaction. Addit. Manuf. **33**, 101071, 2020.
2) Rafael Cardoso, P Silva, A Lima, D Rocha, T Oliveira, T Prado, E Fava, O Filho, E Richter and R.Muñoz. 3D-Printed graphene/polylactic acid electrode for bioanalysis: Biosensing of glucose and simultaneous determination of uric acid and nitrite in biological fluids. Sens. Actuators B Chem. **307**, 127621, 2020.
3) E Oztemel and S Gursev. Literature review of Industry 4.0 and related technologies. J Intell Manuf. 31, 127, 2020.

4) A Lee, A Hudson, D Shiwarski, J Tashman, T Hinton, S Yerneni, J Bliley, P Campbell and A Feinberg. 3D bioprinting of collagen to rebuild components of the human heart. Science, **365**, 482, 2019.
5) N Noor, A Shapira, R Edri, I Gal, L Wertheim and T Dvir. 3D printing of personalized thick and perfusable cardiac patches and hearts. Adv. Sci. **6**, 1900344, 2019.
6) M Luo, T Fan, Y Zhou, H Zhang and L Mei. 2D black phosphorus–based biomedical applications. **29**, 1808309, 2019.
7) X Wang, M Jiang, Z Zhou, J Gou and D Hui. 3D printing of polymer matrix composites: A review and prospective. Compos. B. Eng. **110**, 442, 2017.
8) F Melchels, J Feijen and D Grijpma. A review on stereolithography and its applications in biomedical engineering. Biomaterials, **31**, 6121, 2010.
9) R Goodridge, M Shofner, R Hague, M McClelland, M Schlea, R Johnson and C Tuck. Processing of a Polyamide-12/carbon nanofibre composite by laser sintering. Polym Test. **30**, 94, 2011.
10) S Murphy, A Atala. 3D bioprinting of tissues and organs. Nat Biotechnol. **32**, 773, 2014.
11) A Sood, R Ohdar and S Mahapatra. Parametric appraisal of mechanical property of fused deposition modelling processed parts. Mater Des, **31**, 287, 2010.
12) S Leigh, R Bradley, C Purssell, D Billson and D Hutchins. A Simple, Low-cost conductive composite material for 3D printing of electronic sensors. PloS one. **7**, e49365, 2012.
13) J Odent, T Wallin, W Pan, K Kruemplestaedter, R Shepherd and E Giannelis. Adv. Funct. Mater. **27**, 1701807, 2017

Chapter 5 Electromechanical Properties and Structure of Stretchable and Highly Conductive Polymer Hydrogels

5.1 Introduction

Organic electronics originated from low cost, lightweight, and flexible electronics is developing through printed electronics, stretchable electronics, and recently into wearable electronics for the applications to flexible displays and touch panels, soft sensors and actuators[1,2]. Conductive polymers with high electrical conductivity have been extensively studied in organic electronic devices, such as transparent electrodes, organic light-emitting diodes, organic field-effect transistors, organic solar cells, and electrochemical capacitors[3,4]. However, the conductive polymers are intrinsically hard and brittle because of their rigid π-conjugated structures and strong intermolecular π-π interactions[5,6]. In contrast, polymer hydrogels are soft and wet materials consisting of a three-dimensional polymer network swollen in water, which undergo significant changes of their physicochemical properties in response to various environmental stimuli, such as temperature, pH, light, biomolecules, salts, electric field, etc.[7,8] Furthermore, the hydrogels have been paid considerable attention as biocompatible materials for a variety of applications such as biosensors, bio-separation, drug delivery system, tissue engineering scaffolds, and artificial muscles[9]. However, the hydrogels have poor electrical conductivity due to the ionic conduction, which limits the application of hydrogels to the organic electronics. Therefore, combination between the highly conductive polymer and soft and wet hydrogel at the molecular level may generate a novel composite of electro-conductive hydrogels[10-14]. Indeed, many composites of conductive polymer hydrogels have been so far prepared by in situ polymerization of the conductive polymer inside the hydrogel matrices[15-21], but the composites were still mechanically weak with poor electrical conductivity. Kishi et al. fabricated mechanically tough electro-conductive double-network (E-DN) gels by oxidative polymerization of 3,4-ethylenedioxythiophene (EDOT) in a double-network hydrogel matrix composed of poly(styrenesulfonic acid) as the first network and poly(*N*,*N*-dimethylacrylamide) as the second network[20]. The E-DN gels showed Young's modulus and fracture stress of 3 MPa and 2 MPa, respectively, with a conductivity on the order of 1 S cm^{-1}.

In this study, novel stretchable and highly conductive polymer (S-CP) hydrogels were

fabricated by casting a water solution of poly(3,4-ethylenedioxythiophene) doped with poly(4-styenesulfonic acid) (PEDOT:PSS) and polyacrylamide (PAAm) and subsequent swelling in water. The results demonstrated that the S-CP gel containing 64 wt% of PAAm showed excellent stretchability over 100% and the electrical conductivity of 17 S cm^{-1} in the swollen state, which will open up a new field of soft and wet electronics using hydrogels, namely, "gelectronics".

5.2 Experimental methodologies

5.2.1 Materials

The PEDOT:PSS water dispersion (1.5 wt%) used in this study was synthesized in our laboratory by oxidative polymerization of EDOT monomer (Aldrich) in the presence of PSS (M_w = 75,000 g/mol, Aldrich) where the composition ratio between the repeating units of PEDOT and PSS was 1:2.5[22]. Polyacrylamide (PAAm) ($M_w = 5\times10^6$ g mol^{-1}, Wako Pure Chemistry) was purchased and used without further purification. Ethylene glycol (EG, Tokyo Chemistry Industry) as a secondary dopant to improve the electrical conductivity of the PEDOT:PSS[23-26] was used as received.

5.2.2 Fabrication of S-CP gels

The PAAm was dissolved in deionized water by stirring at room temperature for 2 h to prepare 1.5 wt% solution. Then, the PAAm solution was mixed with the PEDOT:PSS water dispersion with 5 wt% of EG at the different feed weight ratios of PAAm ($W_{PAAm\ feed}$). The mixed solution was cast on a slide glass and dried at 140 °C with a moisture analyzer (MOC-120H, Shimadzu). Subsequently the films were immersed in pure water overnight to prepare the water swollen S-CP gels. Fig. 5-1 shows relation between $W_{PAAm\ feed}$ and actual weight ratio of PAAm (W_{PAAm}). When the PEDOT:PSS film without PAAm ($W_{PAAm\ feed}$ = 0 wt%) was immersed in water, no notable weight loss was measured after drying, which can be explained by crosslinking of anionic PSS chains through electrostatic interaction with cationic PEDOT nanocrystals[26,27]. On the other hand, the dry weight of the S-CP gels decreased after immersing in water until 30 min and reached a constant values, indicating that the water-soluble PAAm on the surface was partially dissolved in water.

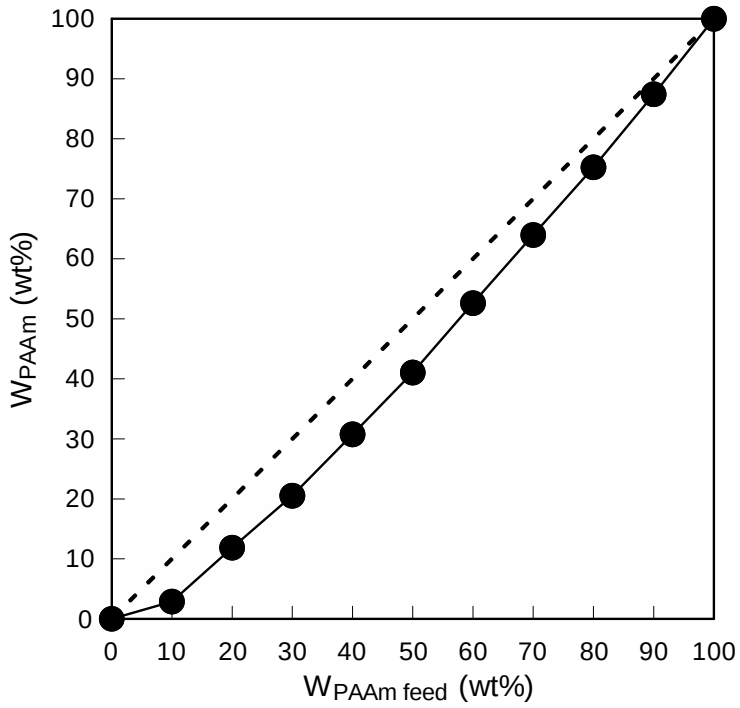

Figure 5-1 Relation between feed weight ratio of PAAm ($W_{PAAm\ feed}$) and actual weight ratio of PAAm (W_{PAAm}) in S-CP gels. The dotted line represents the theoretical straight line.

5.2.3 Characterization of S-CP gels

The electrical conductivity of the S-CP gels was measured with a Loresta-GP (MCP-T610, Mitsubishi Chemical Analytech) equipped with a four-point probe (LSP, Mitsubishi Chemical Analytech), where the water content was evaluated with a moisture analyzer (MOC-120H, Shimadzu). The mechanical properties of the S-CP gels (20 mm long, 2 mm wide, and 70-280 μm thick) were measured with a tensile tester (EZ-TEST, Shimadzu) equipped with a 500 N load cell at a constant strain rate of 20 %/min. Young's modulus, fracture stress, and fracture strain were calculated from the stress-strain curves. Time dependence of water content of the S-CP gel (W_{PAAm} = 64 wt%) was measured and the result was shown in Fig. 5-2. The S-CP gel was almost dry after 4 h in air, but the weight was nearly constant up to 30 min. Therefore, all measurement were carried out in air within 30 min. The morphology of the S-CP gels were evaluated with a scanning electron microscope (SEM) (S-4300, Hitachi) at an accelerating voltage of 3 kV, where the S-CP gels were freeze-dried with a freeze dryer (DC401, Yamato Scientific). The distributions of oxygen, nitrogen, and sulfur elements in the freeze-dried S-CP gels were characterized with an electron probe micro analyzer (EPMA) (JXA-8200, JEOL) at an accelerating voltage of 10 kV. The resistance change

of the S-CP gel at W_{PAAm} = 64 wt% was measured by a two-probe method with a potentiostat (HA-30, Hokuto Denko) under stretching using the tensile tester.

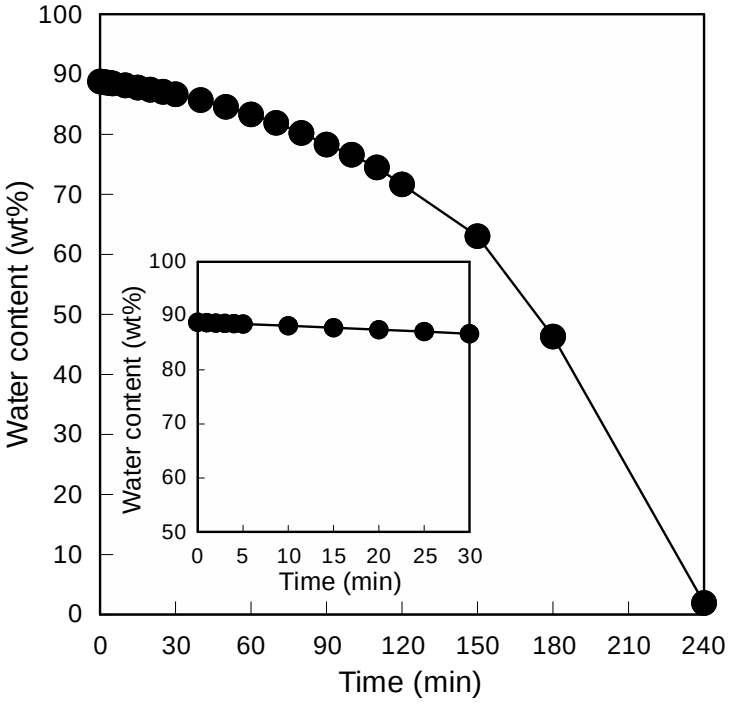

Figure 5-2. Time dependence of water content of S-CP gel (W_{PAAM} = 64 wt%) measured in air.

5.3 Results and discussion

5.3.1 Mechanical properties

Fig. 5-3 shows stress-strain curves and water content of the S-CP gels with different weight ratios of the PAAm (W_{PAAm}). It was found that the PEDOT:PSS gel (W_{PAAm} = 0 wt%) with a water content of 86% was soft but brittle because hydrogen bonding between sulfonic acid groups of the PSS on the PEDOT:PSS colloidal particles forms a network structure and/or PEDOT nanocrystals may crosslink the PSS chains through formation of polyion complex by electrostatic interactions[26,27]. It is seen from Fig. 5-4 that the mechanical properties are strongly dependent on the W_{PAAm}: Upon adding 3 wt% of PAAm, the water content drops but Young's modulus and fracture stress significantly increase and the values attain 142 MPa and 16.8 MPa, respectively, which are more than one order of magnitude higher than those of the E-DN gels[20].

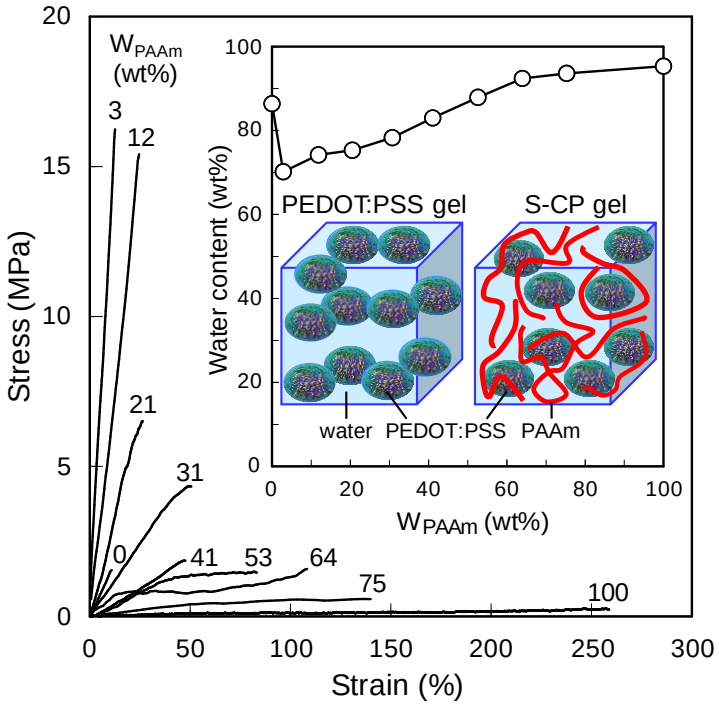

Figure 5-3 Stress-strain curves of S-CP gels with different W_{PAAm}. Inset: Dependence of water content of S-CP gels on W_{PAAm} and schematic diagrams of PEDOT:PSS and S-CP gels.

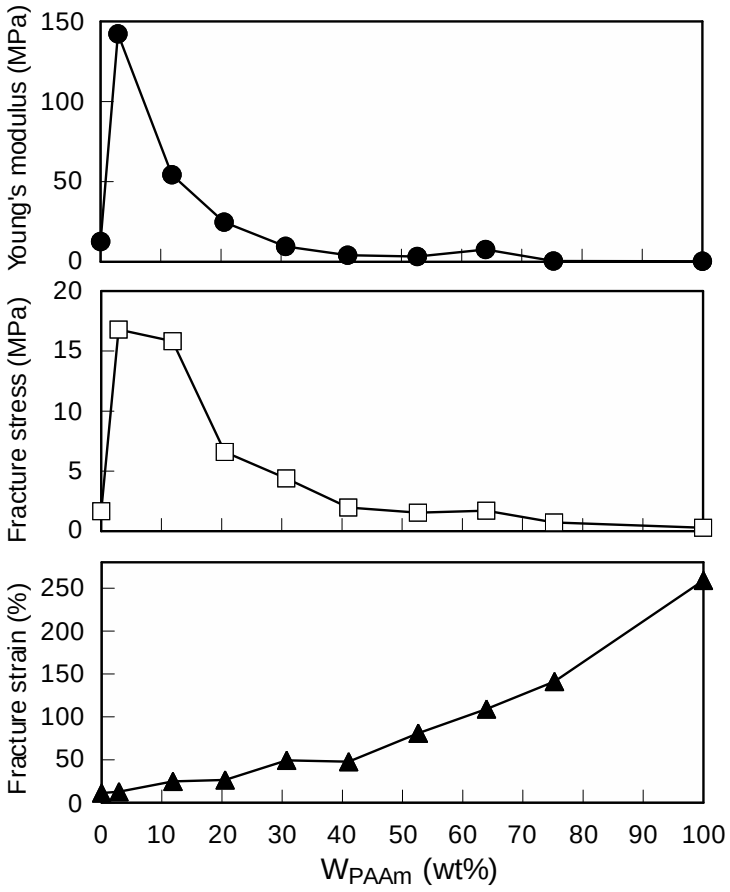

Figure 5-4 Dependence of Young's modulus, fracture stress, and fracture strain of S-CP gels on W_{PAAm}.

This suggests that the PAAm penetrates into the spatial gaps of the PEDOT:PSS network as a filler, similarly to double-network gels[28-30], in which the soft and flexible PAAm suppresses stress concentration on the fragile PEDOT:PSS network. An increase of the W_{PAAm} decreases both Young's modulus and fracture stress but increases fracture strain and water content, demonstrating that the S-CP gel becomes soft and stretchable due to the PAAm. Indeed, the pure PAAm gel (W_{PAAm} = 100 wt%) having a water content of 95% showed low values of Young's modulus (0.34 MPa) and fracture stress (0.28 MPa). It should be noted that the fracture strain attained as high as 100% at W_{PAAm} > 64 wt%.

5.3.2 Electrical properties

A clear indication of the importance of PEDOT:PSS on electrical conductivity is demonstrated in Fig. 5-5. In the solid state, the highest electrical conductivity of the PEDOT:PSS dry film (781 S cm^{-1}) linearly decreases with increasing the W_{PAAm} because the PAAm is an insulator. According

to the percolation theory [31], the electrical conductivity (σ) can be described using a volume fraction of the PEDOT:PSS (φ) as follows

$$\sigma = \sigma_0 (\varphi - \varphi_c)^t \qquad (5\text{-}1)$$

where φ_c, t, and σ_0 are the percolation threshold, critical exponent, and constant, respectively. As shown in the inset of Fig. 5-5, the electrical conductivity of the S-CP solid films can be expressed by the percolation theory where the parameters calculated using the densities of the PEDOT:PSS (1.43 g cm^{-3}) and PAAm (1.31 g cm^{-3}) are φ_c = 0.46 vol%, t = 1.65, and σ_0 = 766 S cm^{-1}. Here, the φ_c value is smaller than that of the carbon black-polyethylene composite (φ_c = 11%)[32], indicative of a predominant conduction path. Furthermore, the t value suggests that the S-CP solid films can be applied to two-dimensional percolation (t = 1.33)[31] which will be discussed later. On the other hand, the percolation theory does not apply to the S-CP gels in the swollen state: The conductivity of the PEDOT:PSS gel (95 S cm^{-1}) significantly increased to 243 S cm^{-1} by adding 3 wt% of PAAm and subsequently decreased with increasing the W_{PAAm}, which is probably due to the variation of water content (Figure 5-1) and/or phase segregation of the S-CP gels. We should emphasize here that the S-CP gel at W_{PAAm} = 64 wt% shows excellent electrical conductivity (17 S cm^{-1}) and fracture strain (110%) in spite of the high water content (92%). The performance of the S-CP gel is much higher than the E-DN gels containing 74% of water with electrical conductivity and fracture strain of ca. 1 S cm^{-1} and 76%, respectively[20]. Moreover, the S-CP gels can be fabricated by a fast and facile casting technique, whereas the E-DN gels were synthesized by oxidative polymerization of EDOT monomer for one week in a double-network hydrogel[20].

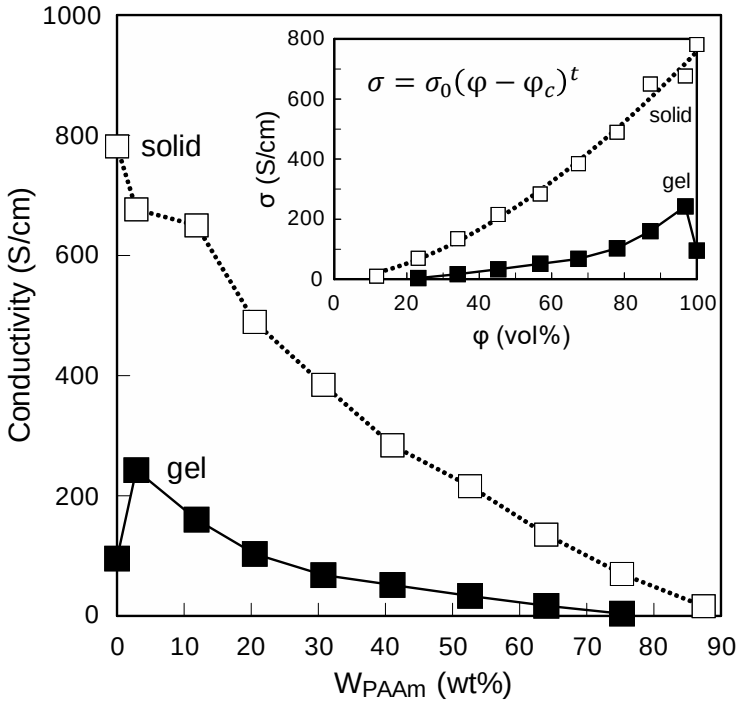

Figure 5-5 Dependence of electrical conductivity of S-CP on W_{PAAm} in gel and solid states. Inset: Relation between the electrical conductivity (σ) and volume fraction of PEDOT:PSS (φ) for S-CP in gel and solid states.

5.3.3 Structure and morphology

In order to clarify the mechanism of high conductivity and stretchability of the S-CP gels, morphology was measured by a scanning electron microscope (SEM) and results are shown in Fig. 5-6. It was found that the PEDOT:PSS gel (W_{PAAM} = 0 wt%) shows layered structure, in which a number of layers with a thickness of several hundred nm stuck in parallel in the direction of the film thickness. The S-CP gel at W_{PAAm} = 3 wt% also shows the layered structure where the PAAm may be filled in between the layers, which will be responsible for the lower water content (Fig. 5-3) and higher values of Young's modulus and fracture stress (Fig. 5-4). In contrast, the PAAm gel (W_{PAAm} = 100 wt%) shows a porous uniform network structure formed by entanglement of ultrahigh molecular weight of the PAAm ($M_w = 5\times10^6$ g mol^{-1}). With increasing the W_{PAAm}, the layered structure gradually changed to porous network structure, which increased water content and fracture strain of the S-CP gels.

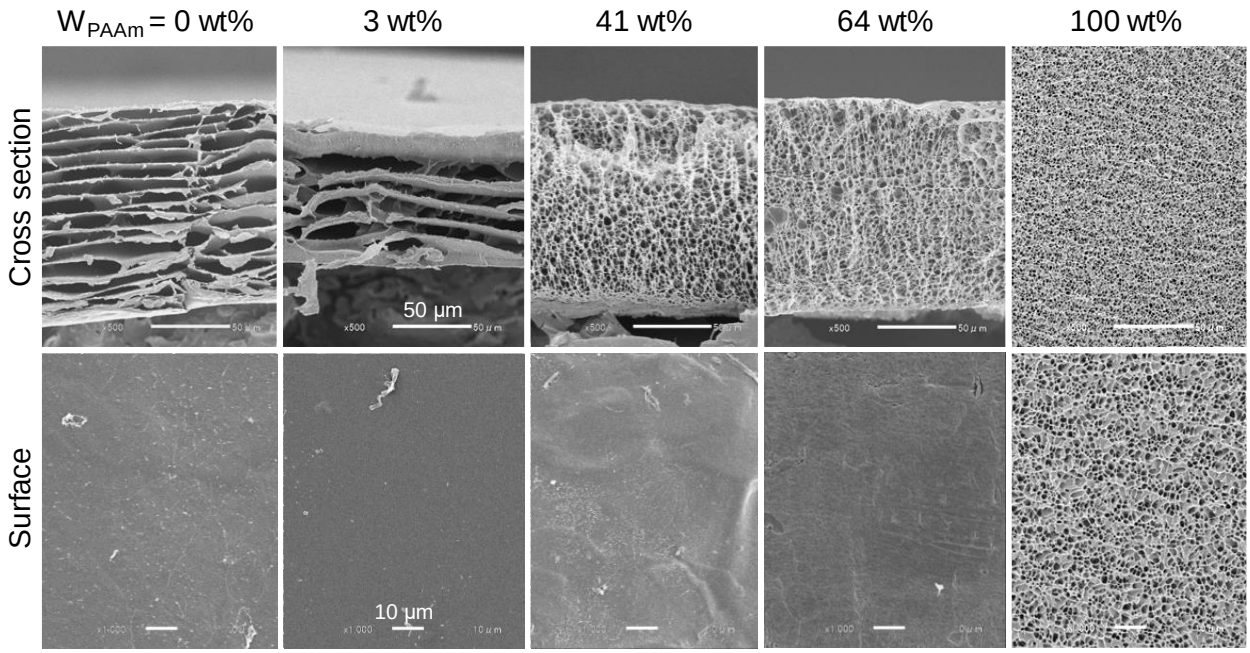

Figure 5-6. SEM micrographs of cross section and surface of freeze-dried S-CP gels with different W_{PAAm}.

Furthermore, EPMA was carried out to investigate the detailed structure, and element mapping images of the S-CP gel at W_{PAAm} = 64 wt% were shown in Fig. 5-7. One can see the oxygen is distributed throughout the cross section and surface of the S-CP gel since both PEDOT:PSS and PAAm contain oxygen atoms. On the other hand, the nitrogen originated from the PAAm is seen both on the surface and in the cross section, but more distributed inside the S-CP gel, which is in good agreement with the SEM micrographs exhibiting the porous network structure (Fig. 5-6). In contrast, the sulfur contained in the PEDOT:PSS was localized on both surfaces and less inside the S-CP gel. Thus, the EPMA clearly indicates that the S-CP gels are composed of soft and stretchable PAAm-rich porous network structure formed by swelling in water surrounded by the PEDOT:PSS-rich conductive network layers probably formed by dissolution of PAAm on the surface when immersed in water. Indeed, the sulfur was uniformly and densely distributed in the cross section of the S-CP dry film before immersion in water (Fig. 5-8). The results are consistent with two-dimensional percolation as shown in Fig. 5-5 where the electric current flows though the conduction paths in the two-dimensional PEDOT:PSS-rich conductive network layers, leading to the high electrical conductivity even in the swollen state.

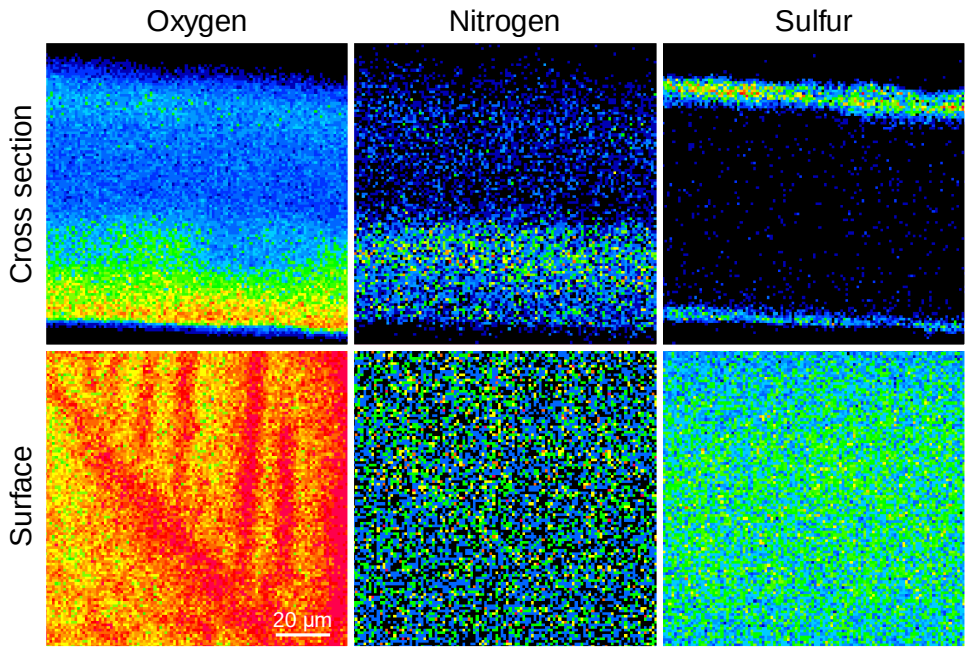

Figure 5-7 EPMA element mapping images of cross section and surface of S-CP gel (W_{PAAm} = 64 wt%).

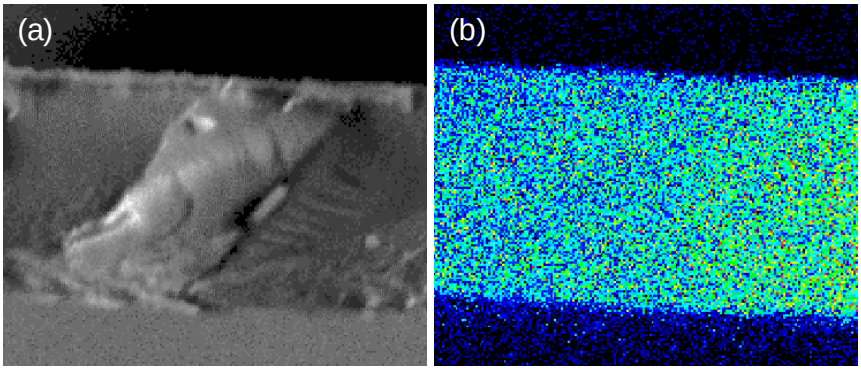

Figure 5-8 (a) SEM and (b) EPMA sulfur mapping images of cross section of S-CP dry film ($W_{PAAm\ feed}$ = 70 wt%) before immersing in water.

5.3.4 Electromechanical properties

Fig. 5-9 shows resistance change of the S-CP gel (10 mm long, 2 mm wide, and 130 μm thick) at W_{PAAm} = 64 wt% under repeated stretching by 50%. It was found that upon stretching the S-CP gel, the resistance was kept almost constant about 50-57 Ω despite of the fact that the distance between electrodes increases and the cross sectional area of the gel decreases. The similar phenomenon was observed at different strain rates of 150 %/min and 50 %/min (Fig.5-10), indicating that the electrical properties of the S-CP gel change rapidly in response to these strain

rates.

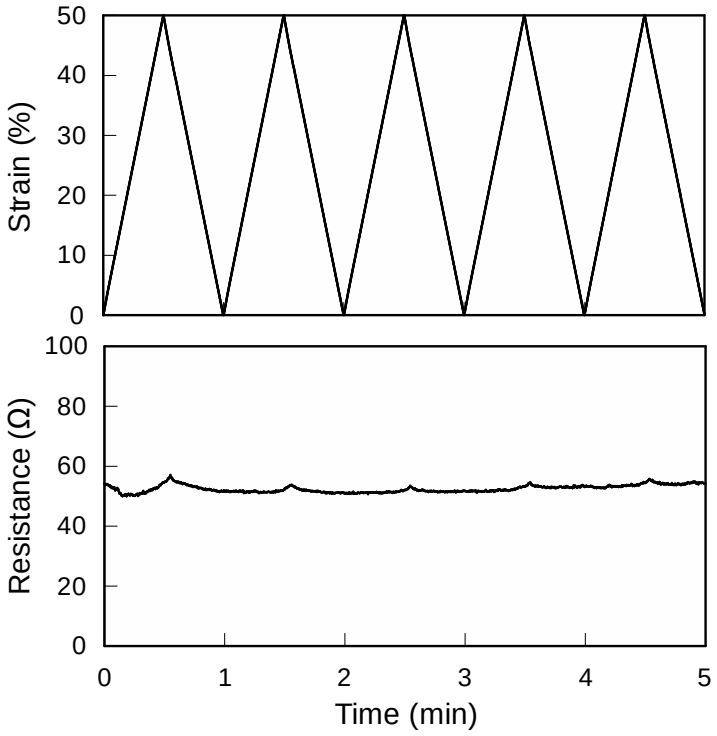

Figure 5-9 Resistance change of S-CP gel (10 mm long, 2 mm wide, and 130 μm thick) at W_{PAAm} = 64 wt% under repeated stretching by 50% at a constant strain rate of 100 %/min (applied voltage = 1 V).

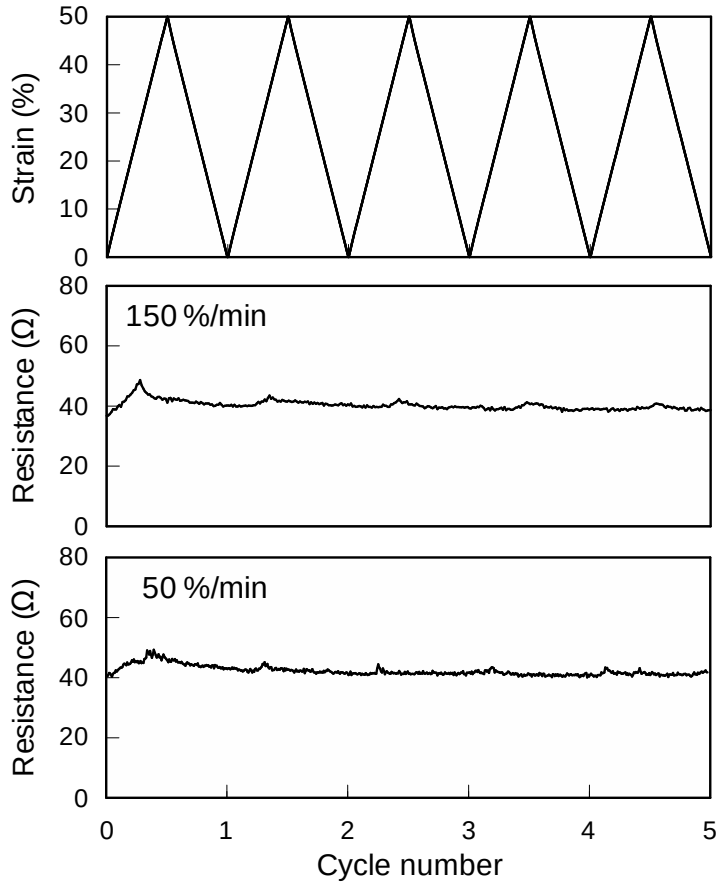

Figure 5-10 Resistance changes of S-CP gel (10 mm long, 2 mm wide, and 140 μm thick) at W_{PAAm} = 64 wt% under repeated stretching by 50% at constant strain rates of 150 %/min and 50 %/min (applied voltage = 1 V).

To evaluate the electromechanical properties in more detail, the electrical conductivity (σ) of the S-CP gel under stretching was calculated using the resistance (R), initial length (L) and cross sectional area (A) as follows[33)]

$$\sigma = L(1 + \varepsilon) / RA(1 - \nu\varepsilon)^2 \qquad (5\text{-}2)$$

where ε and ν are the strain and Poisson's ratio, respectively. Assuming that the Poisson's ratio of the S-CP gel is similar to that of the PAAm gel (ν = 0.46)[34)], the change in the electrical conductivity by stretching the S-CP gel was calculated using the resistance change. It is seen from Fig. 5-11 that no marked increase in the resistance was observed by stretching up to 75%, which clearly indicates an increase of the electrical conductivity. Indeed, the conductivity of the S-CP gel linearly increases from 10.4 S cm^{-1} to 23.8 S cm^{-1} with increasing the strain. On the other hand, the resistance sharply increases at strains higher than 75%, which corresponds to a drop of the

conductivity. Therefore, the mechanism can be considered as shown in Fig.5-12. The electric current flows through conduction paths in the PEDOT:PSS-rich conductive network layers on both sides of the gel, leading to the high electrical conductivity. Upon stretching the S-CP gel up to 75%, the PEDOT:PSS-rich conductive network layers are oriented along the stretching direction, which enhances the contact between the networks in the vertical direction and increases the conduction paths. This may enhance transport of charge carriers, thereby improving the electrical conductivity[35,36]. However, further stretching of the S-CP gel at strains higher than 75% results in an irreversible breakdown of the conduction paths in the PEDOT:PSS-rich conductive network layers by generating microcracks (Fig. 5-13), thereby dropping the electrical conductivity. In fact, even after removal of the stress, both length and conductivity of the S-CP gel did not recover to the initial values.

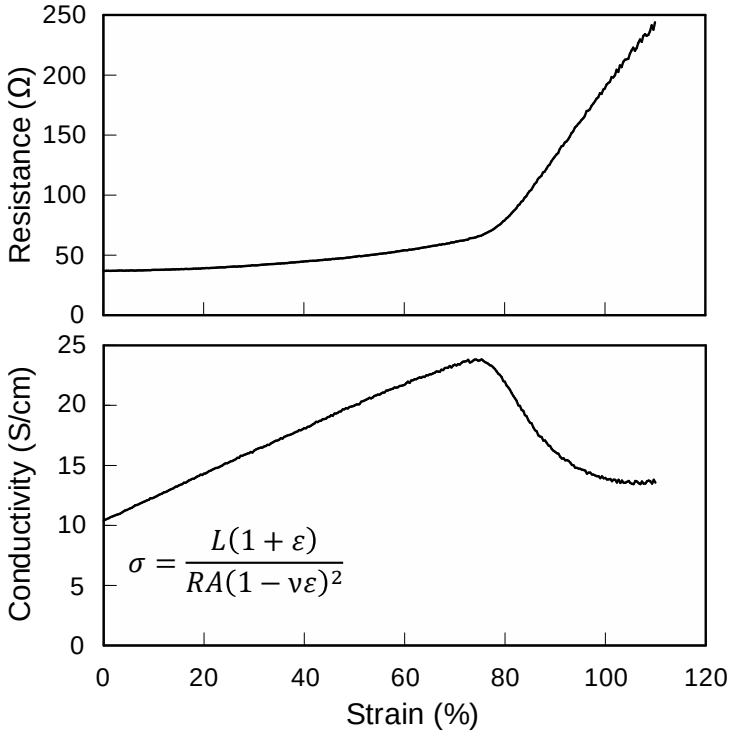

Figure 5-11 Changes in resistance and electrical conductivity of S-CP gel (10 mm long, 2 mm wide, and 130 μm thick) at W_{PAAm} = 64 wt% by stretching at a constant strain rate of 100 %/min.

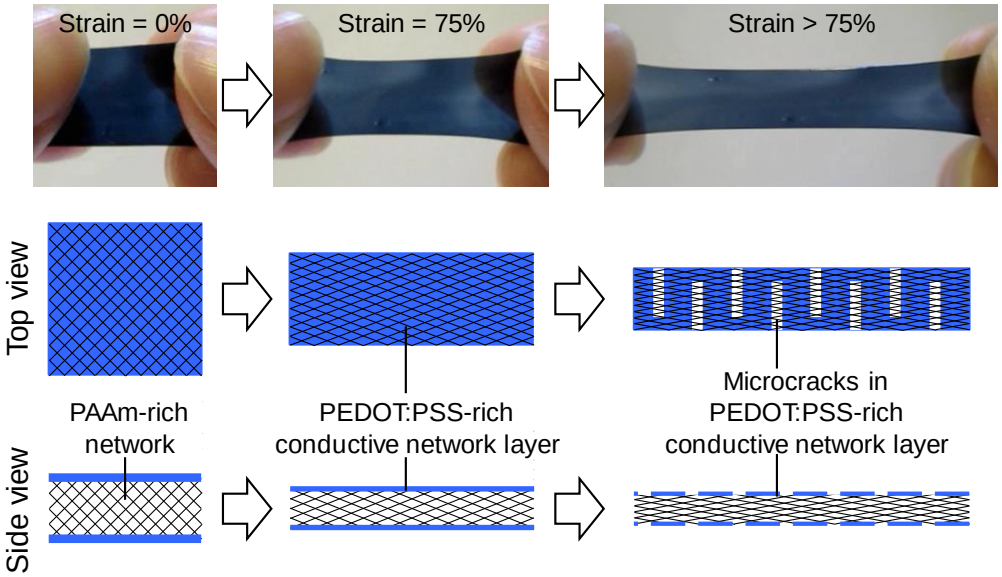

Figure 5-12 Possible mechanism of electromechanical properties of S-CP gels.

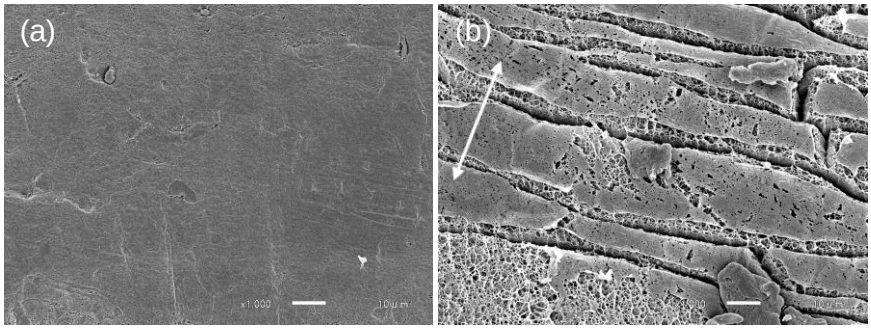

Figure 5-13 SEM micrographs of S-CP gel (W_{PAAm} = 64 wt%) surface (a) before and (b) after stretching by 100%. The scale bars correspond to 10 μm and the arrow indicates the stretching direction.

5.4 Conclusion

We have succeeded in fabricating novel stretchable and highly conductive S-CP gels consisting of PEDOT:PSS and PAAm with excellent electromechanical properties. At W_{PAAm} = 64 wt% the S-CP gel containing 92% of water exhibited the electrical conductivity and fracture strain of 17 S cm^{-1} and 110%, respectively. The SEM and EPMA measurements clearly demonstrated that the S-CP gel was composed of soft and stretchable PAAm-rich porous network surrounded by the PEDOT:PSS-rich conductive network layers. Unlike the conventional conductive rubbers with embedded conductive fillers such as carbon black in which the resistance rises by stretching[37], the

S-CP gels spontaneously improved the electrical conductivity in response to the external stimulus of stretching so as to keep the resistance constant. Thus, the S-CP gels have potential applications to smart electrodes of soft sensors and actuators as a novel intelligent material, which will open up a new field of organic electronics using soft and wet hydrogels, namely, “gelectronics”.

5.5 References

1) H. Klauk ed. Organic Electronics: Materials, Manufacturing and Applications Wiley-VCH, Weinheim, 2006.
2) H. Klauk ed. Organic electronics II: More Materials and Applications Wiley-VCH, Weinheim, 2010.
3) A. Elschner, S. Kirchmeyer, W. Lövenich, U. Merker and K. Reuter eds. PEDOT Principles and Applications of an Intrinsically Conductive Polymer CRC Press, 2010.
4) H. Okuzaki ed. PEDOT: Material Properties and Device Applications, Science & Technology, 2012.
5) H. Okuzaki, N. Ikeda, I. Kubota and T. Kunugi. Mechanical properties and structure of poly(p-phenylenevinylene) films prepared by the zone-reaction method. Macromolecules **32**, 5606, 1999.
6) H. Okuzaki and M. Ishihara. Spinning and characterization of conducting microfibers. Macromol. Rapid Commun. **24**, 261, 2003.
7) Y. Osada, H. Hori and H. Okuzaki. A polymer gel with electrically driven motility. Nature **355**, 242, 1992.
8) K. Asaka and H. Okuzaki eds. Soft Actuators: Materials, Modeling, Applications, and Future Perspectives Springer, 2014.
9) F. Carpi ed. Electromechanically Active Polymers - A Concise Reference Springer, 2016.
10) F. Zhao. J. Bae, X. Zhao, Y. Guo and G. Yu. Nanostructured functional hydrogels as an emerging platform for advanced energy technologies. Adv. Mater. **30**, 1801796, 2018.
11) P. Li, Z. Jin, L. Peng, F. Zhao, D. Xiao, Y. Jin and G. Yu. Stretchable all-gel-state fiber-shaped supercapacitors enabled by macromolecularly interconnected 3D graphene/nanostructured conductive polymer hydrogels. Adv. Mater. **30** 1800124, 2018.
12) F. Zhao, Y. Shi, L. Pan and G. Yu. Multifunctional nanostructured conductive polymer gels: synthesis, properties, and applications. Acc. Chem. Res. **50**, 1734, 2017.

13) Y. Shi, C. Ma, L. Peng and G. Yu. Conductive “smart” hybrid hydrogels with PNIPAM and nanostructured conductive polymers. Adv. Funct. Mater. **25**, 1219, 2015.

14) Y. Zhao, B. Liu, L. Pan and G. Yu. 3D nanostructured conductive polymer hydrogels for high-performance electrochemical devices. Energy Environ. Sci. **6**, 2856, 2013.

15) B. Kim, G. Spinks, G. Wallace and R. John. Electroformation of conducting polymers in a hydrogel support matrix. Polymer. **41**, 1783, 2000.

16) F. Vidal, C. Plesse, D. Teyssié and C. Chevrot. Long-life air working conducting semi-IPN/ionic liquid based actuator. Synth. Met. **142** 287, 2004.

17) S. Siddhanta and R. Gangopadhyay. Conducting polymer gel: formation of a novel semi-IPN from polyaniline and crosslinked poly (2-acrylamido-2-methyl propanesulphonicacid). Polymer. **46**, 2993, 2005.

18) T. Yamauchi, S. Tansuriyavong, K. Doi, K. Oshima, M. Shimomura, N. Tsubokawa, S. Miyauchi and J. Vincent. Preparation of composite materials of polypyrrole and electroactive polymer gel using for actuating system. Synth. Met. **152**, 45, 2005.

19) R. Kishi, K. Hiroki, T. Tominaga, K. Sano, H. Okuzaki, J. Martinez, T. Otero and Y. Osada. Electro-conductive double-network hydrogels. J. Polym. Sci. Polym. Phys. **50**, 790, 2012.

20) R. Kishi, K. Kubota, T. Miura, T. Yamaguchi, H. Okuzaki and Y. Osada. Mechanically tough double-network hydrogels with high electronic conductivity. J. Mater. Chem. C. **2**, 736, 2014.

21) A. Maziz, C. Plesse, C. Soyer, C. Chevrot, D. Teyssié, E. Cattan and F. Vidal. Demonstrating kHz frequency actuation for conducting polymer microactuators. Adv. Funct. Mater. **24** 4851, 2014.

22) T. Horii, H. Hikawa, M. Katsunuma and H. Okuzaki. Synthesis of highly conductive PEDOT:PSS and correlation with hierarchical structure. Polymer. **140**, 33, 2018.

23) S. Ashizawa, R. Horikawa and H. Okuzaki. Effects of solvent on carrier transport in poly (3,4-ethylenedioxythiophene)/poly (4-styrenesulfonate). Synth. Met. **153**, 5, 2005.

24) T. Takano, H. Masunaga, A. Fujiwara, H. Okuzaki and T. Sasaki. PEDOT nanocrystal in highly conductive PEDOT: PSS polymer films. Macromolecules **45** 3859, 2012.

25) H. Yan and H. Okuzaki. Effect of solvent on PEDOT/PSS nanometer-scaled thin films: XPS and STEM/AFM studies. Synth. Met. **159**, 2225, 2009.

26) T. Horii, Y. Li, Y. Mori and H. Okuzaki. Correlation between the hierarchical structure and electrical conductivity of PEDOT/PSS. Polym. J. **47**, 695, 2015.

27) H. Okuzaki, H. Suzuki and T. Ito. Electromechanical properties of poly (3, 4-ethylenedioxythiophene)/poly (4-styrene sulfonate) films. J. Phys. Chem. B. **113**, 11378, 2009.

28) J. Gong, Y. Katsuyama, T. Kurokawa and Y. Osada. Double-network hydrogels with extremely high mechanical strength. Adv. Mater. **15** 1155, 2003.

29) M. Huang, H. Furukawa, Y. Tanaka, T. Nakajima, Y. Osada and J. Gong. Importance of entanglement between first and second components in high-strength double network gels. Macromolecules **40**, 6658, 2007.

30) T. Nakajima, N. Takedomi, T. Kurokawa, H. Furukawa and J. Gong. A facile method for synthesizing free-shaped and tough double network hydrogels using physically crosslinked poly(vinyl alcohol) as an internal mold. Polym. Chem. **1**, 693, 2010.

31) D. Stauffer and A. Aharony. Introduction to Percolation Theory: Revised Second Edition CRS Press, 1994.

32) H. Yoon, K. Kwon, K. Nagata and K. Takahashi. Changing the percolation threshold of a carbon black/polymer composite by a coupling treatment of the black. Carbon. **42**, 1877, 2004.

33) I. Sokolnikoff. Mathematical Theory of Elasticity Krieger Malabar FL, 1983.

34) T. Takigawa, Y. Morino, K. Urayama and T. Masuda. Polym. Gels Networks **4**, 1, 1996.

35) T. Kunugi and H. Okuzaki. Electrical and mechanical properties of the zone-drawn polypyrrole films. J. Polym. Sci. Polym. Phys. **34**, 1269, 1996.

36) S. Pomfreta, P. Adamsa, N. Comfortb and A. Monkmana. Electrical and mechanical properties of polyaniline fibres produced by a one-step wet spinning process. Polymer **41**, 2265, 2000.

37) J. Donnet and A. Voet. Carbon Black: Physics, Chemistry, and Elastomer Reinforcement M. Dekker, 1976.

Chapter 5 General Conclusions and Outlook

5.1 General conclusions

In this study, novel electric SMP and ionic SMP were fabricated using shape memory polymer. The electric SMP exhibits actuation after applying voltage while the ionic SMP shows electric response under mechanical stimulate. Furthermore, a stretchable conductive polymer gel with high electric conductivity was fabricated using PAAm and PEDOT:PSS, which can be used as stretchable electrodes in the flexible and wearable devices.

The electric SMP was fabricated by compositing shape memory polymer with novel conductive polymer (S-PEDOT) in DMSO solution. The crystalline S-PEDOT formed conductive networks in the SMP matrix, leading to high electric conductivity and extremely low percolation threshold. The glass transition temperature (T_g) of the electric SMPs was ~50ºC at $W_{S\text{-}PEDOT} \leq 30$ wt%. The shape memory properties of the electric SMPs were evaluated by TMA. The electric conductivity of the electric SMP increased in proportion to S-PEDOT contents while the shape memory properties decreased with increasing S-PEDOT ratios in the electric SMP. The electric SMP at $W_{S\text{-}PEDOT} = 10$ wt% exhibited electric conductivity (σ), shape fixing ratio (R_f) and shape recovery ratio (R_r) of 29 S cm^{-1}, 95.4 % and 90.1 %, respectively. The electrical and shape memory properties were better than other electric SMPs which were fabricated by carbon black, graphene, carbon nanotubes or PEDOT:PSS composited with SMP, due to the good miscibility between S-PEDOT and SMP. The good electric and shape memory properties of the electric SMP indicated it can be applied electro-active actuators. Furthermore, an electro-active SMP soft actuator was fabricated using the electric SMP with 10 wt% of S-PEDOT, quickly recovered from the temporary bent shape to its original open shape with 5 s upon application of 6 V.

The ionic SMP was fabricated using shape memory polymer and ionic liquid (EMI^+TFSI^-). The ionic SMP/PEDOT:PSS exhibited sensing behaviors under mechanical stimulate. The ionic SMPs were used as acceleration sensors and displacement sensors. The electric charges increased in proportion to the IL content, leading to the increasing of acceleration sensitivity. The highest acceleration sensitivity was achieved as 13.7 nC m^{-1} s^2 at $W_{IL} = 30$ wt%. Due to the difference of the molar ionic conductivity between cations and anions, the transfer number of cations and anions are different, leading to the potential difference between the two electrodes under the mechanical stimulate. The generated voltage increased in proportion in the bending displacements while less

dependent on the accelerations, indicated the ionic SMP can be used as non-powered displacement sensors. Furthermore, we claimed that the generated voltage is strongly dependent on the total transferred charges (ΔQ) under the mechanical stimulate and the capacitance (C) of the ionic gel sensors. The highest voltage was achieved at W_{IL} = 30 wt%, as high as 5.96 mV, which can be explained by the largest ΔQ and relative lower C. Furthermore, the ionic SMP exhibited shape memory property of R_f = 86.9 %, R_r = 89.8 % at W_{IL} = 10 wt%.

Furthermore, a novel stretchable and highly conductive S-CP gel was fabricated using PAAm and PEDOT:PSS. The S-CP gel exhibited highly electrical conductivity and large fracture strain of 17 S cm^{-1} and 110% at W_{PAAm} = 64 wt%. The S-CP gel was composed of soft and stretchable PAAm-rich porous network surrounded by the PEDOT:PSS-rich conductive network layers. The S-CP gels spontaneously improved the electrical conductivity in response to the external stimulus of stretching so as to keep the resistance constant. The S-CP gels have potential applications to smart electrodes of soft sensors and actuators as flexible and stretchable electrodes, namely, 'gelectronics'.

5.2 Outlook

In the view of energy consumption, non-powered sensors and energy generators will play very important roles in future. Compared with electromagnetic[1)], piezoelectric[2-6)] and triboelectric[7-11)] non-powered sensors or energy generator, piezoionic sensors exhibit some distinguished advantages, such as stable output voltage signals, response to not only the displacements but also the accelerations and directions and so on. Piezoionic gels are a good candidate for the flexible non-powered sensors and generators. The output voltage should be improved much more.

In this research, the sensing performance of the ionic SMP and the mechanism of the piezoionic effect were investigated in detail. The results clearly indicated that the generated voltage strongly dependent on the combination of total transferred electric charges (ΔQ) under mechanical bending and capacitance (C) of the ionic SMP gels, as shown in follow equation:

$$V = \frac{\Delta Q}{C} = \frac{Q_+ - Q_-}{C}$$

The measured voltage was highly agreed with that calculated by the equation. This equation provides a direction for increasing the sensitivity of the non-powered displacement sensors. By increasing the total transferred charges (ΔQ) and reducing the capacitance (C) of the ionic polymer

gels, the generated voltage will be improved. ΔQ was determined by the difference between transferred cations (Q+) and anions (Q-). Q+ and Q- related to the transfer number of cations (t_+) and anions (t_-) of the ionic liquid in the polymer matrix. Large Q+ and small Q- will result in large ΔQ, leading to the larger voltage. The selection of ionic liquid is important for the generated voltage. It is potential to applying piezoionic gels to non-powered sensors and energy generator.

On the other hand, the fundamental theory of the piezoionic effect is related to the elastic modulus of the materials, mobility of the ions, diffusion constant, cation and anion concentration, dielectric constant of the materials and so on. In order to understanding on the ionic sensing mechanisms, investigating the transport process of ions of ionic polymer gels is necessary. Many multi-physical models of cation and water transport in ionic polymer-metal composite sensors (single ion transferred) had been built[12-15]. But there is no model to discuss the ionic liquid-polymer gels (double ions transferred). So developing of multi-physical model of the ionic liquid polymer gels is an effect way to understanding on the sensing mechanism.

5.3 References

1) S. Li, J. Yuan and H. Lipson. Ambient wind energy harvesting using cross-flow fluttering, J. Appl. Phys. **109**, 026104, 2011.
2) J. Smoker, M. Nouh, O. Aldraihem and A. Baz. Energy harvesting from a standing wave thermoacoustic-piezoelectric resonator, J. Appl. Phys. **111**, 787, 2012.
3) D. Li, S. Hong, S. Gu, Y. Choi, S. Nakhmanson, O. Heinonen, D. Karpeev and K. No. Polymer piezoelectric energy harvesters for low wind speed, Appl. Phys. Lett. **104**, 604, 2014.
4) M. Lee, C Chen, S. Wang, S. Cha, Y. Park, J. Kim, L. Chou and Z. Wang. A hybrid piezoelectric structure for wearable nanogenerators. Adv. Mater. **24**, 1759, 2012.
5) J. Chang, M. Dommer, C. Chang and L. Lin. Piezoelectric nanofibers for energy scavenging applications. Nano Energy. **1**, 356, 2012.
6) W. Wu, S. Bai, M. Yuan, Y. Qin, Z. Wang and T. Jing. Lead zirconate titanate nanowire textile nanogenerator for wearable energy-harvesting and self-powered devices. ACS Nano. 6, 6231, 2012.
7) Z. Wang, J. Chen and L. Lin, Progress in triboelectric nanogenerators as a new energy technology and self-powered sensors. Energy Environ. Sci. **8**, 2250, 2015.

8) F. Fan, Z. Tian and Z. Wang, Flexible triboelectric generator. Nano Energy. **1**, 328, 2012.

9) Z. Lin, G. Zhu, Y. Zhou, Y. Yang, P. Bai, J. Chen and Z. Wang, A self-powered triboelectric nanosensor for mercury ion detection. Angew. Chem. Int. Ed. **52**, 5065, 2013.

10) Z. Lin, Y. Xie, Y. Yang, S. Wang, G. Zhu and Z. Wang, Enhanced triboelectric nanogenerators and triboelectric nanosensor using chemically modified TiO2 nanomaterials. ACS Nano. **7**, 4554, 2013.

11) S. Wang, L. Lin, Y. Xie, Q. Jing, S. Niu and Z. Wang, Sliding-triboelectric nanogenerators based on in-plane charge-separation mechanism. Nano Lett. **13**, 2226, 2013.

12) Z. Zhu, L. Chang, T. Horiuchi, K. Takagi, A. Aabloo, and K. Asaka. Multi-physical model of cation and water transport in ionic polymer-metal composite sensors. J. Appl. Phys. **119**, 124901, 2016.

13) T. Stalbaum, D. Pugal, S. Nelson, V. Palmre, and K. Kim. Physics-based modeling of mechano-electric transduction of tube-shaped ionic polymer-metal composite. J. Appl. Phys. **117**. 114903, 2015.

14) Z. Zhu, K. Asaka, L. Chang and K. Takagi. Multiphysics of ionic polymer-metal composite actuator. J. Appl. Phys. **114**, 084902, 2013.

15) Z. Zhu, Y. Wang, Y. Liu, K. Asaka, X. Sun, L. Chang and P. Lu. Application-oriented simplification of actuation mechanism and physical model for ionic polymer-metal composites. J. Appl. Phys. **120**, 034901, 2016.

Research achievements

Peer-reviewed journal articles

1) **Y. An**, K. Iwashita, H. Okuzaki, Electromechanical properties and structure of stretchable and highly conductive polymer hydrogels, *Multifunct. Mater.*, **2**, 014001 (2019)
2) **Y. An**, H. Okuzaki, Novel electro-active shape memory polymers for soft actuators, *Jpn. J. Appl. Phys.*, **59**, 6 (2020)

Manuscripts to be submitted

1) **Y. An**, H. Okuzaki, Multi-functional shape memory polymer-ionic liquid gel sensors based on piezoionic effect.

Oral presentations

1) **Y. An**, H. Okuzaki, "Novel Composites of Conductive Polymer and Shape Memory Polymer for Electroactive Soft Actuators", *MRS-J 2018,* Dec. 20th, Kitakyushu, Japan. (Oral, F4-020-005)
2) **Y. An**, H. Okuzaki, "Fabrication of Conducting Polymer:Shape Memory Polymer Composites and their Electroactive Shape Memory Properties", *The 68th SPSJ Annual Meeting 2019*, May 29-31th, Osaka, Japan. (Oral, 1L14)
3) **Y. An**, H. Okuzaki, "Novel Conducting Polymer:Shape Memory Polymer Composites for Electroactive Actuators", *The 80th JSAP Autumn Meeting 2019*, Sep. 18-21th, Hokkaido, Japan. (Oral, 19a-B12-2)
4) **Y. An**, H. Okuzaki, "Novel Conductive Polymer:Shape Memory Polymer Composites for Electroactive Soft Actuators", *The 8th International Seminar on Green Energy Conversion Science and Technology 2019*, Oct. 22-23, Kofu, Japan. (Oral, 02)
5) **Y. An**, H. Okuzaki, "Electromechanical Behavior of Carbon Nanotube and Ionic Liquid Polymer Gel Actuators Based on Oxidation/Reduction Reaction", *MRS-J 2019*, Nov. 20th, Yokohama, Japan. (Oral, 2209)

Poster presentations

1) **Y. An**, K. Iwashita, H. Okuzaki, "Stretchable and Highly Conductive PEDOT:PSS-PAAm

Composited Hydrogels", *The 65th JSAP Spring Meeting 2018*, Mar. 17-18, Tokyo, Japan. (Poster, 17p-P6-10)

2) **Y. An**, K. Iwashita, H. Okuzaki, "Fabrication of Stretchable and Highly Conductive Polymer Hydrogels", *The 67th SPSJ Annual Meeting 2018*, May 23-25, Nagoya, Japan. (Poster, 1Pd102)
3) **Y. An**, K. Iwashita, H. Okuzaki, "Stretchable and Highly Conductive Polymer Gels", *ICSM 2018*, July 1-6, Busan, Korea. (Poster, TuP-091)
4) **Y. An**, H. Okuzaki, "Conducting Polymer:Shape Memory Polymer Composites", *The 7th International Seminar on Green Energy Conversion Science and Technology 2018*, Aug. 22-23, Kofu, Japan. (Poster, P46)
5) **Y. An**, H. Okuzaki, "Novel Composites of Conductive Polymer and Shape Memory Polymer for Electroactive Soft Actuators", *Japan-China Joint Workshop on Recent Advances on Active Soft Materials 2018*, Aug. 28th, Tokyo, Japan. (Poster, 02)
6) **Y. An**, H. Okuzaki, "Novel Composites of Conductive Polymer and Shape Memory Polymer for Electroactive Soft Actuators", *AMSM 2018*, Oct. 23-26th, Daejeon, Korea. (Poster, PS-47)
7) **Y. An**, H. Okuzaki, "Fabrication of Conducting Polymer:Shape Memory Polymer Composites and their Electroactive Shape Memory Properties", *APMSR 2019*, Aug. 25-28th, Xi'an, China. (Poster, 06)

Acknowledgements

My PhD studies began in October of 2017 at Laboratory of Organic Robot, Applied Chemistry Department, and Interdisciplinary Graduate School of Medicine and Engineering in University of Yamanashi. This dissertation presented the results of three year research. This would not have been accomplished without the assistance of a large number of people, I cannot name them all here, but I am grateful for their support.

Foremost, I would like to express my deepest thanks to Prof. Hidenori Okuzaki for his continuous guidance and support during the last three years. He was always careful and considerate in instructing me about the research process, the skills to write paper and how to make a good presentation. I also appreciate his great help in planning my career paths.

I am especially grateful to Prof. Kinji Asaka for the kind help during my internship in the National Institute of Advanced Science and Technology (AIST). I am luck to follow him to finished my internship.

I would like to thank Mr. Takahiro, Mr. Haruki Saito, Mr. Asuka Noda, Mr. Kazuki Kudo and Mr. Naoya Katsyama for teaching me the fabrication and characterization of sensor, the operation of scanning electron microscope (SEM), X-ray diffraction (XRD) and atomic force microscope (AFM).

I also want to thank Mr. Kazumasa Marumo, Ms. Yukino Fujiwara, Ms. Ayana Tomioka, Ms. Fumika Miyai, Mr. Furuyama Takaya, Ms. Tomokazu Shimura, Mr. Yudai Fukuzawa, Mr. Yusuke Fukasawa, Mr. Naoto Yamaguchi, Mr. Haruki Yoshida and Ms. Yuxin Jing for their kind help.

I would like to express my sincere gratitude to Ms. Maki Endo, Ms. Tomomi Hashizume, Ms. Nozomi Toyoda and Ms. Michiyo Midorikawa for the clerical assistance. Their kindness and patience accompanied me throughout my PhD life.

I specially thanks Prof. Hu Yan from Zhengzhou University, China. He provided me the opportunity to study here for PhD. His continual warm care and advice has been motivating me to do better and better.

I profoundly thank my parents, sister, and my brother for their love and support over the years.

Finally, the financial support from Special Doctoral Program for Green Energy Conversion Science and Technology is gratefully acknowledged.

Yingjun An

June 2020